THE PLASMA IN A MAGNETIC FIELD

The Plasma in a Magnetic Field

A Symposium on

MAGNETOHYDRODYNAMICS

Edited by

ROLF K. M LANDSHOFF

STANFORD UNIVERSITY PRESS

Stanford, California, 1958

The Library of Congress has cataloged this book as follows:

Landshoff, Rolf Karl Michael, 1911– *ed.*
The plasma in a magnetic field; a symposium on magnetohydrodynamics. Stanford, Calif., Stanford University Press, 1958.

vii, 130 p. illus. 24 cm.
Includes bibliographies.

1. Magnetohydrodynamics — Congresses. 2. Nuclear physics — Congresses. I. Title.

QC711.L34 1958 537.5 58–11698

Library of Congress

STANFORD UNIVERSITY PRESS
STANFORD, CALIFORNIA
LONDON: OXFORD UNIVERSITY PRESS

PREFACE

The present volume is the second to grow out of a Lockheed-sponsored symposium on magnetohydrodynamics. That second symposium was held at the Palo Alto laboratory of the Missile Systems Division on December 16, 1957.

The general remarks of the Preface to the first volume concerning the intent of both the symposium and the book still apply. The changed title reflects the much wider interest in phenomena involving plasmas rather than liquid metals. Actually, all papers presented dealt with plasmas.

For large values of the temperature, electrons and ions travel quite long distances before the cumulative effect of collisions becomes appreciable. Some configurations of importance which are discussed in Section 1 can for this reason be studied best through an individual orbit analysis. Anyone who would rather avoid the complicated averaging procedure which relates particle orbits and electrical currents will welcome the derivation of a modified macroscopic theory which gets around contradictions with the individual orbit analysis.

The use of magnetic fields appears to be the most promising means for confining a hot deuterium plasma long enough to produce controlled thermonuclear power. However, the interface between a plasma and a magnetic field tends to be unstable. In Section 2 evidence is presented for such an instability from both pinch effect studies and astrophysical observations. It is cautioned that observed fusion reactions can and in some cases must be interpreted as being due to instabilities rather than to a high temperature. A discussion of the effectiveness of axial magnetic fields and conducting walls to stabilize a pinch is followed by a theoretical study of plasma confinement by radiation pressure.

The tight coupling between magnetic field and plasma makes it possible to transfer energy from one to the other. Section 3 shows how high-speed flow can be generated as well as modified by magnetic forces. Several arrangements for magnetically driving shock waves are presented. Effects which a magnetic field has on existing plasma flow, which are discussed in this section, include an observed channeling of a plasma stream passing through an axial magnetic field and the effect of a transverse field

on drag and heat transfer deduced theoretically for simple viscous flow patterns.

I wish to thank the speakers at the symposium for their cooperation in preparing their papers for publication. I am also greatly indebted to D. Bershader for reading parts of the manuscript and to J. Todd from the LMSD publications staff for his valuable assistance in editing the manuscript and preparing it for publication.

ROLF K. M. LANDSHOFF
Consulting Scientist

Lockheed Missile Systems Division
Palo Alto, California
April 1958

CONTENTS

SECTION 1

KINETIC THEORY

ADIABATIC INVARIANTS IN THE MOTIONS OF CHARGED PARTICLES

S. CHANDRASEKHAR*

I. INTRODUCTION

In current treatments of plasma physics one often considers the motions of charged particles in varying magnetic fields in a so-called guiding center approximation. In this approximation one separates the spiraling motion of the charged particles about the lines of force, from the motion along the lines of force. This separation of the motion into the two parts is possible only so long as the magnetic field remains sensibly constant, spatially, over several Larmor radii and, temporally, over several Larmor periods. When these latter conditions are fulfilled, one generally supposes that the transverse kinetic energy ($w_\perp$) of the spiraling motion divided by the strength of the magnetic field (B) remains constant during the motion. This constancy of

$$\mu = \frac{w_\perp}{B} = \frac{mv_\perp^2}{2B} \tag{1}$$

is not strictly an integral of the equations of motion; it is an *adiabatic invariant* in the sense that it is a constant in the limit of infinitely slow variation of the field.

If in virtue of the constancy of μ, the particle should be trapped between two regions of relatively strong field,† then one supposes that the integral

$$\oint v \cdot \frac{dB}{B} \tag{2}$$

* The Enrico Fermi Institute for Nuclear Studies, University of Chicago.

† If W ($= w_\perp + w_\parallel$) denotes the total kinetic energy of the particle, then the points between which the particle will be trapped will be determined by $B_{max} = W/\mu$.

of the component of the velocity parallel to the field taken over a complete cycle is a further adiabatic invariant.*

In this paper we shall examine the precise meaning which must be attached to the notion of adiabatic invariance with a view to clarifying the limitations in its use in plasma physics.

II. THE NOTION OF ADIABATIC INVARIANCE

The notion of adiabatic invariance played an important role in the early developments of the quantum theory in the context of formulating the general rules of quantization. Historically, it arose from a question proposed by Lorentz at the first Solvay Congress in 1911. Lorentz's question was: How does a simple pendulum behave when the length of the suspending thread is gradually shortened? The relevance of this question for the quantum theory of the time was the following: If an oscillator has originally the correct energy appropriate to an elementary quantum ($h\nu$), would the energy suffice to make up a quantum at the end of a process

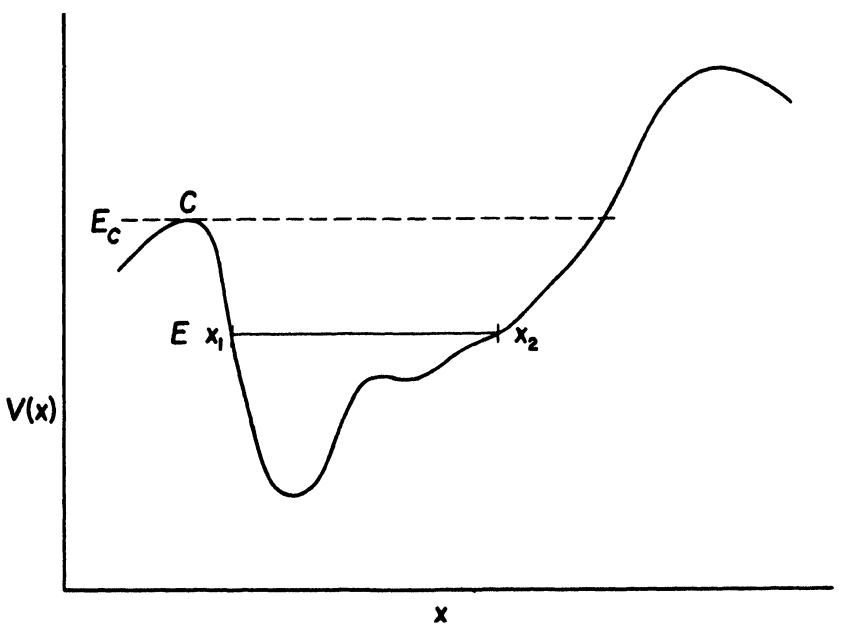

FIG. 1. Potential field with a barrier

* The conditions which must prevail in order that Eq. (2) may be an adiabatic invariant are very much more stringent than those which must obtain for $w_\perp/B$ to be an invariant (see Section XII).

(such as shortening the length of a pendulum) in which the frequency has been increased? To Lorentz's question, Einstein furnished the correct answer by saying that if the suspending thread is shortened infinitely slowly, then the energy, E, will increase proportionately to the "instantaneous" frequency, ν, so that a quantum of energy remains a quantum of energy; in other words, E/ν *is an adiabatic invariant.* We shall presently return to a somewhat more precise formulation of what this adiabatic invariance of E/ν really means; but it may be noted here, parenthetically, that the invariance of E/ν to slow changes was extended by Ehrenfest into a general "adiabatic hypothesis" applicable to multiply periodic systems. In this paper we shall, however, be concerned with adiabatic invariance as a concept in classical mechanics and, indeed, only for one-dimensional systems.

III. THE ADIABATIC INVARIANCE OF THE ACTION INTEGRAL

Consider the motion of a particle (of unit mass) in a potential field $V(x)$ (see Fig. 1). The equation governing its motion is

$$\frac{d^2x}{dt^2} + \frac{dV(x)}{dx} = 0. \tag{3}$$

This equation allows the energy integral

$$\frac{1}{2}\left(\frac{dx}{dt}\right)^2 + V(x) = E = \text{constant}; \tag{4}$$

from this we deduce that

$$t = \int \frac{dx}{\{2[E - V(x)]\}^{\frac{1}{2}}}. \tag{5}$$

If two points x_1 and x_2 exist such that (see Fig. 1)

$$E = V(x_1) = V(x_2) \qquad (x_2 > x_1), \tag{6}$$

then the particle will oscillate between x_1 and x_2; and the period of the oscillation will be given by

$$P = 2\int_{x_1}^{x_2} \frac{dx}{\{2[E - V(x)]\}^{\frac{1}{2}}} = \oint \frac{dx}{\{2[E - V(x)]\}^{\frac{1}{2}}}. \tag{7}$$

Associated with such periodic motions one defines the *action integral*

$$J = \oint dx\{2[E - V(x)]\}^{\frac{1}{2}} = \oint dx\left(\frac{dx}{dt}\right). \tag{8}$$

Suppose that $V(x)$ depends (apart from x) on a set of parameters a_j $(j=1,\ldots,n)$ such that

$$V(x) = V(x; a_1, \ldots, a_n). \tag{9}$$

Now let the a_j's instead of being constants be slowly varying functions of time. "Slowly varying" in this connection means that the particle executes several oscillations (appropriate to a set of a_j's which occur) before any of the a_j's change appreciably; in other words, we require:

$$\left|\frac{1}{a_j}\frac{da_j}{dt}\right| << \frac{1}{P(a_1, \ldots, a_n)} \qquad (j = 1, \ldots, n). \tag{10}$$

When this is the case, we may characterize the motion by a certain energy, $\bar{E}$, appropriate for a single oscillation, namely,

$$\begin{aligned}\bar{E} &= \oint \frac{dx}{\dot{x}}\left[\frac{1}{2}\left(\frac{dx}{dt}\right)^2 + V(x; a_1, \ldots, a_n)\right] \Big/ \oint \frac{dx}{\dot{x}} \\ &= \oint dt\left[\frac{1}{2}\left(\frac{dx}{dt}\right)^2 + V(x; a_1, \ldots, a_n)\right] \Big/ \oint dt.\end{aligned} \tag{11}$$

It will be observed that in defining $\bar{E}$ in this way, we are averaging the energy during an oscillation, weighting each element of the orbit by the fraction of the time the particle spends in that element.

The theorem on adiabatic invariance is to the effect that *the action integral,*

$$J = \oint dx\,\{2[\bar{E} - V(x; a_1, \ldots, a_n)]\}^{\frac{1}{2}}, \tag{12}$$

defined in terms of $\bar{E}$ is a constant for infinitely slow variations of the a_j's. The arguments by which one attempts to establish this constancy of J are, essentially, as follows:

We have

$$\frac{dJ}{dt} = \frac{\partial J}{\partial \bar{E}}\frac{d\bar{E}}{dt} + \sum_{j=1}^{n}\frac{\partial J}{\partial a_j}\frac{da_j}{dt}. \tag{13}$$

On the other hand, from the definition of J we have

$$\left.\begin{aligned} \frac{\partial J}{\partial a_j} &= -\oint \frac{\partial V}{\partial a_j} \frac{dx}{\{2\,[\bar{E} - V]\}^{\frac{1}{2}}} \\ \text{and} \\ \frac{\partial J}{\partial \bar{E}} &= \oint \frac{dx}{\{2\,[\bar{E} - V]\}^{\frac{1}{2}}} = \oint \frac{dx}{\dot{x}}; \end{aligned}\right\} \tag{14}$$

while from the definition of $\bar{E}$ we have

$$\frac{d\bar{E}}{dt} = \oint dt \left[\frac{dx}{dt}\frac{d^2x}{dt^2} + \frac{\partial V}{\partial x}\frac{dx}{dt} + \sum_{j=1}^{n} \frac{\partial V}{\partial a_j}\frac{da_j}{dt} \right] \Big/ \oint dt. \tag{15}$$

Making use of the equation of motion governing x, we can reduce the foregoing equation to the form

$$\begin{aligned} \frac{d\bar{E}}{dt} &= \sum_{j=1}^{n} \frac{da_j}{dt} \oint \frac{\partial V}{\partial a_j}\, dt \Big/ \oint dt \\ &= \sum_{j=1}^{n} \frac{da_j}{dt} \oint \frac{\partial V}{\partial a_j} \frac{dx}{\{2\,[\bar{E} - V]\}^{\frac{1}{2}}} \Big/ \oint \frac{dx}{\dot{x}}. \end{aligned} \tag{16}$$

Combining Eqs. (13), (14), and (16), we have

$$\begin{aligned} \frac{dJ}{dt} &= \sum_{j=1}^{n} \frac{da_j}{dt} \oint \frac{\partial V}{\partial a_j} \frac{dx}{\{2\,[\bar{E} - V]\}^{\frac{1}{2}}} \\ &\quad - \sum_{j=1}^{n} \frac{da_j}{dt} \oint \frac{\partial V}{\partial a_j} \frac{dx}{\{2\,[\bar{E} - V]\}^{\frac{1}{2}}} = 0, \end{aligned} \tag{17}$$

which establishes the constancy of J.

IV. ADIABATIC INVARIANCE IN THE SMALL AND IN THE LARGE

The proof of the constancy of the action integral given in Section III, for slow changes in the parameters which occur in the potential function, contains many heuristic elements. For example, the proof at no stage involved any explicit estimate of the error involved in the concept of $\bar{E}$ and

of the action integral defined in terms of it. Indeed, the notion of adiabatic invariance was taken as equivalent to a justification of $\overline{E}$ and J as defined. This is not altogether satisfactory; and we shall accordingly try to formulate more explicitly the conceptual prerequisites underlying the notion of adiabatic invariance. In order that we may clarify the essential physical concepts without any of the formal complexities which a completely general formulation will require, we shall consider the relevant questions explicitly in the context of Lorentz's original problem and leave the generalizations to the reader.

Consider then the equation of motion of a simple pendulum. We have

$$\frac{d^2x}{dt^2} + \omega^2 x = 0, \tag{18}$$

where ω denotes the circular frequency. If ω is a constant, the general solution of this equation can be written as

$$x = A \cos(\omega t + \varepsilon), \tag{19}$$

where A and ε are constants. From this solution it follows that

$$\langle \dot{x}^2 \rangle = \tfrac{1}{2} A^2 \omega^2; \quad \langle x^2 \rangle = \tfrac{1}{2} A^2; \tag{20}$$

and, further, that

$$\overline{E} = \tfrac{1}{2}\{\langle \dot{x}^2 \rangle + \omega^2 \langle x^2 \rangle\} = \tfrac{1}{2} A^2 \omega^2. \tag{21}$$

The adiabatic invariance of the action integral as applied to this problem states the following:

Let ω, instead of being a constant, be a slowly varying function of time such that

$$\left| \frac{1}{\omega} \frac{d\omega}{dt} \right| << \omega. \tag{22}$$

For such slow variations

$$\overline{E}/\omega \text{ is a constant.} \tag{23}$$

If one wants to formulate the principle of adiabatic invariance without any of the heuristic elements implied in the forgeoing statement, then it would appear that the physical premises should be restated somewhat differently.

Clearly, the concepts of energy and period taken over from the case when ω is a constant cannot strictly apply to a dynamical system in which ω is some function of time no matter how slowly varying. They can apply only if certain limiting conditions are satisfied. Thus, let ω (t) be a func-

tion of time such that

$$\omega(t) \to \omega_1 \text{ as } t \to -\infty,$$

and

$$\omega(t) \to \omega_2 \text{ as } t \to +\infty; \tag{24}$$

and also that

$$\frac{d^n\omega}{dt^n} \to 0 \quad \text{as } t \to +\infty \quad \text{and } t \to -\infty \quad \text{for all } n \geqslant 1. \tag{25}$$

When these conditions are satisfied, the system is a simple harmonic oscillator, in the strict sense, both when $t \to -\infty$ and when $t \to +\infty$. Accordingly, $\langle x^2 \rangle$ can be defined uniquely for both these limits and we may consider the ratio

$$\lambda = \frac{\omega_2 \langle x^2 \rangle_{t \to +\infty}}{\omega_1 \langle x^2 \rangle_{t \to -\infty}}. \tag{26}$$

This will clearly depend on the manner in which ω varies between ω_1 and ω_2. Let $d\omega/dt$ be bounded and

$$\text{Maximum of } \left| \frac{1}{\omega} \frac{d\omega}{dt} \right| = \frac{1}{T} \qquad (-\infty < t < +\infty). \tag{27}$$

A precise statement of the theorem on adiabatic invariance would be the assertion:

$$\lambda \to 1 \quad \text{as} \quad T \to \infty. \tag{28}$$

The remarkable aspect of this assertion is that it is not restricted by any limitation on ω_2/ω_1. Nevertheless, it will be convenient to distinguish two cases: the case when

$$\delta = \tfrac{1}{2} \left| \frac{\omega_2 - \omega_1}{\omega_2 + \omega_1} \right| << 1; \tag{29}$$

and when no such restriction applies. If, in the former case, we can show that

$$\lambda = 1 + O(\delta^2) \quad \text{as} \quad T \to \infty, \tag{30}$$

then we shall say that we have *adiabatic invariance in the small*. If on the other hand, Eq. (28) holds with no restriction on ω_2/ω_1, we shall say that we have *adiabatic invariance in the large*.

The principle of adiabatic invariance in the large can be formulated somewhat differently as follows: Let

$$\omega \equiv \omega(\alpha t) \tag{31}$$

represent a one-parameter family of time variations satisfying the requirements (24) and (25). For such a family of time variations, λ defined as in Eq. (26) will depend on α; and adiabatic invariance in the large implies that

$$\lambda(\omega_1, \omega_2; \alpha) \to 1 \quad \text{as} \quad \alpha \to 0, \tag{32}$$

independently of ω_1 and ω_2.

It is clear that the foregoing ideas formulated in the context of Lorentz's original problem can be extended to include the more general problem considered in Section III.

V. THE RELATION OF THE ADIABATIC INVARIANCE OF $w_\perp/B$ TO THE INVARIANCE OF $\omega \langle |x|^2 \rangle$ IN THE PENDULUM PROBLEM

Before discussing in some detail the adiabatic invariance of $\omega \langle |x|^2 \rangle$ in the problem of the simple pendulum, it will be useful to relate this problem to the invariance of $w_\perp/B$ in the motion of a charged particle in a varying magnetic field.

With the substitution

$$\zeta = x \exp\left(-i \int \omega \, dt\right), \tag{33}$$

the equation

$$\frac{d^2x}{dt^2} + \omega^2 x = 0 \tag{34}$$

becomes

$$\frac{d^2\zeta}{dt^2} + 2i\omega \frac{d\zeta}{dt} + i \frac{d\omega}{dt} \zeta = 0; \tag{35}$$

and this is the equation of motion of a charged particle in a spatially uniform but a temporally varying magnetic field, if we identify 2ω as the Larmor frequency ($= eB/mc$) and the real and the imaginary parts of ζ (regarded as a complex variable) as the Cartesian coordinates of the particle in a plane normal to the lines of force. The transverse kinetic energy divided by the instantaneous strength of the field is, apart from constant factors of proportionality, given by

$$\frac{1}{\omega} \left| \frac{d\zeta}{dt} \right|^2 = \frac{1}{\omega} \left| \frac{dx}{dt} - i\omega x \right|^2. \tag{36}$$

The adiabatic invariance of $w_\perp/B$ in the motion of a charged particle in a uniform but time-dependent magnetic field is, therefore, very directly related to the adiabatic invariance of $\overline{E}/\omega$ in the problem of the simple pendulum; they represent, in fact, the same problem.

VI. THE ADIABATIC INVARIANCE OF $\omega\langle|x|^2\rangle$ IN THE SMALL

The proof of the adiabatic invariance of $\omega\langle|x|^2\rangle$ in the small can be accomplished very simply.

By letting

$$t_1 = \int \omega dt \quad \text{and} \quad dt_1 = \omega dt, \tag{37}$$

we find that Eq. (34) becomes

$$\frac{d^2x}{dt_1^2} + x = -\left(\frac{1}{\omega}\frac{d\omega}{dt_1}\right)\frac{dx}{dt_1}. \tag{38}$$

We solve this equation by an iteration procedure, i.e., by evaluating the right-hand side of the equation in terms of the solution obtained when this side is ignored; and solving the resulting equation as a non-homogeneous equation for x. Thus, if

$$x = e^{it_1} \tag{39}$$

is the solution appropriate for $t_1 \to -\infty$, the equation we have to solve is

$$\frac{d^2x}{dt_1^2} + x = -i\left(\frac{1}{\omega}\frac{d\omega}{dt_1}\right)e^{it_1}. \tag{40}$$

The solution of Eq. (40) which tends to (39) as $t_1 \to -\infty$ is readily found to be

$$x = e^{it_1}\left(1 - \tfrac{1}{2}\log\frac{\omega}{\omega_1}\right) + \tfrac{1}{2}\,e^{-it_1}\int_{-\infty}^{t_1}\frac{1}{\omega}\frac{d\omega}{dt_1'}\,e^{2it_1'}\,dt_1'. \tag{41}$$

From this solution it follows that

$$\lim_{t_1 \to +\infty}\left\{\omega\langle|x|^2\rangle\right\} = \omega_2\left(1 - \tfrac{1}{2}\log\frac{\omega_2}{\omega_1}\right)^2 + \omega_2|P|^2, \tag{42}*$$

where

$$P = \tfrac{1}{2}\int_{-\infty}^{+\infty}\frac{1}{\omega}\frac{d\omega}{dt_1}\,e^{2it_1}\,dt_1. \tag{43}$$

* In writing this equation we have further averaged over all initial phases.

Accordingly [cf. Eq. (26)]

$$\lambda = \frac{\omega_2}{\omega_1}\left(1 - \tfrac{1}{2}\log\frac{\omega_2}{\omega_1}\right)^2 + \frac{\omega_2}{\omega_1}|P|^2. \tag{44}$$

If we now suppose that

$$\omega_2 = \omega_1 + \delta\omega, \tag{45}$$

as is permissible when considering adiabatic invariance in the small, then we deduce from Eq. (44) that

$$\lambda = 1 + O(\delta\omega^2) + \frac{\omega_2}{\omega_1}|P|^2. \tag{46}$$

It is evident that in the limit of infinitely slow variation,

$$|P|^2 \to 0. \tag{47}$$

The adiabatic invariance in the small is therefore established.

VII. THE ADIABATIC INVARIANCE OF $\omega\langle|x|^2\rangle$ IN THE LARGE

The adiabatic invariance of $\omega\langle|x|^2\rangle$ in the large is more difficult to establish. It can, however, be made to "look obvious" by a further transformation of Eq. (38). Thus, by introducing the variable

$$x_1 = \sqrt{\omega}\, x \tag{48}$$

in place of x, we find that Eq. (38) becomes

$$\frac{d^2x_1}{dt_1^2} + x_1 + \Omega x_1 = 0 \tag{49}$$

where

$$\Omega = \tfrac{1}{4}\left(\frac{1}{\omega}\frac{d\omega}{dt_1}\right)^2 - \frac{1}{2\omega}\frac{d^2\omega}{dt_1^2}. \tag{50}$$

It will be observed that in contrast to Eq. (38), the "correction terms" included in Ω in Eq. (49) are of the second order in $d\omega/dt$. If we can ignore the term in Ω in Eq. (49), then it is clearly a consequence of this equation that $\langle|x_1|^2\rangle$ is indeed a constant; and the constancy, in this approximation, of $\omega\langle|x|^2\rangle$ directly follows. More precisely, we may try to solve Eq. (49) by an iteration procedure by evaluating the term Ωx_1 in terms of the solution obtained by ignoring this term; and solving the resulting equation as an inhomogeneous equation for x_1. In this manner we

find that the solution of Eq. (49), which tends to e^{it_1} as $t_1 \to -\infty$, is given by

$$x_1 = e^{it_1} + \tfrac{1}{2} i \left\{ e^{it_1} \int_{-\infty}^{t_1} \Omega\,(t_1')\, dt_1' - e^{-it_1} \int_{-\infty}^{t_1} \Omega\,(t_1')\, e^{2it_1'}\, dt_1' \right\}. \quad (51)$$

If we now suppose that

$$\omega(t) \equiv \omega(\alpha t) = \omega(\tau) \qquad (\tau = \alpha t), \quad (52)$$

as in Eq. (31), we may conclude from Eq. (51) that

$$x_1 \to e^{it_1} + i\alpha\,(e^{it_1} X - e^{-it_1} Y) \qquad (t_1 \to +\infty), \quad (53)$$

where

$$X = \tfrac{1}{2} \int_{-\infty}^{+\infty} \Omega(\tau_1) d\tau_1; \quad Y = \tfrac{1}{2} \int_{-\infty}^{+\infty} \Omega(\tau_1) e^{2i\tau_1/\alpha} d\tau_1, \quad (54)$$

$$\Omega(\tau_1) = \tfrac{1}{4} \left(\frac{1}{\omega} \frac{d\omega}{d\tau_1} \right)^2 - \frac{1}{2\omega} \frac{d^2\omega}{d\tau_1^2} \qquad [\omega \equiv \omega(\tau_1) \text{ and } \tau_1 = \alpha t_1]. \quad (55)$$

If the integral defining X exists, then it clearly follows from Eq. (53) that

$$x \to e^{it} \text{ as } \alpha \to 0 \qquad (\text{and } t_1 \to +\infty). \quad (56)$$

From this, the adiabatic invariance of $\omega\langle|x|^2\rangle$ in the large follows.

While the foregoing suffices to establish the adiabatic invariance of $\omega\langle|x|^2\rangle$ in the large, it is not sufficient to yield the error term with exactitude for $\alpha \to 0$. This arises from the fact that the iteration scheme by which we obtained the solution (51) is not uniformly convergent for the entire (infinite) range of t_1. A method which appears sufficient to establish the true order of the error term as $\alpha \to 0$ was discovered by Hertweck and Schlüter.[1] In this method, we start from Eq. (40) and make the following sequence of transformations. First, we let

$$x = \exp\,(\int \gamma dt_1), \quad (57)$$

when Eq. (40) becomes

$$\frac{d\gamma}{dt_1} + \gamma^2 + 1 + \left(\frac{1}{\omega} \frac{d\omega}{dt_1} \right) \gamma = 0. \quad (58)$$

Next, we let

$$y = \frac{\gamma + i}{\gamma - i}, \quad (59)$$

and obtain

$$\frac{dy}{dt_1} - 2iy + \frac{1}{2\omega}\frac{d\omega}{dt_1}(1 - y^2) = 0. \tag{60}$$

Hertweck and Schlüter now show that by neglecting y^2 in comparison with 1 in this equation and solving the equation consistently in this approximation, one obtains

$$\lambda = 1 + |P|^2 \tag{61}$$

where

$$P = \tfrac{1}{2}\int_{-\infty}^{+\infty} \frac{1}{\omega}\frac{d\omega}{dt_1} e^{-2it_1}\, dt_1. \tag{62}$$

[Note that this definition of P agrees with that given in Eq. (43).] In this way, Hertweck and Schlüter establish the adiabatic invariance of $\omega\langle|x|^2\rangle$ in the large and obtain at the same time the correct order of the error term as $\alpha \to 0$.

VIII. THE HIERARCHY OF INVARIANTS

Starting from the equation

$$\frac{d^2x}{dt^2} + \omega^2 x = 0, \tag{63}$$

where ω is a function of time, we have found that the substitutions

$$dt_1 = \omega\, dt \quad \text{and} \quad x_1 = \sqrt{\omega}\, x \tag{64}$$

lead to an equation of the same form as the original, namely [cf. Eqs. (49) and (50)]

$$\frac{d^2x_1}{dt_1^2} + \omega_1^2 x_1 = 0, \tag{65}$$

where

$$\omega_1^2 = 1 + \Omega = 1 + \tfrac{1}{4}\left(\frac{1}{\omega}\frac{d\omega}{dt_1}\right)^2 - \frac{1}{2\omega}\frac{d^2\omega}{dt_1^2}$$

$$= 1 + \frac{1}{\omega^{3/2}}\frac{d^2}{dt^2}\frac{1}{\sqrt{\omega}}. \tag{66}$$

Consequently, by the further transformations

$$dt_2 = \omega_1\, dt_1 \quad \text{and} \quad x_2 = \sqrt{\omega_1}\, x_1, \tag{67}$$

Eq. (65) can be brought once again to the form

$$\frac{d^2x_2}{dt_2{}^2} + \omega_2{}^2\, x_2 = 0, \tag{68}$$

where

$$\omega_2{}^2 = 1 + \frac{1}{\omega_1{}^{3/2}} \frac{d^2}{dt_1{}^2} \frac{1}{\sqrt{\omega_1}}. \tag{69}$$

More generally, by defining the transformations

$$dt_n = \omega_{n-1}\, dt_{n-1}, \quad x_n = \sqrt{\omega_{n-1}}\, x_{n-1}, \tag{70}$$

by induction, we can derive the sequence of equations

$$\frac{d^2x_n}{dt_n{}^2} + \omega_n{}^2\, x_n = 0 \tag{71}$$

where

$$\omega_n{}^2 = 1 + \frac{1}{\omega_{n-1}{}^{3/2}} \frac{d^2}{dt_{n-1}{}^2} \frac{1}{\sqrt{\omega_{n-1}}}. \tag{72}$$

We have seen that whenever we have an equation of the form (63) in which ω^2 is a slowly varying function of time,

$$\omega \langle |x|^2 \rangle \quad \text{is an adiabatic invariant.} \tag{73}$$

By applying this principle to Eq. (71), we obtain the hierarchy of invariants

$$\begin{aligned} \mu_n &= \omega_n \langle |x_n|^2 \rangle = \omega_n\, \omega_{n-1} \langle |x_{n-1}|^2 \rangle \\ &= \ldots = \omega_n \omega_{n-1} \ldots \omega_1 \omega \langle |x|^2 \rangle. \end{aligned} \tag{74}$$

IX. THE HIGHER-ORDER INVARIANTS FOR THE MOTION OF CHARGED PARTICLES; AN EXAMPLE

We shall now consider some applications of the higher-order invariants to the motion of charged particles in varying magnetic fields.

We have seen in Section V that the equation

$$\frac{d^2\zeta}{dt^2} + 2i\omega \frac{d\zeta}{dt} + i \frac{d\omega}{dt} \zeta = 0, \tag{75}$$

representing the motion of a charged particle in a uniform but a time-dependent magnetic field, becomes

$$\frac{d^2x}{dt^2} + \omega^2 x = 0, \tag{76}$$

by the transformation

$$x = \zeta \exp\,(i\int \omega dt) = \zeta\, e^{it_1}. \tag{77}$$

Since by the succession of transformations [cf. Eq. (70)]

$$(x, t) \to (x_1, t_1) \to (x_2, t_2) \to \ldots \to (x_n, t_n) \to \ldots, \tag{78}$$

Eq. (76) can be repeatedly brought to the same form, it is clear that by a corresponding sequence of transformations

$$(\zeta, t) \to (\zeta_1, t_1) \to (\zeta_2, t_2) \to \ldots \to (\zeta_n, t_n) \to \ldots, \tag{79}$$

Eq. (75) can be similarly brought, repeatedly, to the same form. According to Eqs. (70) and (77), the required transformations (79) are, inductively, defined by

$$\left.\begin{aligned} \zeta_n = x_n e^{-it_{n+1}} = \sqrt{\omega_{n-1}}\, x_{n-1}\, e^{-it_{n+1}} = \sqrt{\omega_{n-1}}\, e^{i(t_n - t_{n+1})}\, \zeta_{n-1}, \\ \text{and} \\ dt_n = \omega_{n-1}\, dt_{n-1} \quad (n = 1, 2, \ldots,), \end{aligned}\right\} \tag{80}$$

where the ω_n's are given, as before, by Eq. (72).

As an example we may note that the transformations

$$\zeta_1 = \sqrt{\omega}\, e^{i(t_1 - t_2)}\, \zeta, \quad dt_1 = \omega\, dt, \tag{81}$$

will lead to an equation of the form

$$\frac{d^2\zeta_1}{dt_1^2} + 2i\omega_1 \frac{d\zeta_1}{dt_1} + i\,\frac{d\omega_1}{dt_1}\,\zeta_1 = 0, \tag{82}$$

where ω_1 is given by Eq. (66).

We have seen that whenever an equation of the form (75) obtains in which ω is a slowly varying function of time, the quantity

$$\mu = \frac{1}{\omega}\left|\frac{d\zeta}{dt}\right|^2 \tag{83}$$

is an adiabatic invariant. Since ζ_n satisfies, with respect to t_n, a differential equation of the same form as (75), we may conclude that

$$\mu_n = \frac{1}{\omega_n}\left|\frac{d\zeta_n}{dt_n}\right|^2 \tag{84}$$

represents a hierarchy of adiabatic invariants for the motion of a charged particle in a time-dependent magnetic field.

The relation in which the various higher-order invariants stand with respect to each other and to the basic invariant (83) can be seen by considering the first of these higher-order ones, namely,

$$\mu_1 = \frac{1}{\omega_1} \left| \frac{d\zeta_1}{dt_1} \right|^2 . \tag{85}$$

Reverting to the original variables by means of Eqs. (81), we readily find:

$$\mu_1 = \frac{1}{\omega\omega_1} \left| \frac{d\zeta}{dt} + \zeta \left\{ \tfrac{1}{2} \frac{d}{dt} \log \omega + i\,\omega\,(1 - \omega_1) \right\} \right|^2 . \tag{86}$$

If we set in Eq. (86) the derivatives of ω equal to zero, we recover the basic invariant (83).

By averaging over all relative phases between ζ and $d\zeta/dt$, we obtain from Eq. (86), the invariant

$$\mu_1 = \frac{1}{\omega\omega_1} \left[\left| \frac{d\zeta}{dt} \right|^2 + |\zeta|^2 \left\{ \omega^2 (1 - \omega_1)^2 + \tfrac{1}{4} \left(\frac{d}{dt} \log \omega \right)^2 \right\} \right]. \tag{87}$$

The (relative) constancy of μ_1 under circumstances in which μ may not be treated as a constant, may have some practical applications.

X. THE CHANGE IN THE INVARIANT WHEN THERE IS A DISCONTINUITY IN B OR A HIGHER DERIVATIVE OF B

By rewriting Eq. (75) in the manner

$$\frac{d}{dt} \left(\frac{d\zeta}{dt} + 2i\omega\zeta \right) - i \frac{d\omega}{dt} \zeta = 0, \tag{88}$$

and integrating over t, we get

$$\frac{d\zeta}{dt} + 2i\omega\zeta - i \int^t \frac{d\omega}{dt} \zeta dt = C, \tag{89}$$

where C is a constant. If ω should suffer a discontinuity at $t = 0$ (say), at which time it jumps discontinuously from a value ω^- to a value ω^+, we may deduce from Eq. (89) that

$$\frac{d\zeta}{dt} + 2i\omega^-\zeta = C \quad (t < 0), \tag{90}$$

and

$$\frac{d\zeta}{dt} + 2i\omega^+\zeta - i\,(\omega^+ - \omega^-)\,\zeta_0 = C \quad (t > 0), \tag{91}$$

where ζ_0 is the value of ζ at $t = 0$. From the foregoing equations we readily find that

$$\frac{\mu^+}{\mu^-} = \frac{1}{\omega^+}\left|\frac{d\zeta}{dt}\right|^2_{t\to+0} \Big/ \frac{1}{\omega^-}\left|\frac{d\zeta}{dt}\right|^2_{t\to-0} = \frac{(\omega^+ + \omega^-)^2}{4\omega^+\omega^-}, \tag{92}$$

if ζ is assumed to be of the form $\rho e^{-2i\omega^- t}$ (ρ real) for $t < 0$.

If instead of ω a derivative of ω should suffer a discontinuity at $t = 0$, then we can obtain a result similar to (92) for one of the higher invariants μ_n. Thus, if ω_n is the first of the ω_n's which experience a discontinuity at $t = 0$, then by treating the equation satisfied by ζ_n in a similar manner, we shall obtain the result

$$\frac{\mu_n{}^+}{\mu_n{}^-} = \frac{(\omega_n{}^+ + \omega_n{}^-)^2}{4\,\omega_n{}^+\omega_n{}^-}. \tag{93}$$

XI. THE CHANGE IN $w_\perp/B$ FOR A SLOW BUT A FINITE RATE OF VARIATION OF B

We have seen that $w_\perp/B$ is strictly a constant only in the limit of infinitely slow variation of B. For any finite rate of variation, $w_\perp/B$ will change by calculable amounts; and the asymptotic dependence of this change on the rate of variation of B, as it tends to zero, can be ascertained by Hertweck and Schlüter's method. In this method one starts from the equation of motion of a simple harmonic oscillator (with ω^2 a function of time) and obtains by the sequence of transformations [cf. Eqs. (57) and (59)]

$$x \to \gamma \to y \quad \text{and} \quad t \to t_1, \tag{94}$$

the differential equation [Eq. (60)]

$$\frac{dy}{dt_1} - 2iy + \frac{1}{2\omega}\frac{d\omega}{dt_1}(1 - y^2) = 0. \tag{95}$$

By neglecting the term in y^2 in this equation and solving the equation

$$\frac{dy}{dt_1} - 2iy + \frac{1}{2\omega}\frac{d\omega}{dt_1} = 0 \tag{96}$$

consistently in this approximation, Hertweck and Schlüter show that for sufficiently slow variations of B

$$\frac{\mu^{+\infty}}{\mu^{-\infty}} - 1 \simeq |P|^2 \tag{97}$$

where

$$P = \tfrac{1}{2}\int_{-\infty}^{+\infty} \frac{1}{\omega}\,\frac{d\omega}{dt_1}\, e^{-2it_1}\, dt_1. \tag{98}$$

It is clear that we may improve upon Hertweck and Schlüter's method by starting from Eq. (71) for x_n and treating this equation in a similar fashion. We shall then obtain

$$\frac{\mu^{+\infty}}{\mu^{-\infty}} - 1 \simeq |P_n|^2 \tag{99}$$

where

$$P_n = \tfrac{1}{2}\int_{-\infty}^{+\infty} \frac{1}{\omega_n}\,\frac{d\omega_n}{dt_{n+1}}\, e^{-2it_{n+1}}\, dt_{n+1}. \tag{100}$$

Integrating the expression on the right-hand side of this equation by parts and remembering that $d\omega_n/dt_{n+1}$ tends to zero at both limits of integration for all $n > 1$, we obtain

$$P_n = i\int_{-\infty}^{+\infty} (\log \omega_n)\, e^{-2it_{n+1}}\, dt_{n+1}, \tag{101}$$

or [cf. Eq. (70)]

$$P_n = i\int_{-\infty}^{+\infty} (\omega_n \log \omega_n)\, e^{-2it_{n+1}}\, dt_n. \tag{102}$$

We shall illustrate the use of these higher-order approximations for $(\mu^{+\infty}/\mu^{-\infty}) - 1$ by considering the case $n = 1$. In this case Eq. (102) takes the form

$$P_1 = \tfrac{1}{2}i\int_{-\infty}^{+\infty} [(1+\Omega)^{\frac{1}{2}} \log (1+\Omega)] \exp\{-2i\textstyle\int (1+\Omega)^{\frac{1}{2}}\, dt_1\}\, dt_1, \tag{103}$$

where we have substituted for ω_1 in accordance with Eq. (66). When $\Omega \to 0$, we can write

$$P_1 = \tfrac{1}{2}i\int_{-\infty}^{+\infty} \Omega(t_1)\, e^{-2it_1}\, dt_1. \tag{104}$$

In Hertweck and Schlüter's paper the case when $\omega(t)$ has the form

$$\omega(t) = \omega_0 \, (3/2 + 1/2 \tanh \alpha t), \tag{105}$$

where ω_0 and α are constants, is treated in some detail. For this form of $\omega\,(t)$ it can be readily shown that

$$\Omega = \left(\frac{\alpha}{\omega_0} \right)^2 \frac{2Q^{3/2} - 5Q + 3}{4Q^2} \tag{106}$$

where

$$Q = 1 + 8\, e^{2y} \text{ and } y = \alpha t_1/\omega_0. \tag{107}$$

The integral defining P_1 [Eq. (104)] can be evaluated explicitly and we find

$$|\, P_1 \,|^2 = \frac{\pi^2 q^2}{16 \left(\sinh \dfrac{\pi}{2q} \right)^2} \left| 1 - \frac{3i}{4q} - \frac{1}{\sqrt{\pi}} \frac{\Gamma\left(\dfrac{1}{2} + \dfrac{i}{2q} \right)}{\Gamma\left(1 + \dfrac{i}{2q} \right)} \right|^2, \tag{108}$$

where

$$q = 1/2 \, (\alpha/\omega_0). \tag{109}$$

Equation (108) may be contrasted with

$$|\, P \,|^2 = \frac{\pi^2}{16 \left(\sinh \dfrac{\pi}{2q} \right)^2} \left| 1 - \frac{1}{\sqrt{\pi}} \frac{\Gamma\left(\dfrac{1}{2} + \dfrac{i}{2q} \right)}{\Gamma\left(1 + \dfrac{i}{2q} \right)} \right|^2, \tag{110}$$

obtained by Hertweck and Schlüter. The values of $|\, P \,|^2$ and $|\, P_1 \,|^2$ given by the foregoing formulae for some values of q are listed in Table 1, and are further compared with the results of exact numerical integrations.* It will be observed that $|\, P_1 \,|^2$ gives for intermediate values of q a better representation of the exact results than does $|\, P \,|^2$.

XII. THE LONGITUDINAL INVARIANT

As we have stated in Section I, in treating the motions of charged particles in the guiding center approximation, we separate the motions parallel and perpendicular to the field. The variation of $w_\perp$ along the lines of force is determined from the (assumed) constancy of $w_\perp / B$ as an adiabatic invariant. The variation of the velocity ($v_\parallel$) parallel to the lines of

* I am indebted to Dr. R. Lüst for supplying me with these.

force is, then, determined from the equation of motion [cf. Spitzer[2] or Rosenbluth and Longmire[3]]

$$\frac{dv_{\parallel}}{dt} = -\frac{w_{\perp}}{B}\frac{\partial B}{\partial s}, \tag{111}$$

where ds denotes the element of arc along $\boldsymbol{B}$. The content of Eq. (111) is that the motion along the line of force is governed by the potential function

$$V(s) = \frac{w_{\perp}}{B}B(s). \tag{112}$$

If the particle should describe a periodic orbit in this potential function, then the considerations of Section III apply and we may infer the adiabatic invariance of the action integral

$$J = \oint v_{\parallel}\, ds = \oint \boldsymbol{v}\cdot\frac{d\boldsymbol{B}}{B}. \tag{113}$$

This is the longitudinal invariant of Chew, Goldberger, and Low.[4] It is, however, clear that this invariant can be used only if the variation of B with time takes place very slowly in the time scale of the period of oscillation of the particle in the potential field (112). Also, it is necessary that during the variation of B, particles which are initially "trapped" do not escape over the potential barrier (as at C in Fig. 1); and, conversely, particles, once "free," are not trapped. For these reasons the conditions

TABLE 1

THE CHANGE IN $w_{\perp}/B$ FOR FINITE RATES OF VARIATION OF B IN ACCORDANCE WITH EQ. (105)

q	$\lvert P\rvert^2$	$\lvert P_1\rvert^2$	Exact
0.20	2.223×10^{-7}	1.914×10^{-7}	
0.25	4.823×10^{-6}	4.291×10^{-6}	
0.3333	1.013×10^{-4}	9.384×10^{-5}	1.13×10^{-4}
0.50	1.956×10^{-3}	1.903×10^{-3}	2.04×10^{-3}
0.625	6.066×10^{-3}	6.028×10^{-3}	
0.8333...	1.762×10^{-2}	1.788×10^{-2}	
1.00	2.884×10^{-2}	2.958×10^{-2}	2.99×10^{-2}
1.25	4.527×10^{-2}	4.694×10^{-2}	
2.00	7.919×10^{-2}	8.411×10^{-2}	8.26×10^{-2}
2.50	9.141×10^{-2}	9.869×10^{-2}	
∞	...	...	1.25×10^{-1}

which must obtain for a valid use of the longitudinal invariant are very much more stringent than for the use of $w_\perp/B$ as an invariant during the motion.

REFERENCES

1. F. Hertweck and A. Schlüter, "Die 'adiabatische Invarianz' des magnetischen Bahnmomentes geladener Teilchen," Z. Naturforsch. **12A**, 844 (1957); see also R. Kulsrud, "Adiabatic Invariant of Harmonic Oscillator," Phys. Rev. **106**, 205 (1957).
2. L. Spitzer, Physics of Fully Ionized Gases. Interscience Publishers, New York (1956).
3. M. N. Rosenbluth and C. L. Longmire, "Stability of Plasma Confined by Magnetic Fields," Ann. Phys. **1**, 120 (1957).
4. G. F. Chew, M. L. Goldberger, and F. E. Low, "An Adiabatic Invariant for Motion Along the Magnetic Lines of Force" (September 1955), Los Alamos Report LA-2055 T-767.

HYDROMAGNETIC BASIS FOR TREATMENT OF PLASMAS*

The standard kinetic theory derivation of the hydrodynamic equations—and of their magnetohydrodynamic counterparts as well —starts from the assumption that collisions are so frequent as to keep the velocity distribution close to Maxwellian. Under these conditions one expands the deviation of the distribution function from the Maxwellian form and derives the equations in the manner demonstrated by Enskog. The question arises if one can expect these equations to be valid for plasmas in which effective collsions are so infrequent as to be completely negligible. We shall see below that a large part of the structure of magnetohydrodynamics is quite independent of any assumption concerning collisions. There remains, however, some doubt concerning a part of the theory, where frequent collisions are indeed essential to the derivation given by Enskog. The present paper proposes a different approach in which the Debye length and the Larmor radius rather than the mean free path of the electrons are considered to be small.

The kinetic theory description of a plasma can be based on the Boltzmann equation

$$\frac{\partial f}{\partial t} + \boldsymbol{v} \cdot \nabla f + \frac{e}{m}(\boldsymbol{E} + \boldsymbol{v} \times \boldsymbol{B}) \cdot \nabla_v f = 0 \qquad (1)$$

where one regards $\boldsymbol{E}$ and $\boldsymbol{B}$ as the macroscopic fields, neglects the collision terms, and does not worry about how to separate macroscopic fields from fluctuating ones. The macroscopic fields are created by the electric currents and charge densities and they obey Maxwell's equations. It is usually assumed that

$$\boldsymbol{E} + \boldsymbol{u} \times \boldsymbol{B} = 0 \qquad (2)$$

where $\boldsymbol{u}$ stands for the macroscopic velocity of the plasma. This equation may be interpreted as saying that the fluid moves with the electric field

* This discussion is based on the symposium talk by M. Rosenbluth.

drift velocity. In conjunction with Maxwell's equation

$$\frac{\partial \boldsymbol{B}}{\partial t} = -\nabla \times \boldsymbol{E} \tag{3}$$

Eq. (2) also implies that the magnetic field lines and the particles of the fluid are interlocked so that they move together.

By taking zero and first-order moments of the Boltzmann equation in velocity space one obtains the equations

$$\frac{\partial \rho}{\partial t} + \nabla\,(\rho \boldsymbol{u}) = 0 \tag{4}$$

$$\rho\left(\frac{\partial \boldsymbol{u}}{\partial t} + (\boldsymbol{u}\cdot\nabla)\,\boldsymbol{u}\right) + \nabla\,\mathbf{P} = j \times \boldsymbol{B} \tag{5}$$

It should be noted that $\mathbf{P}$ is a tensor, whereas in magnetohydrodynamics one customarily assumes that the pressure is a scalar. Except for this difference the equations of continuity and of momentum or pressure balance are therefore exact consequences of kinetic theory. The energy balance equation of ordinary hydrodynamics follows if one takes the v^2 moment of the Boltzmann equation. By this procedure one unfortunately introduces third moments of the distribution function, the components of the heat flow vector. For ordinary fluids one can make use of the nearly Maxwellian form of the distribution function maintained by the collisions and relate the heat flow to the temperature gradient, so that the system of equations is closed. In addition the heat flow is often so small that it can be ignored, and, in that case, one is led to the entropy conservation equation

$$\frac{d}{dt}\,(p\rho^{-\gamma}) = 0 \tag{6}$$

which states that the pressure varies by an adiabatic law. For plasmas the heat flow term prevents the equations from forming a closed system unless one arbitrarily sets it equal to zero. This procedure leads to the no-heat-flow equations in which the components of the pressure tensor parallel and perpendicular to the magnetic field lines vary by separate adiabatic laws.[1]

$$\frac{d}{dt}\left(\frac{P_{\parallel} B^2}{\rho}\right) = 0 \tag{7a}$$

$$\frac{d}{dt}\left(\frac{P_{\perp}}{\rho B}\right) = 0 \tag{7b}$$

This double adiabatic hypothesis is rather different from the single one given in Eq. (6) and adoption of one or the other would certainly lead to different results. In particular, we shall consider the important question of whether some equilibrium situation is stable against small perturbations. One convenient way of treating this problem is to calculate the change in energy which results from a small perturbation. This method leads to a variational principle which was first formulated by Frieman, Kruskal, Kulsrud, and Bernstein.[2]

One finds rather different criteria depending on which law one uses. The equilibrium seems to be considerably more stable if the double adiabatic hypothesis is assumed to be correct. Since there appears to be no very good a priori reason, however, for believing either the single or double adiabatic hypothesis, it seems worth while to try to solve the Boltzmann equation directly.

Let us then consider an equilibrium situation where the distribution function $f_0(\boldsymbol{r},\boldsymbol{v})$ is known and where we introduce a small perturbation. The terms in the Boltzmann equation that are linear in the perturbation give rise to the equation

$$\frac{\partial f_1}{\partial t} + \boldsymbol{v}\cdot\nabla f_1 + \frac{e}{m}(\boldsymbol{E}_0 + \boldsymbol{v}\times\boldsymbol{B}_0)\cdot\nabla_v f_1 = -\frac{e}{m}(\boldsymbol{E}_1 + \boldsymbol{v}\times\boldsymbol{B}_1)\cdot\nabla_v f_0 \tag{8}$$

On the left-hand side we have the terms which are linear in the perturbed distribution function f_1 acted on by the zero order fields and on the right-hand side the zero order equilibrium distribution acted on by the perturbed fields. The left-hand side of Eq. (8) is the total time derivative of f_1 following the unperturbed motion of particles in the six-dimensional space of $\boldsymbol{r}$ and $\boldsymbol{v}$. This observation permits one to write down the solution of Eq. (8).

$$f_1(\boldsymbol{r},\boldsymbol{v},t) = -\frac{e}{m}\int_0^t (\boldsymbol{E}_1 + \boldsymbol{v}'\times\boldsymbol{B}_1)\cdot\nabla_v f_0(\boldsymbol{r}',\dot{\boldsymbol{v}}')dt' + f_1(\boldsymbol{r}_0,\boldsymbol{v}_0,0) \tag{9}$$

It is essential to remember that this formulation presupposes that one knows the particle orbits in the unperturbed field $(\boldsymbol{E}_0,\boldsymbol{B}_0)$ because the initial value of f_1 and the terms of the integrand must be taken at the starting point $\boldsymbol{r}_0,\boldsymbol{v}_0$ and at the "in-between" points $\boldsymbol{r}',\boldsymbol{v}'$ of the path in phase space which at the time t passes through the point $\boldsymbol{r},\boldsymbol{v}$. Since the calcula-

tion of orbits is fairly well developed, Eq. (9) seems to offer a convenient method for approaching the problem.

At this point of the development one obviously would like to get rid of the distribution function in favor of macroscopic concepts. That can be achieved in a fairly straightforward way, namely, by taking appropriate moments of Eq. (9) in velocity space to get such quantities as densities, current, pressure, or whatever is needed to yield a complete set of equations.

To clarify this procedure a little, let us briefly discuss a slightly different problem—that of plasma oscillations—which can be solved by applying Eq. (9).

Let us consider the simplest case where one starts with space uniformly filled with an ionized gas at constant pressure but without magnetic fields. The zero-order distribution function is $f_0 = C\, e^{-mv^2/2kT}$. Since there are no fields in zero order the orbits are very simple; the velocity remains constant and, consequently, $\boldsymbol{r}(t') = \boldsymbol{r}(t) + \boldsymbol{v}\,(t' - t)$. We consider only longitudinal plasma oscillations with a field that can be obtained from a scalar potential assumed to be of the form

$$\phi(\boldsymbol{r}, t) = \phi_{\boldsymbol{k}}(t) e^{i(\boldsymbol{k}\cdot\boldsymbol{r})}$$

Then, of course, the electric field will be $\boldsymbol{E} = i\,\boldsymbol{k}\,\phi$. Substitution into Eq. (9) leads to the equation

$$f_1(\boldsymbol{r}, \boldsymbol{v}, t) = -i\frac{e}{kT}\int_0^t (\boldsymbol{k}\cdot\boldsymbol{v})\,\phi(r', t')\, f_0\, dt' + f_1(\boldsymbol{r}_0, \boldsymbol{v}, 0) \qquad (10)$$

Now, as outlined above, we get rid of the distribution function in favor of a macroscopic quantity which here clearly should be the charge density so that we can make use of the fact that

$$\nabla\cdot\boldsymbol{E} = -4\pi\rho = -k^2\phi \qquad (11)$$

We therefore multiply by e and integrate over all velocities which results in the integral equation

$$\phi_{\boldsymbol{k}}(t) = \frac{4\pi ne^2}{m}\int_0^t \phi_{\boldsymbol{k}}(t')(t' - t)e^{-\frac{kT}{2m}k^2(t'-t)^2}\, dt' + \qquad (12)$$

a term which results from the initial distribution $f_1(r_0,v,0)$. Since $\boldsymbol{r}_0 = \boldsymbol{r} - \boldsymbol{v}t$, the quantity $f_1(r_0,v,0)$ will oscillate like $e^{-i(\boldsymbol{k}\cdot\boldsymbol{v})t}$ and its inte-

gral over velocity space will for sufficiently large t go to zero about as the Gaussian

$$e^{-\frac{kT}{2m}\kappa^2 t^2}$$

Thus one obtains an integral equation relating the field at time t to that at time t' through a displacement kernel, i.e., a kernel which depends only on the difference $(t' - t)$. Since this time difference occurs in the equation because of the way in which the orbits enter the consideration, equations of this structure will be typical of any plasma problem.

The way to solve Eq. (12) is by a Laplace transform where one can use the well-known convolution theorem. In general, if one is interested in stability problems one has to make sure there are no poles of the transform to the right of the imaginary axis, but we shall not go further into this part of the discussion here.

If one restricts the analysis to large values of t, one finds asymptotic solutions of Eq. (12) of the form e^{pt} where p is obtained from an eigenvalue equation. The results obtained in this manner agree with those of Landau.[3]

In the limit where the Gaussian term in the integral equation would tend to one, one obtains $p = i\omega_0$, where $\omega_0 = \sqrt{4\pi ne^2/m}$ is the plasma frequency. On the other hand with the Gaussian present it is rather easy to show that p cannot be purely imaginary but rather of the form $p = -\alpha + i\omega$ which signifies a damped oscillation. The physical meaning of this damping is rather clear from the integral equation formulation. The velocity spread due to the thermal motion gradually causes the particles to come back at the wrong phase so that the contribution from very long previous times gets smeared out; this smearing out leads to the damping. It seems likely that such damping may be expected to be characteristic of any plasma problem.

In the somewhat more complex case where the plasma is in a uniform magnetic field the orbits become slightly more complicated, but one can still carry out the velocity integrals. The resulting dispersion relations show that magnetohydrodynamic sound waves suffer damping of the same character as found in the preceding analysis.

Let us return to the problem of magnetohydrodynamic stability. Both the plasma distribution and the electromagnetic field of an equilibrium configuration are in general more complicated than those in the preceding discussion. Since these complications make it impossible to write down closed expressions for the orbits, some sort of an expansion procedure will have to be used. The one which appears to be relevant is based on the as-

sumption that the magnetic field varies only by a small amount between two points which are one Larmor radius apart. For such fields there are well-known methods for expanding the orbits in powers of a parameter, η, which is the Larmor radius divided by some characteristic distance in the field. The zero-order term of this expansion is essentially the orbit in a homogeneous magnetic field. As a particle spirals along a magnetic field line, its energy remains constant. However, the partition of energy between the parallel and the perpendicular components of the motion will change depending upon the magnetic field strength. As discussed in some detail in the chapter by Chandrasekhar, the quantity $W_\perp / B$ is an adiabatic invariant and remains nearly constant.

The first-order corrections to the orbits are given by such well-known drifts as

$$\frac{W_\perp}{eB^3} \boldsymbol{B} \times \nabla B$$

and others which can be found in standard texts.[4]

In addition to the orbits we also have to expand the undisturbed distribution function. Let us consider the case where the zero-order distribution function is locally isotropic in velocity space but varying as one moves from one magnetic field line to another, so that it can be written in the form $F(v^2,\boldsymbol{r})$. One could generalize the discussion by assuming an initially anisotropic distibution function $F(v^2, v_{\|}{}^2, \boldsymbol{r})$ with different components $p_\perp$ and $p_\|$ of the pressure tensor, but for our discussion this is not necessary.

A plasma will in general carry electric currents. In the zero-order isotropic distribution function currents are absent, but one can easily add a first-order correction to account for a current density $\boldsymbol{j}$. The resulting distribution function is

$$f_0 = F(v^2, \boldsymbol{r}) \left(1 + \frac{e}{m} \frac{\boldsymbol{v} \cdot \boldsymbol{j}}{p} \right) \tag{13}$$

Inserting the expansions for the orbits and for the distribution function one can expand Eq. (9). We notice that the zero-order term in $\nabla_v f_0$ points in direction of the velocity $\boldsymbol{v}'$ and its dot product with the Lorentz force $\boldsymbol{v}' \times \boldsymbol{B}$ therefore drops out of the integrand.

Following the method of solution suggested earlier in this paper one has to make a choice of macroscopic variables which will yield the correct number of moment relations to close the system of equations. It is convenient to regard the components of $\boldsymbol{E}_1$ as these variables for the reason that one can make use of the relation between electric field and charge

density to derive moment relations, and that one can always obtain the magnetic field $\boldsymbol{B}_1$ from $\boldsymbol{E}_1$ by applying Eq. (3).

The zero-order velocity $\boldsymbol{v}$ which occurs in the non-vanishing term $(\boldsymbol{E}_1 \cdot \boldsymbol{v})$ of the integrand in Eq. (9) is essentially constant along the lines of the field $\boldsymbol{B}_0$ with a Larmor precession in the perpendicular direction. The contribution of the electric field component perpendicular to $\boldsymbol{B}_0$ therefore tends to average out since it is multiplied by the oscillating velocity perpendicular to the field. A more careful analysis shows that a contribution remains in the next higher order. However, the component of $\boldsymbol{E}_1$ parallel to the magnetic field will give rise to a zero-order term.

The arguments which will be presented below are aimed at obtaining some fairly general conclusions which can be based on order of magnitude considerations rather than on algebraic detail. One can estimate the order of magnitude of that part of the integral in Eq. (9) which matters in obtaining moments, by inspecting Eq. (12) which resulted from the simple but in many respects similar problem of plasma oscillations. The Gaussian factor in Eq. (12) indicates that contributions from times sufficiently far back are damped out and lost to the integral. The damping time is the ratio of a distance λ which is typical of the structure of the fields [in Eq. (12) λ is $1/k$] to the velocity spread of the unperturbed distribution. Therefore the order of magnitude of the part of f_1 that matters is

$$f_1 \sim \frac{e}{m} (E_1 + vB_1) \frac{\lambda}{v^2} f_0 \tag{14}$$

By previous arguments, B_1 and $E_{1_\perp}$ drop out of the lowest order, therefore

$$f_1 \sim \frac{e}{m} E_{1_\parallel} \frac{\lambda}{v^2} f_0$$

If one performs the integration in velocity space to obtain this perturbed charge density and applies

$$4\pi\rho_1 = \nabla \cdot \boldsymbol{E}_1 \sim E_1/\lambda$$

one is led to a relation

$$E_{1_\parallel} \sim \left(\frac{\lambda_D}{\lambda}\right)^2 E_1$$

where λ_D stands for the Debye distance. Now by the assumption which underlies the expansion procedure λ is large compared to the Larmor radius which in turn is generally large compared to the Debye lengths. From this one can conclude that $E_{1_\parallel}$ is smaller than $E_{1_\perp}$ by a factor of the

order η^2 and one is therefore justified to set $E_{1_{||}} = 0$. This leaves no contributions to f_1 which result from the zero-order terms of the expansions made for the orbits and the distribution function. The order of the first non-vanishing contribution to f_1 is therefore obtained by multiplying the right-hand side of Eq. (14) by η. Dropping E_1 because it is of the same order as vB_1 leads to

$$f_1 \sim \frac{eB_1}{mv}\lambda\eta f_0 \sim \frac{B_1}{B_0} f_0$$

The pressure tensor that we calculate by taking appropriate moments of f_1 will be of zero order in the parameter η; hence, the pressure will not, for example, contain the electric charge. Substituting the pressure into Eq. (5) which, as pointed out, is exact, one is led to an equation in which the electric charge does not occur explicitly. This is, of course, just the classical magnetohydrodynamic formulation; it would appear, therefore, that this is as far as we have to carry the expansion to recover the analogue of the magnetohydrodynamic theory.

This then is the prescription. One chooses the two components of the electric field $\boldsymbol{E}_1$ perpendicular to the magnetic field as the variables; one calculates f_1 to the order η by keeping first-order terms in f_0; then one calculates the perturbed pressure tensor and the perturbed velocity, substitutes them into Eq. (5), uses Maxwell's equation to eliminate j_1 and $\boldsymbol{B}_1$ in terms of $\boldsymbol{E}_1$, and one finally winds up with a macroscopic equation for $\boldsymbol{E}_1$ which looks a good deal like Eq. (2).

In fact one can go a little further and construct a variational principle for the energy completely analogous with the magnetohydrodynamic variational principle and use that to determine stability.

Skipping the detail of the calculation the results are as follows: First this formulation indicates that particles in magnetic fields fall naturally into two classes. If one considers particles which orbit in some arbitrary configuration, some will have most of their energy directed along the field lines and will be able to pass through all the maxima of the magnetic fields. Other particles with less of their energy directed along the field lines will be localized by reflections between maxima of the magnetic field. In a simple configuration like the pinch geometry the first-mentioned class of particles will go round and round all the time and never get reflected. The effect of a periodic perturbation, where the electric field is alternately positive and negative, on these non-localized particles will on the average cancel.

On the other hand, particles which are reflected and confined to some

small region will only "see" one phase of the perturbation with no chance for cancellation. This sounds a good deal like the difference between the two points of view on what to use for the law of energy conservation. If a particle is allowed to wander up and down the field and sample all the different regions, this is analogous to the magnetohydrodynamic description that one allows sound to travel down a field line and to equalize any inequalities of pressure that may develop along a field line in the course of the perturbation. It turns out that if the field geometry is such that there are no reflected particles, which is true if

$$\boldsymbol{B} \cdot \nabla B = 0$$

then one obtains exactly the magnetohydrodynamic results. The variational principle one gets in that case can be shown to be equivalent to the magnetohydrodynamic one, which uses Eq. (6).

On the other hand, when particles are confined locally one does get differences. In particular, if somehow all particles are confined to a region which is small compared to the wave length of the perturbation so they all "see" a constant phase of the perturbation, then one gets essentially Eqs. (7), which is not surprising because obviously there is no heat flow along the lines.

In the general case where there are both localized and non-localized particles the variational principle will have a fairly complicated form, but it will always lead to results which lie between the two extreme cases which we have considered.

REFERENCES

1. G. F. Chew, M. L. Goldberger, and F. E. Low, Proc. Roy. Soc. **236,** 112 (1956).
2. E. A. Frieman, M. D. Kruskal, R. M. Kulsrud, and I. B. Bernstein, Proc. Roy. Soc. **244,** 17 (1958).
3. L. Landau, J. Phys. USRR **10,** 25 (1946).
4. Lyman Spitzer, Physics of Fully Ionized Gases. Interscience Publishers, New York (1956).

SECTION 2

CONFINEMENT AND INSTABILITIES OF A PLASMA

MECHANISM OF ION ACCELERATION BY DYNAMIC PINCH INSTABILITIES*

Pinch discharges with deuterium have led to the observation of large neutron bursts.[1] This fact which has been known for several years suggests that heating due to the dynamic pinch can produce a sufficiently high temperature to cause thermonuclear reactions. It is of great importance to ascertain whether this is, indeed, the case or whether some other mechanism causes the fusion reactions.

A series of careful measurements[2] eventually proved that the observed neutrons are *not* thermonuclear, although earlier experiments seemed to indicate that they were. The main features of the experimental arrangement which produced the data specifically discussed below follow. A 12-μf condenser was discharged through a linear tube 7.5 cm in diameter, 45 to 90 cm long, and surrounded by a metal cylinder returning the current. The inductance external to the pinch tube was about 2×10^{-7} henry. The initial voltage on the condenser and the initial deuterium pressure were varied from 30 to 50 kv and from 50 to 500 microns, respectively. Further details are given in Ref. 2.

The part of the evidence which could be interpreted as supporting the thermonuclear origin concerns the simultaneous appearance of the neutron burst all along the axis of the tube at the time of maximum compression, a quenching of the yield by impurities, and a proof that the emission originates away from the walls and from the electrodes. Not completely fitting into the picture but ruling out some other possibilities are results concerning the variation of the yield with voltage and pressure and a considerable quenching of the yield by even a weak axial magnetic field.

One crucial experiment, however, definitely ruled out the assumption of a thermonuclear origin of the neutrons. This evidence came from recoil proton tracks in nuclear emulsions placed at the two ends of the pinch

* This discussion is based on the conference report by Stirling A. Colgate, University of California Radiation Laboratory, Livermore, California, and on the preprint of an article by S.A.C. and his associates which has been submitted to the *Physical Review.*

tube. The lengths of these tracks are a measure of the energy of the neutrons causing the recoil protons. If the neutrons came from a thermonuclear reaction they would be isotropic in space in regard to their energy. The histogram of tracks presented in Fig. 1 shows that the neutrons

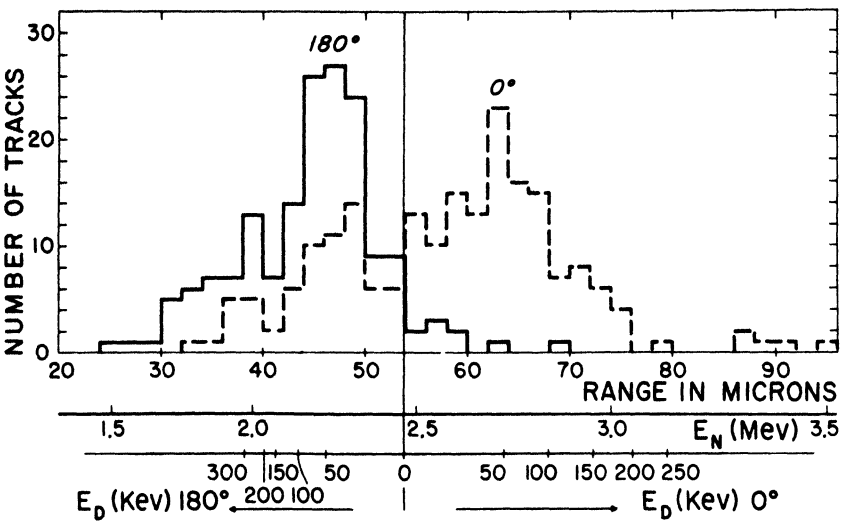

FIG. 1. Histogram of recoil proton tracks

emitted at 0° and 180° to the applied electric field have energies respectively above and below the distribution which one would expect from a thermonuclear reaction. This energy shift corresponds to 50 kev deuterons moving in direction of the applied electric field and reacting with deuterons at rest.

An attempt will be made to demonstrate in an intuitive fashion how an instability which has grown beyond the linear small-perturbation limit can accelerate ions to high energies. The above results on neutrons from the pinch will be interpreted in terms of the $m = 0$ or sausage mode of instability. This by no means exhausts all possibilities but indicates the kind of thinking that probably must be applied to account for the observed neutrons.

The deformations of the sausage type derive their name from their similarity to a string of sausages with constrictions where the individual ones are held together. The designation $m = 0$ indicates the absence of a variation with the angle around the axis. At the time when the ionized deuterium is compressed about 60- to 100-fold it is surrounded by a strong

magnetic field. The magnetic pressure which causes the pinch is inversely proportional to the square of the radius. Any small constriction which may be present due to random fluctuations will therefore give rise to a more rapid inward acceleration at the narrowest point and thereby cause an exponential build-up of the constriction.

Ripples which contain small wave-length components will initially grow most rapidly but there appears to be a non-linear coupling between neighboring constrictions which will make them coalesce. Only those constrictions which are of the order of one or two radii apart will remain separate.

The manner in which these instabilities grow after non-linear effects set in is quite complicated. For the considerations to be made one is, however, really only interested in some kind of average behavior. Roughly speaking, the inward velocity stops growing in an exponential fashion when it catches up with the speed of the shock which the magnetic pressure is able to send into the plasma. From this argument one can estimate that inward velocity to be about

$$-\dot{r} = \sqrt{B^2/8\pi\rho} = \frac{1}{10\sqrt{2\pi\rho}}\frac{I}{r} \tag{1}$$

If the plasma has a radius r which varies along the length z of the tube the inductance of a pinch discharge is given by

$$L = 2 \times 10^{-9} \int ln\left(\frac{R}{r}\right) dz \tag{2}$$

where R is the radius of the metallic conductor on the outside. At a section where a neck is forming one can locally obtain large values of dL/dt and correspondingly large voltages across the instability

$$V = I\frac{dL}{dt} = 2 \times 10^{-9} I \int \frac{-\dot{r}}{r} dz \tag{3}$$

The inductance of the entire pinch tube is fairly large and the current I is therefore quite steady so that one can ignore the local contribution to the voltage arising from the rate of change of the current. Another way to derive the expression in Eq. (3) is based on the theorem that in a moving conductor, $\boldsymbol{E} = -\boldsymbol{v} \times \boldsymbol{B}$.

The integrand in Eq. (3) obviously has a maximum at the neck and a width Δz which is some fraction of the average radius $\bar{r}$ of the pinch.

If Eq. (1) is used at the neck where the radius has the value r_n, the expression for the voltage simplifies to

$$V = \frac{\sqrt{2} \times 10^{-10} I^2}{\sqrt{\pi \rho \bar{r}^2}} \frac{\bar{r} \Delta z}{r_n^2} \tag{4}$$

The mass per unit length is $\pi\rho(\bar{r})^2 = 1.4 \times 10^{-6}$ gm/cm when the deuterium is at an initial pressure of 170 microns. A typical value of the current at the second bounce time of the pinch when neutrons are usually observed is 150,000 amp. With these data

$$V = 2.5 \times 10^3 \frac{\bar{r} \Delta z}{r_n^2} \tag{5}$$

There seems to be no difficulty in picking reasonable values, such as $\bar{r} = 0.4$ cm, $\Delta z = 0.125$ cm, and $r_n = 0.05$ cm, which will lead to 50 kv as suggested by the data on recoil protons.

The deuterons in the surface layer separating the plasma from the magnetic field will be accelerated to 50 kev in the direction of the applied electric field. However, if the Larmor radii which they acquire when they enter the magnetic field are shorter than the width of the gap they will be turned back. This imposes another condition which agrees with the lengths picked in the previous paragraph.

On the basis that there are about 50 such instabilities along the length of the discharge, the neutron yield per burst was estimated at about 10^7 to 10^8 in agreement with observed numbers.

It seems surprising at first that in a discharge there could be large voltage spikes adding up to many times the externally applied voltage. Such a structure of the field implies that the tube is essentially a magnetic bottle within which large currents circulate. These currents are quite isolated from the external circuit and are similar to the observed secondary current sheath which is discussed in the article by Karr. Under similar conditions but when the instabilities are relatively weak a voltage spike can be observed on the outside. The larger voltages, however, which occur when neutrons are observed apparently short the external conductor and make the inside glass wall a conducting surface.

If an axial magnetic field is applied before starting the pinch it gets trapped and compressed along with the plasma. This causes it to increase as $(1/r)^2$ and theory shows that there will be a certain radius below which the axial field B_z stabilizes the $m = 0$ instabilities. For an initial field of 100 gauss this occurs at a radius of about 0.05 cm. By increasing B_z to values where the radius for stabilization becomes larger, one very definitely cuts down the observed neutron yield.

When disturbances of the $m = 0$ type are stabilized, it becomes more difficult to distinguish if neutrons which are observed are due to an acceleration mechanism or to thermonuclear reactions, because both produce isotropic distributions. Accelerations can result from random collisions with moving magnetic field inhomogeneities. A mechanism of this type was first proposed by Fermi[3] for explaining the acceleration of cosmic ray particles in interstellar space. Parker[4] who applied the same idea to the production of cosmic rays in solar flares gives the mean velocity after n Fermi-type collisions with fields moving at a speed v as $w = \sqrt{8n}\, v$.

This formula applies only if the slowing down caused by collisions with other particles is negligible. Since the effective cross section for collisions between particles, which interact by a Coulomb law, goes as the inverse square of the energy, only particles which are faster than a minimum value can build up their energy by Fermi collisions.

A moving magnetic field inhomogeneity can, for example, result from the growth of an $m = 1$ or screw-type instability. When the discharge is confined to a radius $\bar{r}$ the distance a particle would travel between Fermi collisions is about $2\pi\bar{r}$. The slowing-down length should not be shorter than this distance. Using a slowing-down cross section for deuterium of $\sigma = 6 \times 10^{-19}/E^2$ cm^2 with E expressed in kev and a value of the radius $\bar{r} = 0.4$ cm as in the previous example, the "injection energy" is about 1 kev.

The magnetic field moves with the Alfvén velocity which turns out to be about the same as the speed of a 200-ev deuteron. A deuteron can therefore acquire somewhat more than the injection energy in a single collision. As in Parker's case electrons which are slowed down more effectively would require a much higher injection energy and the Fermi mechanism cannot get started for them.

To obtain a large fusion reaction yield the deuterons must be accelerated to at least 40 kev, which requires 25 collisions. The time required for this is $w\, 2\pi r/4v^2 = 0.6$ μsec which though somewhat longer than the observed 0.3 μsec is of the correct order of magnitude.

REFERENCES

1. I. V. Kurchatov, Nucleonics **14**, 37 (1956); Los Alamos group, J. Appl. Phys. **28**, 519 (1957).
2. O. A. Anderson, W. R. Baker, S. A. Colgate, H. P. Furth, J. Ise, Jr., R. V. Pyle, R. E. Wright, Phys. Rev. **109**, 612 (1958).
3. E. Fermi, Phys. Rev. **75**, 1169 (1949); Astrophys. J. **119**, 1 (1954).
4. E. N. Parker, Phys. Rev. **107**, 830 (1957).

EXPERIMENTAL STUDIES OF THE PINCH EFFECT*

HUGH J. KARR†

INTRODUCTION

One of the devices that have been considered hopefully in the Sherwood Program as a possible basis for a thermonuclear reactor has been the plasma pinch. However, even the early observations[1] of the pinch effect in gas discharges have all indicated that the pinch discharge tends to have only a brief transient existence due to rapid breakup in various modes of deformation. Figure 1 shows a smear camera trace of a line section of a typical unstabilized, simple pinch. The camera trace shows that the discharge initially fills the tube but quickly pulls away from the tube walls and pinches, as desired. However, no sustained contraction is obtained. The discharge is observed to undergo a series of contractions and partial expansions which is then followed by a succession of turbulent waves and kinks until detail of structure is lost and breakup is complete in a few microseconds. It is apparent that this unstable behavior is an obstacle in the development of the pinch method for obtaining thermonuclear reactions even on a low-level laboratory scale. Because of this effect, much of the effort in the pinch program has been devoted to understanding plasma instabilities with the ultimate intent of their elimination or control. This report is a brief review of some of the experimental work at Los Alamos Scientific Laboratory in the pinch study program. The work to be discussed can be conveniently divided into two parts: I. Stability Studies of the Straight Pinch and II. Current Distribution Within the Pinch Discharge.

* Work performed under the auspices of the U.S. Atomic Energy Commission.

This review was compiled from results of work done at Los Alamos during the period from 1952 to 1956. In particular the contributions by L. Burkhardt, R. Lovberg, J. Mather, J. Phillips, G. Sawyer, and T. Stratton are to be cited.

† University of California, Los Alamos Scientific Laboratory, Los Alamos, New Mexico.

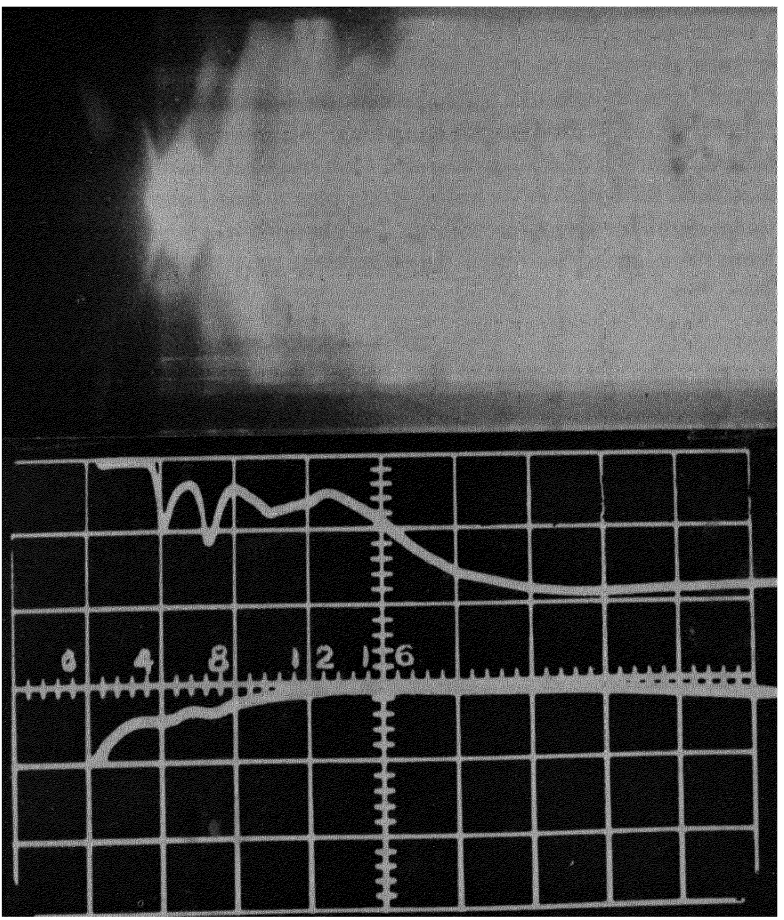

FIG. 1. Smear camera trace of pinch discharge in helium ($I_{max} = 1.1 \times 10^5$ amp., $V = 3.5$ kv, $p = 450$ micron). Oscilloscope traces show total light intensity (upper) and discharge current (lower) vs. time.

1. STABILITY STUDIES OF THE STRAIGHT PINCH WITH LONGITUDINAL MAGNETIC FIELD[2]

The general experimental approach in the study of the unstable pinch has been to detect the onset of the instability, to determine the nature or type of perturbation leading to the breakup, and to investigate parameters that correct or effect the instability with the guidance of existing theoretical predictions.

Of the several existing theoretical treatments[3,4,5] of the pinch instabilities, that of Kruskal and Tuck[3] is most adaptable to interpretation of the experimental work to be discussed here. In their analysis, the stability of a plasma cylinder against perturbations or deformations is determined from the magnetohydrodynamic equations. An infinite cylinder of plasma is assumed initially at equilibrium and each physical quantity in the equations is then set equal to its initial value plus a small perturbation term. The magnetohydrodynamic solution is obtained as a superposition of elementary solutions in which the dependent variables are functions of

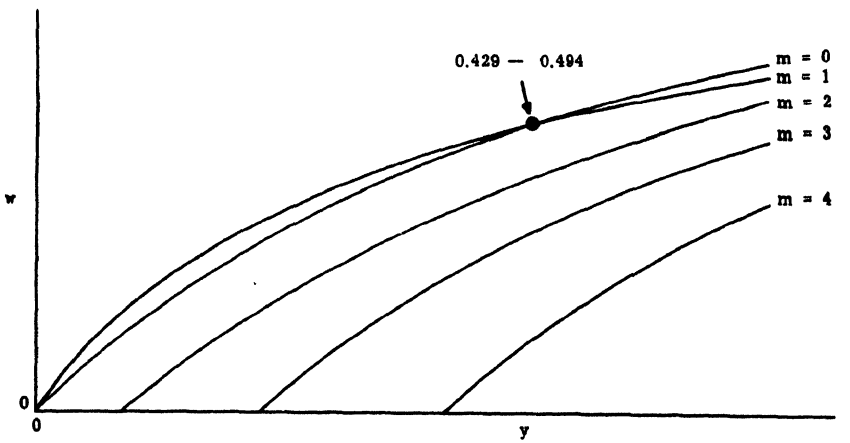

FIG. 2. Exponent growth rate vs. wave number: uniform case ($\alpha_P = \alpha_V$), purely external case ($\alpha_P = 0$).

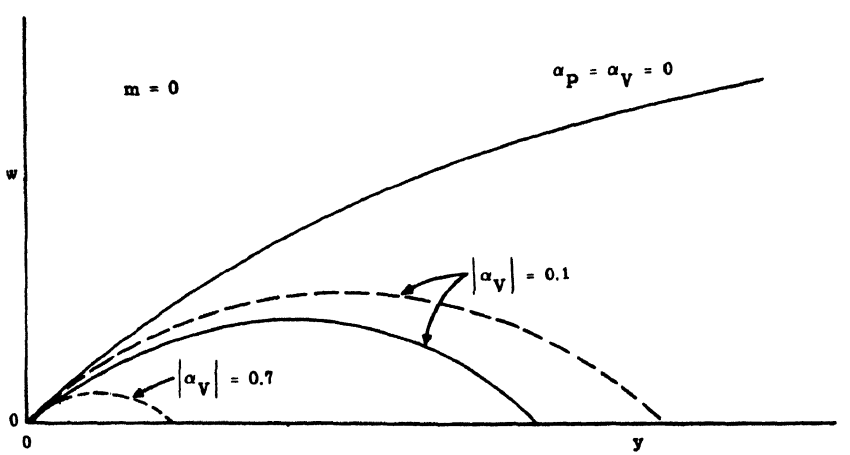

FIG. 3. Exponent growth rate vs. wave number: uniform case ($\alpha_P = \alpha_V$), purely external case ($\alpha_P = 0$).

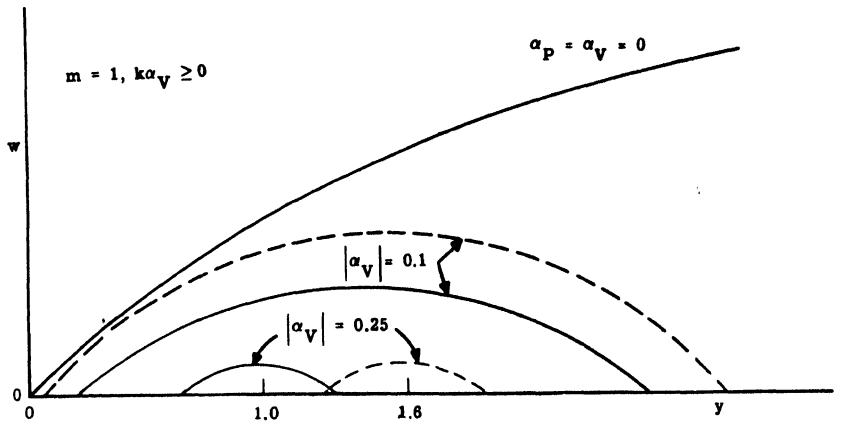

FIG. 4. Exponent growth rate vs. wave number: uniform case ($\alpha_P = \alpha_V$), purely external case ($\alpha_P = 0$).

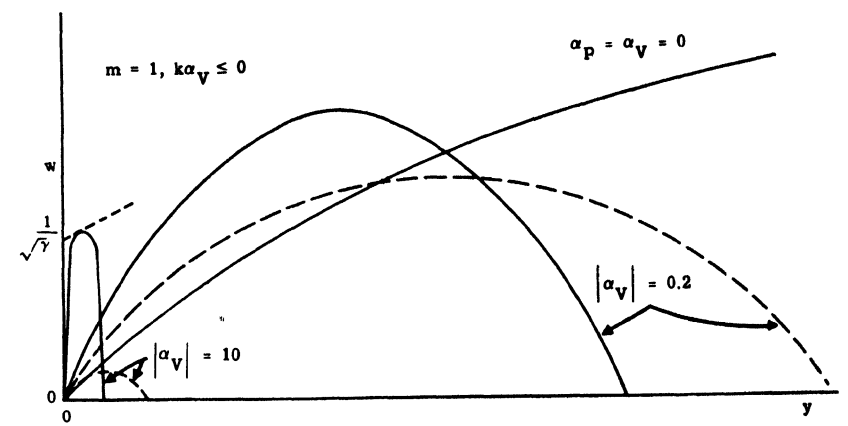

FIG. 5. Exponent growth rate vs. wave number: uniform case ($\alpha_P = \alpha_V$), purely external case ($\alpha_P = 0$).

radius multiplied by $\exp[i(m\phi + kz) + \omega t]$ where m, k, and ω are the characteristic constants of the elementary solutions. Accordingly, a particular instability is customarily identified in terms of m, the azimuthal or mode number, and k, the wave number, or more generally the wave length ($\lambda = 2\pi/k$). The value of ω, determined in the analysis, is indicative of the rate of growth of the instability. Kruskal and Tuck have examined the stabilizing effect of a longitudinal magnetic field superimposed on the azimuthal self-magnetic field characteristic of the pinch current.

Figure 2 shows the results obtained by Kruskal and Tuck for the simple, unstabilized pinch. The abscissa, $y = 2\pi r_0/\lambda$, and the ordinate, $W = r_0\,\omega/s$, both in dimensionless units, indicate the reciprocal instability wave length and relative growth rate for the instability. It is apparent from the figure that the $m = 0$ and $m = 1$ modes are the most serious instabilities of the simple pinch. The results indicate that the short wave length sausage ($m = 0$) instability grows most rapidly of all and will probably ultimately destroy the pinch.* Physically, this instability is one in which the plasma is necked off or constricted in one or more places. The local increase in magnetic field at the plasma surface within the region adjacent to the constriction gives rise to greater magnetic pressure in this area causing the constriction to increase further. This necking off causes axial flow of plasma that expands the region next to the constriction. Thus, a pattern of bulges and constrictions determined by the wave number, k, of the components of the $m = 0$ instability develops along the pinch, giving it a sausage-chain appearance. It is of interest to note that the rapid radial motion at the instability regions can generate very large local voltages due principally to the rate of change of inductance ($V = I\,dL/dt$) at the necked-off regions. Acceleration of plasma ions by these local electric fields has been invoked to account for the instability neutron production[6] observed early in the history of the pinch program. This effect is described by Colgate in this volume. However, the Kruskal and Tuck theory indicates that a longitudinal magnetic field (B_z field) will stabilize the pinch against these $m = 0$ breakups. This theoretical result is shown in Fig. 3, in which $\alpha_V = B_V/B_\theta$ and $\alpha_P = B_P/B_\theta$ where B_V and B_P are the values of B_z outside and inside the plasma surface respectively and B_θ is the azimuthal flux density at the plasma surface. For the case of uniform longitudinal magnetic field ($\alpha_P = \alpha_V$), the Kruskal-Tuck results indicate stability against the $m = 0$ mode for $\alpha_P = 1/\sqrt{2}$. The theoretical prediction of the suppression of the $m = 0$ instability by the B_z magnetic field was verified by the first set of experiments described later in this report.

The $m = 1$ mode has the physical appearance of a helix. This instability develops at a local displacement or bend of the discharge. The magnetic flux is concentrated at the concave side of the bend and attenuated on the convex side. The resulting difference in magnetic pressure, $B_z^2/8\pi$,

* The curves in Fi . 2 indicate that $w \to \infty$ as $y \to \infty$ limplying instantaneous breakup of the pinch by extremely short wave length perturbations. However, the theory is not valid for wave lengths smaller than a limiting value which is probably of the order of a Larmor radius for the plasma ions in the pinch magnetic field.

causes further growth of the deformation. The effect of a B_z field on the $m = 1$ instability is shown in Figs. 4 and 5. The helical instability theory considers two cases: (1) in which the perturbation is assumed to spiral in a direction such that the added B_z field it generates in twisting the plasma current opposes the initial B_z field ($k\alpha_v \geqq 0$), and (2) the perturbation spirals so as to aid the initial B_z field ($k\alpha_v \leqq 0$). The curves in Fig. 4 shrink toward the points on the y-axis with values 1.0 in the uniform case and 1.6 in the purely external case, disappearing at $\alpha_v = 0.266$ and $\alpha_v = 0.312$ respectively. The theory indicates that the first case can be stabilized by addition of an adequate B_z field. The second type of $m = 1$ instability is more persistent, and the long wave length $m = 1$ instability persists no matter how large the added stabilizing B_z field. The curves in Fig. 5 shrink toward the w-axis as $|\alpha_v| \to \infty$. The maximum of w approaches $1/\sqrt{\alpha}$ in the uniform case and zero in the purely external case. The second group of experiments described below investigated this $m = 1$ instability. For the higher instability modes, the theoretical results indicate stability for the uniform field case ($\alpha_P = \alpha_V$) if $(\alpha_P/\alpha_V)^2 > 1/(m-1)$.

The Kruskal-Tuck analysis did not find any region of complete stability. The additions of the axial magnetic fields merely shift the region of instability to the larger wave lengths for $m = 1, 2, \ldots$. Earlier results[7] indicated the stabilizing effect of conducting walls on long wave length instabilities ($m \neq 0, \lambda >$ radius).

The Rosenbluth stability theory[4] combined the two effects and yielded the important conclusion that a region of complete stability exists. The combined effects produce a region of stability for a limited region of values of internal B_z field, external B_z field, ratio of pinch to external conductor radius, azimuthal B_θ field which depends on the discharge current, of course, and the gas pressure NkT. This analysis assumes a highly conducting plasma with the current confined to a thin sheath at the plasma surface. In the experimental work discussed here no attempt was made to meet the Rosenbluth theory requirements. The immediate intent was to explore the $m = 0$ and $m = 1$ instabilities in this series of measurements.

Observation of the Sausage ($m = 0$) Instability

Figure 6 illustrates the discharge system used in this experimental series. The discharge tube was pyrex glass of 6.5 cm I.D. and 30 cm between electrodes. Electrodes were of stainless steel and projected into the glass tube as indicated in the illustration. The coaxial return around the pyrex tube was also of stainless steel of 8.2 cm I.D. and $\frac{1}{16}$ in. wall

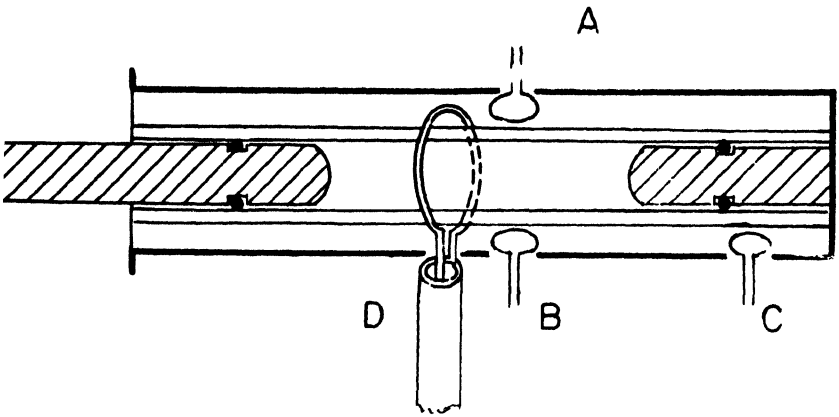

FIG. 6. Probe and loop geometry of discharge tube

thickness. A low inductance coaxial system was used to obtain maximum peak current and to obtain fast rise time of the discharge current since this tends to force the discharge away from the tube walls more quickly. A d.c. solenoid around the coaxial conductor supplied longitudinal magnetic fields up to 3000 gauss. A coaxial resistance voltage divider at the high-voltage electrode and a shielded current coil around one of the supply leads measured voltage and current. Energy was supplied by a 40 μf capacitor bank at voltages up to 20 kv (4500 joules max.). The system was switched by Type 5550 ignitrons, one for each 4 μf; ten RG-8 coaxial cables connected these to the tube feed points. The system constants were:

$$C = 40\ \mu f \qquad I_{\max} = 2.5 \times 10^5 \text{ amp}$$
$$T = 17\ \mu\text{sec} \qquad L_{\text{ext}} = 0.12\ \mu h$$

The observations of the $m = 0$ instabilities were made using an image converter camera which viewed the pinch discharge through a 1.5×3 cm hole in the side of the coaxial return conductor. While the small size of the port made observation of the sheath edges impossible at early times in the discharge process, the $m = 0$ breakup was readily seen since it occurred at the high compressions when an appreciable section of the discharge was visible through the hole.

Figure 7 shows six different instances of the sausage instability, each photograph taken at the maximum development of the sausage perturbation for a series of pressures. For these measurements the stabilizing longitudinal magnetic field was not used ($B_z = 0$). The time of formation

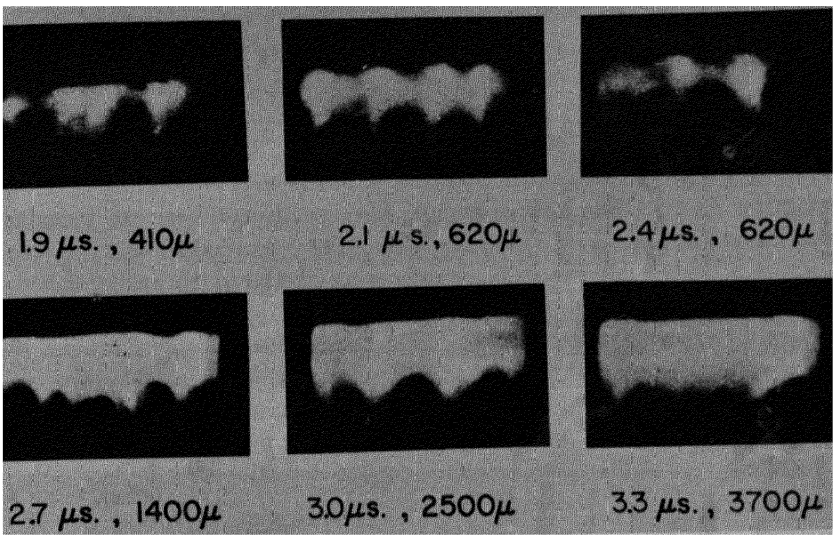

FIG. 7. Image converter pictures of deuterium discharge for $B_z = 0$ showing $m = 0$ instabilities.

measured from the initial gas breakdown is indicated and was observed to increase slowly with the initial deuterium gas pressure. The wave length of the instability remains at about 1 cm for the series of six pictures. The regular spacing of the perturbations is remarkable. The crests and troughs are visible only at the bottom of the picture because the observation port in the metal return wall masked off the upper part of the picture. Next a longitudinal magnetic field of a few hundred gauss was applied to the tube before firing the discharge. The image converter photographs were found to be highly reproducible from shot to shot. Thus, it was possible to follow the time behavior of the pinch with a series of photographs obtained by advancing the exposure delay with each shot. The $m = 0$ or sausage instabilities vanished after the addition of the B_z field and the life of the pinch was observed to increase by an appreciable fraction due essentially to the suppression of the $m = 0$ instability. Both of these results are in agreement with the Kruskal-Tuck theory predictions. The remaining instabilities which later destroyed the pinch could not be identified from the image converter photographs. These instabilities, $m = 1$ and possible higher order, should be of long wave length according to the Kruskal-Tuck theory and would tend to move the discharge off the tube axis out of view of the port.

Observation of the Helical ($m = 1$) Instability

A system of magnetic pickup loops was used to detect and identify the $m = 1$ instability. The experimental layout is illustrated in Fig. 6. The energy supply and discharge tube are the same as those used in the previous set of experiments. The pickup loops A, B, C, and D were added. A, B, and C were small electrostatically shielded coils of 50 turns on 1-mm diameter forms. These three probes were positioned between the glass and metal walls and were oriented to detect the azimuthal B_θ field produced by the discharge current. The signals were displayed on an oscilloscope without integration and their amplitude is proportional to dB_θ/dt or dI/dt where I is the discharge current. The loop D was wrapped around the glass tube in the space between the glass and stainless steel return conductor. The D-loop was, of course, coupled to the longitudinal B_z field. The output of this loop was connected to an oscilloscope through an RC integrator so that the signal amplitude was proportional to the total longitudinal flux within the area of the loop.

The longitudinal magnetic field was first introduced into the discharge tube from the solenoid winding after which the discharge was initiated. The signal obtained from the D-loop can be interpreted from the following elementary considerations. Since the discharge initially developed a highly conducting sheath of plasma at the glass tube inner wall, the B_z field within the sheath could not penetrate through the conducting layer within the time duration of the discharge and was therefore trapped within. As the sheath pinched in, the trapped field was swept in with it. A part of the remaining B_z flux originally residing in the space between the glass and the conducting wall then flowed inward past the D-loop into the region evacuated by the pinch. Therefore a net increase of flux inside the loop resulted and a rising signal was expected as the pinch moved in.

The loop signal that resulted from the expansion of the flux outside the discharge can be computed readily from the geometry of the system, assuming that all the B_z within the discharge is trapped and retained as the pinch moves in and that the flux within the conducting wall does not diffuse in appreciably during the short period of the discharge. The magnitude of the expanding B_z field at any instant is given by

$$B_{ze} = B_{z0} \frac{r_c^2 - r_g^2}{r_c^2 - r_p^2}$$

The flux increase detected by the loop is then:

$$\Delta\phi = (\pi r_c^2 - \pi r_l^2)\,(B_{z0} - B_{ze}) \tag{1}$$

where

B_{z0} = initial axial field
r_c = conductor inner radius
r_g = glass inner radius
r_p = instantaneous plasma radius
r_l = loop radius

However, when deuterium was used in the pinch discharge, a rising signal was at first obtained in agreement with that predicted by Eq. (1), but this was followed by an anomalous rise in the signal. This later rise could not be accounted for by Eq. (1) even assuming a pinch to radius zero. Figure 8 shows the loop signal along with the tube voltage wave form. The anomalous rise appears at 2.8 μsec after the initiation of the discharge. It is interesting to note that the voltage wave form here again

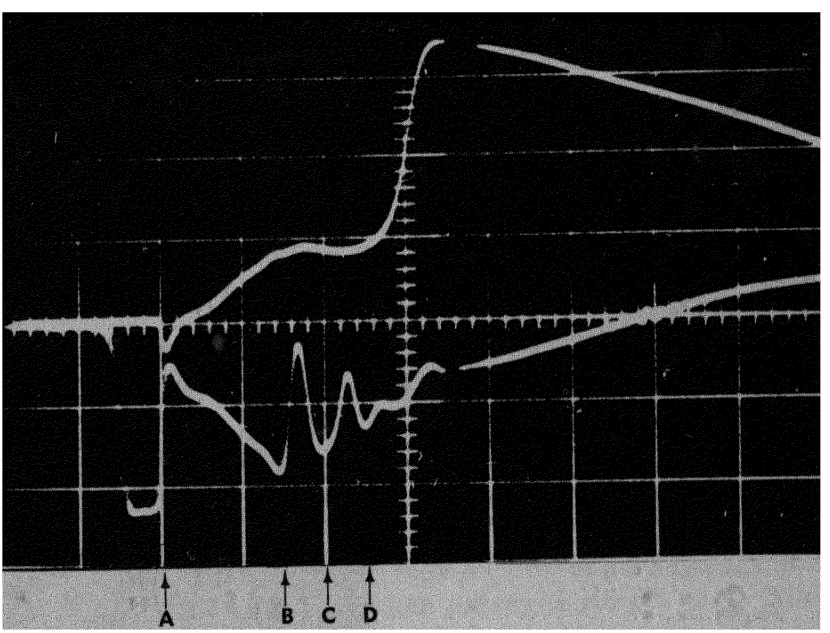

FIG. 8. Loop signal (upper curve) and tube voltage (lower curve) for D_2 pinch when $B_z = 900$ gauss.

indicates that the discharge has gone through the usual succession of pinch compressions and partial expansions before the anomalous rise began. In view of the predictions of the Kruskal-Tuck theory it was suspected that an $m = 1$ instability might be the source of the signal rise. The identification of the apparent instability was established by means of the small probe coils A, B, and C of Fig. 6. Probes A and B were positioned on opposite sides of the tube and probe C was positioned at one electrode and served to normalize the A and B signals. It is clear that as long as the pinch remains cylindrically symmetrical at the tube axis, all three probe signals will be identical and proportional to dI/dt of the gas current. However, if the current channel undergoes any lateral motion bringing it closer to one probe loop, that probe signal will increase and the other decrease. The electrode probe will detect this motion only to the extent that the inductance variation due to this motion affects the total current through the tube.

In Fig. 9, the output of the monitor probe at the electrode is displayed together with the signal from one of the discharge probes. The signals obtained from the two probes were identical for about 2 μsec in the $B_z = 0$ case and 2.8 μsec in the $B_z = 900$ gauss case. The discharge apparently maintains radial symmetry up to these times. Then an abrupt

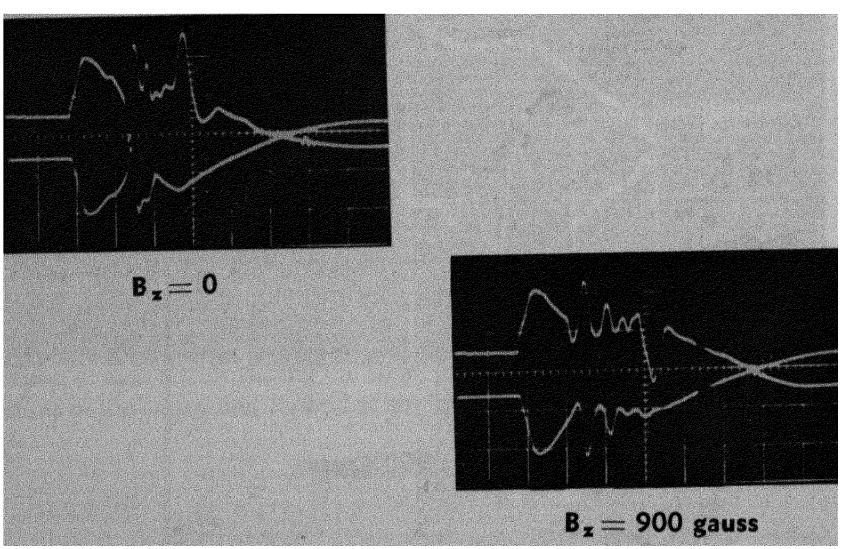

FIG. 9. Outputs from probes A (upper curve) and C (lower curve)

swing of the discharge probe signal not duplicated by the electrode probe output was observed. It should be noted that the rises and dips in the probe signals prior to this anomalous signal are due to the changing inductance of the pinch in its usual dynamic motion of successive cycles of pinching and partial expansion in response to the self-magnetic field pressure. This behavior has been analyzed by Garwin and Rosenbluth,[4] and the pinch velocities and pinch times indicated here are in good agreement with this theory. The rises and dips in the probe signals coincide with the variations in the voltage signal in Fig. 8.

In Fig. 10, the signals from the two opposed discharge probes are dis-

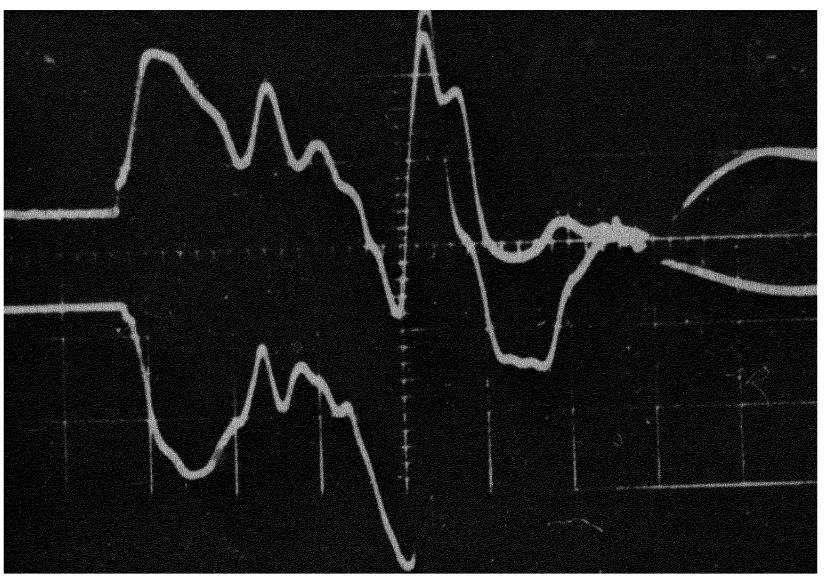

FIG. 10. Outputs from opposed probes A and B when $B_z = 1300$ gauss

played together. The signals are identical for the first 2.8 μsec and then there is an abrupt swing of opposite polarity in the two traces. This shows clearly that the instability is locally a gross sidewise motion as would be expected from either a kink or long spiral in the pinch discharge. In Fig. 11, the D-loop signal and a discharge-probe signal are displayed together. The anomalous behavior is seen to appear simultaneously in both signals. The sudden increase in B_z detected by the loop occurs at the same time that the probes indicate a sidewise motion of the pinch. Now,

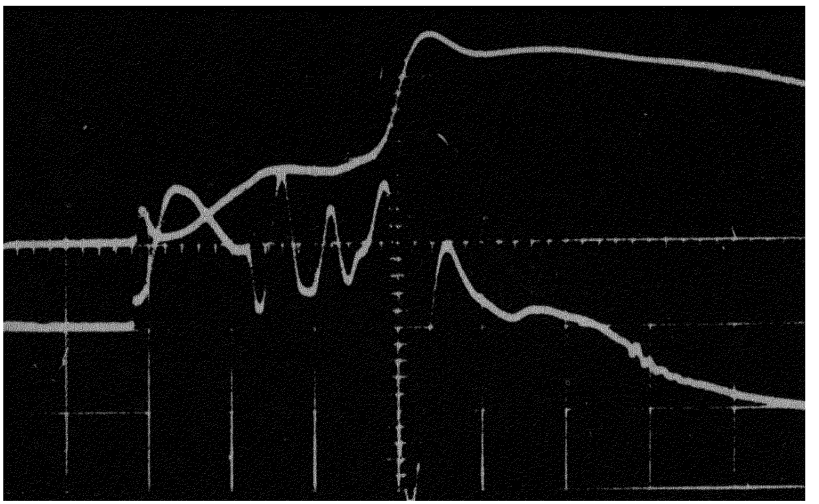

FIG. 11. Output from loop D (upper curve) compared with that from probe A (lower curve) when $B_z = 900$ gauss.

while the probe signals are consistent with either a simple kink instability in which the discharge current axis remains coplanar with the tube axis or with a long spiral motion of the discharge about the tube axis, the loop signal is consistent only with the latter. It is therefore concluded that an $m = 1$ spiral instability has begun to destroy the pinch configuration.

It should be noted that, as expected by the Kruskal-Tuck theory, the corkscrew twist develops in the direction such that the added B_z field is in the same direction at the axis as the initial B_z field, causing the rising anomalous loop signal.

II. CURRENT DISTRIBUTION WITHIN A LINEAR PINCH DISCHARGE[9]

Extension of the use of the small magnetic pickup probes to measuring magnetic fields inside the plasma discharge was first reported[10] by the Russian physicists also studying the pinch effect. Stimulated by the reported Russian success with this method, the technique was adapted at LASL and has proved a valuable diagnostic tool in determining conditions within the pinched plasma and in observing the boundary layer formation

of the pinch. Earlier methods of analyzing the behavior of the pinch discharge channel included optical measurements with the smear camera, frame camera, and image converter, magnetic field measurements by probes and loops external to the discharge, and indirect observations of the pinch motion as indicated by the effect of apparent inductance variations on the current and voltage wave forms of the discharge. These methods did not, however, give any information on the detailed current magnetic field distributions within the pinch. These limitations led to the use of the magnetic probe method in search for the answers to such questions as: Does a current sheath form at the tube wall at the start of the pinch? How thick is the current sheath if one does form? Does the radial velocity of the sheath agree with the predictions of the dynamic pinch theory?[8] Does a current continue to flow along the tube walls? What indications of instability growth are indicated by the magnetic field and current distributions?

The pinch discharge machine used in these measurements, called Columbus I″, was very similar to the device described earlier with respect to energy storage, switching by ignitrons, and coaxial tube assembly. The significant parameters of the circuit were:

Energy storage capacitor bank
—ten 7.5-μf condensers, used at 10 kilovolts (3750 joules)
Discharge tube—pyrex, 30 cm between electrodes, 7 cm I.D.
Electrodes—stainless steel
Coaxial return conductor—stainless steel, 8.2 cm I.D.
Peak current—1.5×10^5 amperes
Period of current—25 μsec
Source inductance—0.19 μh
Gas—deuterium at 600 microns

Figure 12 shows the components of the type of miniature probe used. The device consists essentially of a small coil of wire which is inserted into a slotted stainless steel tube for electrostatic shielding, and this assembly, in turn, is inserted into a quartz or glass tube to insulate it from the plasma discharge. A typical coil consists of 20 to 50 turns of No. 44 enameled wire and has a diameter of 50 to 60 mils and a mean area of about 0.001 sq. in. The coils have an inductance of about 0.3 μh and have a frequency response flat within 5 percent to 30 megacycles. The probes were used with RC integration ($RC = 310 \times 10^{-6}$ sec). A typical probe has a sensitivity of 1×10^5 to 2×10^5 gauss/volt with the value of RC indicated. The shield tubes are of non-magnetic stainless steel 0.055 in. I.D. and

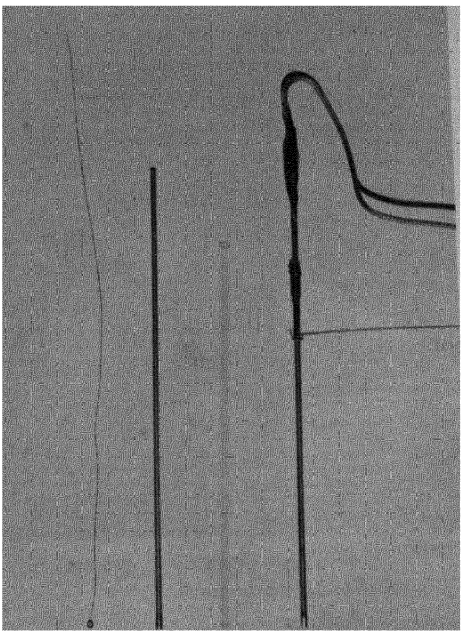

FIG. 12. Miniature probe for exploring magnetic field and current density distributions.

0.010 in. wall thickness. The end containing the coil is further thinned to 0.001 in. and slotted to admit magnetic flux without significant eddy current effects. The leads from the coil pass through the inside of the tube as a twisted pair and are brought out through a shield to a 90-Ω coaxial line. The quartz tube used to insulate the probe had an outside diameter of roughly 0.120 in.

The probe was inserted into the discharge midway between the electrodes through small holes in the metal return conductor and in the pyrex tube wall. A neoprene gasket cemented on the outer glass wall acted as a vacuum seal.

Initially there was some doubt about the use of the probes within the discharge since it was suspected that the probe might seriously disturb the system. There is evidence that the perturbation is very slight: (a) the probe is of such small diameter that its presence could change the magnetic field only slightly at any point since this field is caused by current elements spread over a relatively large region; (b) when two probes are inserted at opposite sides of the discharge and one used as a monitor at several posi-

tions which are kept fixed while the other is moved through the discharge on successive shots, no effect or variation is indicated in the monitor signal until the probes are less than ⅛ in. apart at the tube axis; (c) when one probe is moved completely through the discharge, the magnetic field detected on the far side is identical with that on the near side as a function of time, although the probe extends through the discharge; and (d) spectroscopic measurements indicate that the Si and O impurity introduced by the probe insertion is very small during the period of field distribution measurements.

Figure 13 shows measurements of the B_θ magnetic flux as a function

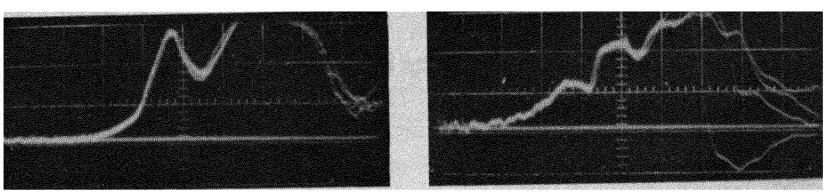

FIG. 13. Superimposed probe signals from successive discharges at a fixed radial position as a function of time.

of time at a fixed radial position within the discharge. It is found that for the first few microseconds (< 2.5 μsec) the traces on successive shots reproduce remarkably well. This fact has made it possible to correlate measurements made at different radii and to determine the complete magnetic field distribution within the pinch at any time until instabilities set in strongly and irreproducibility makes further mapping impractical.

Using the miniature probes, a magnetic field distribution was measured for a simple pinch without the stabilizing B_z field. The probe output after integration was proportional to $B_\theta(t)$. The magnitude of the field as a function of r and t was then determined using the probe calibration factor of 1.5×10^5 gauss/volt for the RC value. Care was exercised in maintaining the probe orientation so that the plane of the coil was always perpendicular to the B_θ flux, and so that the probe moved along a diameter of the discharge tube.

The current density distribution is then determined from Maxwell's equation. Since cylindrical symmetry was indicated in the results of the probe measurements, the longitudinal discharge current density can be obtained from Maxwell's equation expressed in cylindrical coordinates:

$$\frac{1}{r}\frac{\partial r B_\theta}{\partial r} - \frac{\partial B_r}{\partial \theta} = 4\pi j_z$$

Due to the cylindrical symmetry, $B_r = 0$. Thus,

$$j_z = \frac{1}{4\pi}\left(\frac{B_\theta}{r} + \frac{\partial B_\theta}{\partial r}\right)$$

The probe signals at successive radial positions in the discharge give B_θ as a function of r directly and j_z can then readily be determined for any selected time.

Figures 14 and 15 show current distributions obtained in this way for the simple pinch. A current sheath forms at the tube wall as predicted by the dynamic pinch theory,[8] and the sheath moves in radially toward the tube axis as predicted by this theory. The time of the first pinch is 1.8 μsec which agrees well with the theoretically predicted value if the effect of the external inductance is included. The plasma sheath is observed to thicken

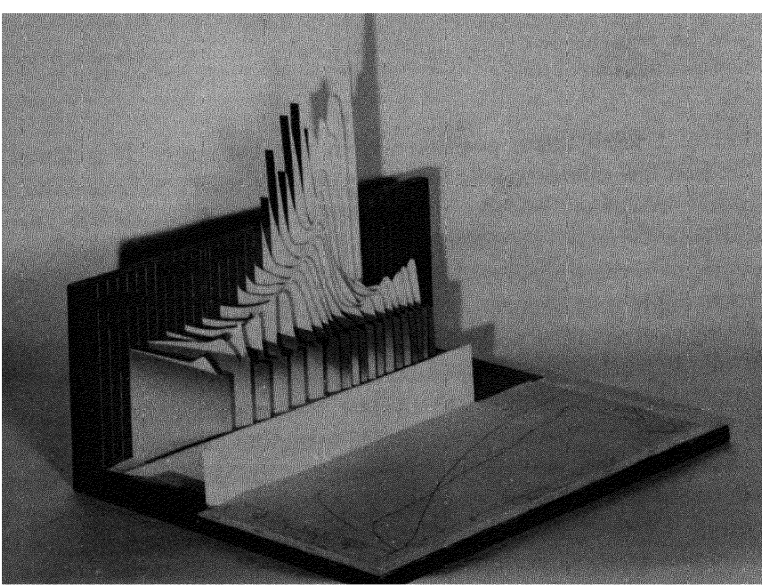

FIG. 14. Current density distribution as function of time and radius for a simple pinch without stabilizing magnetic field. Current density magnitude is indicated vertically, time to the right, and radial position is indicated from the vertical black mounting board as axis of the discharge.

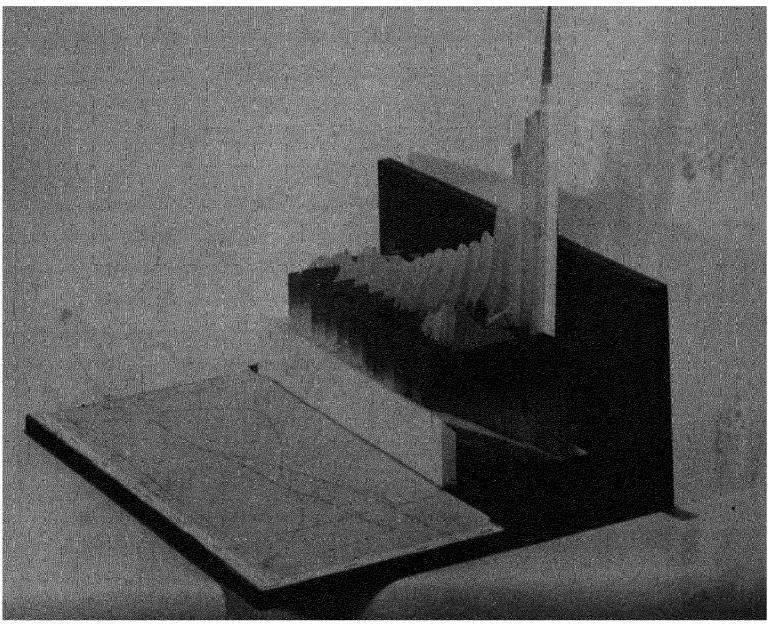

FIG. 15. Rear view of Fig. 14

as the pinch moves in and current density grows in the inner region of the pinch because of the finite conductivity of the plasma. It should also be noted that a reverse current develops at the wall during the first microsecond of the discharge. This "negative" current at the wall persists during the remainder of the pinch discharge. When the initial current sheath approaches the axis of the tube at about 1.7 μsec, a second positive sheath is observed to form near the tube walls. The voltage across the tube has increased during the pinch process of the first sheath due to the $I\dot{L} + L\dot{I}$ variations. Evidently not all the gas was ionized during the first sheath formation and the increased voltage has broken down the residual gas and formed a second sheath. At about 2 μsec, a second reverse current region between the two sheaths is observed.

Figure 16 shows a contour plot of the current distribution as a function of radius and time. At about 2 μsec, a rather remarkable current distribution of four layers is indicated, alternately in opposite directions within the discharge. After about 2.5 μsec, instabilities destroy the distribution and random, turbulent behavior takes over. The dark line on Fig. 16 is a plot of the radial profile of the emitted light of the discharge as observed

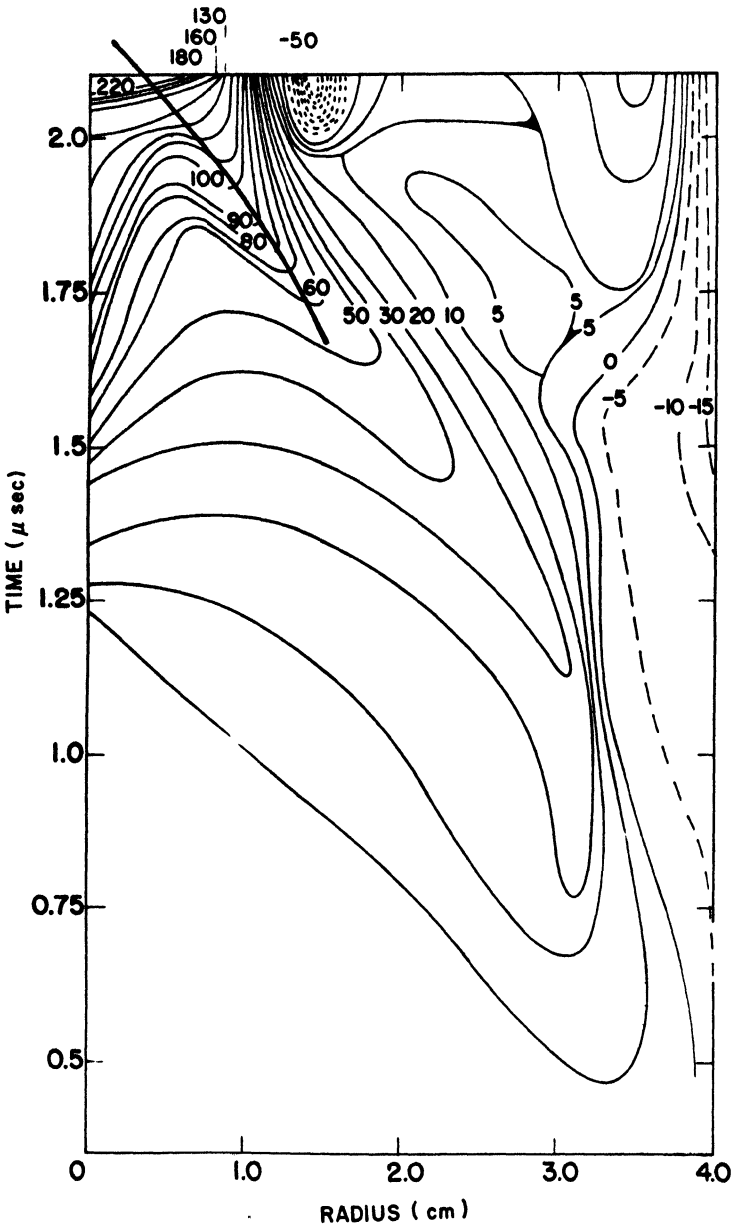

FIG. 16. Contour plot of current density as function of time and radius with no longitudinal magnetic field.

with a smear camera. The agreement between the sheath motion indicated by the light and that of the probe data is very good.

The origin of the reverse current observed in the discharge can be explained qualitatively either as a rarefaction of an Alfvén wave, or in terms of the equivalent description of particle orbit theory. For example, the development of density gradients within the discharge volume gives rise to magnetization currents arising from imperfect Larmor orbit cancellation on an atomic scale. The plasma density, N, usually falls off with increasing radius, and the resulting magnetization current is in the positive current direction. However, in a region where the plasma density increases with radius, as must be the case somewhere in the region between the first and second current sheaths, a negative or reverse current results.

REFERENCES

1. A. A. Ware, Trans. Roy. Soc. (London) **A243,** 863 (1951); S. W. Cousins and A. A. Ware, Proc. Phys. Soc. (London) **64A,** 159 (1951); Artsimovich, Adrianov, Bazilevskaya, Prokhorov, Filippov, Atomnaya Energiya **3,** 76 (1956); I. Kurchatov, reprinted in Nucleonics **14,** 36 (1956); L. Burkhardt, R. Dunaway, J. Mather, J. Phillips, G. Sawyer, T. Stratton, E. Stovall, and J. Tuck, J. Appl. Phys. **28,** 519 (1957).
2. R. Lovberg, L. Burkhardt, G. Sawyer, T. Stratton, to be published.
3. M. Kruskal and J. Tuck, Los Alamos Scientific Laboratory Report LA-1716, Proc. Roy. Soc. **A245,** 222 (1958).
4. M. Rosenbluth, Los Alamos Scientific Laboratory Report LA-2030.
5. C. Longmire and M. Rosenbluth, Ann. Phys. **1,** 120 (1957).
6. R. Dunaway, J. Phillips, "Neutron Generation from Straight Pinches," to be published. O. Anderson, W. Baker, S. Colgate, J. Ise, Jr., and R. Pyle, UCRL-3725 Rev.
7. W. H. Bostick, M. A. Levine, L. S. Combs, I. Moncius, Tufts Laboratory Report (1953).
8. M. Rosenbluth, Los Alamos Scientific Laboratory Report LA-1850; part of this report is contained in Magnetohydrodynamics. Stanford University Press, Stanford, Calif. (1957).
9. L. Burkhardt, R. Lovberg, J. Phillips, Los Alamos Scientific Laboratory Report LA-2131, to be published.
10. I. Kurchatov, reprinted in Nucleonics **14,** 36 (1956); L. Artsimovich *et al.*, *op. cit.*

CONFINEMENT OF A PLASMA COLUMN BY RADIATION PRESSURE

ERICH S. WEIBEL*

I. INTRODUCTION

The equations which govern the interaction between a plasma and the electromagnetic field are so complex that almost always simplifying assumptions must be made to arrive at solutions. One assumption that has been made very often is to drop the displacement current from Maxwell's equations. Thus all electromagnetic wave phenomena are excluded. There exists of course a great deal of work on the transmission of microwaves through and their reflection from a plasma; however, in such work usually little attention is paid to the forces which are exerted by the radiation on the plasma. Another approximation frequently made is to treat the plasma as a single fluid with a fixed conductivity. This model does not allow a consistent treatment of charge separation, so that in addition the charge density is usually set equal to zero.

It seemed worth while to investigate a situation in which these two approximations do not have to be made, a case involving waves reflected and refracted by a plasma which at the same time exert a pressure on this plasma. The problem of charge separation, which is very intriguing mathematically, will also be treated.

Figure 1 shows a configuration which permits a fairly detailed analysis. It consists of an infinitely long cylindrical cavity with a conducting wall. The center is occupied by a column of plasma which is supposed to be completely ionized hydrogen gas. The cavity is excited in such a way that a radial electromagnetic wave is reflected back and forth between the wall and the plasma. It thereby exerts a pressure on the plasma, keeping it separated from the wall. The polarization is chosen such that E is purely

* Aeronautical Research Laboratory, Ramo-Wooldridge Corporation, Los Angeles, California.

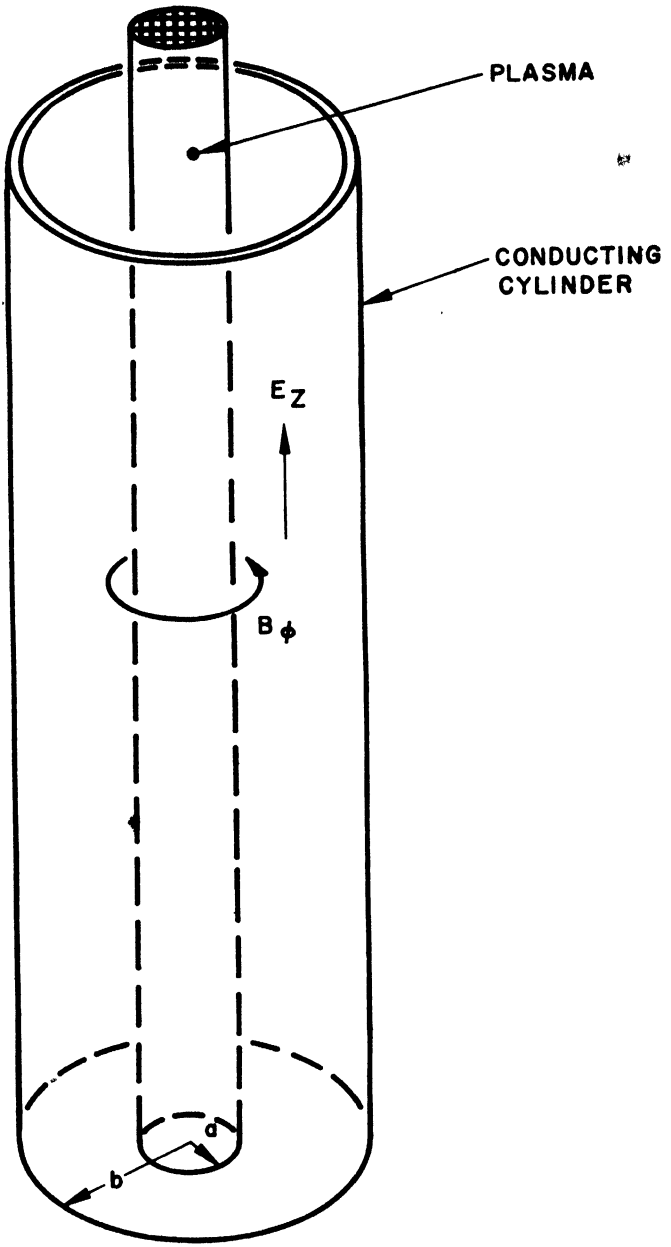

FIG. 1. Disposition of plasma and fields

longitudinal and B purely azimuthal. (TM_{01} mode driven at its cut-off frequency.)

A perfectly sharp boundary can of course not exist. There will be a surface layer of finite thickness through which the field penetrates and in which the density drops gradually from its maximum to zero. The longitudinal electric field causes the ions and electrons to oscillate parallel to the cylinder axis. The axial current thus produced is in phase with the azimuthal magnetic field, so that the Lorentz force $\boldsymbol{j} \times \boldsymbol{B}$ always points in the same direction, namely, toward the axis. This force confines the gases. Because of their greater mass the current carried by the ions is much smaller than the electron current. Hence the electron gas experiences most of the radiation pressure while the ions try to escape. But they do not get very far. Charge separation occurs which gives rise to an electrostatic field which in turn binds the ions to the electrons. The confining forces oscillate about their average value at twice the frequency of the applied radiation. Hence radial plasma oscillations are excited. It is the purpose of this paper to determine these effects quantitatively. Sections II and III derive the pertinent equations, while Sections IV and V give their solution. In Section VI the forced plasma oscillations are treated as a perturbation.

All equations are written in a "natural system of units" in which all coefficients of Maxwell's equations in vacuum are ± 1.

II. THE CONTINUOUS MODEL

The plasma shall be regarded as consisting of two oppositely charged ideal gases which penetrate each other without friction.* The hydrodynamic equations for these gases include the Lorentz force:

$$NM \frac{D\boldsymbol{V}}{Dt} + \text{grad } NkT = eN\ [\boldsymbol{E} + \boldsymbol{V} \times \boldsymbol{B}] \tag{1A}$$

$$nm \frac{D\boldsymbol{v}}{Dt} + \text{grad } nkT = -en\ [\boldsymbol{E} + \boldsymbol{v} \times \boldsymbol{B}] \tag{1B}$$

$$\text{div } (N\boldsymbol{V}) + \frac{\partial N}{\partial t} = 0 \tag{2A}$$

* This approximation is valid if $f\tau \gg 1$ where f is the frequency of the applied radiation and τ is the average time between collisions of electrons with ions. L. Spitzer gives values for τ in Physics of Completely Ionized Gases (Interscience, 1956), Chap. 5.3.

$$\operatorname{div}(n\boldsymbol{v}) + \frac{\partial n}{\partial t} = 0 \tag{2B}$$

Ion and electron temperatures are assumed equal and constant. In Maxwell's equations,

$$\operatorname{div}\boldsymbol{E} = \rho = e(N - n) \tag{3}$$

$$\operatorname{curl}\boldsymbol{B} - \frac{\partial \boldsymbol{E}}{\partial t} = j = e(N\boldsymbol{V} - n\boldsymbol{v}) \tag{4}$$

$$\operatorname{curl}\boldsymbol{E} + \frac{\partial \boldsymbol{B}}{\partial t} = 0 \tag{5}$$

$$\operatorname{div}\boldsymbol{B} = 0 \tag{6}$$

the sources are expressed in terms of the densities and velocities of the two gases (capitals are used for the ions, lower-case letters for electrons). The complexity of this system is reduced considerably owing to the symmetry of the problem, which requires the following forms for the electric field and the velocities:

$$\boldsymbol{E} = \{E_r(r), 0, E_0(r)\cos\omega t\} \tag{7}$$

$$\boldsymbol{V} = \{0,0, V(r,t)\} \tag{8}$$

$$\boldsymbol{v} = \{0,0, v(r,t)\} \tag{9}$$

where the brackets contain the r-, ϕ-, and z-components of the vectors. The z-component of Eq. (7) represents the applied field plus the field due to the plasma current. The radial electrostatic field is due to charge separation. Of the densities we require that they depend only on r. We shall show that with these assumptions the original set of equations can be satisfied if one makes a single approximation: the forces in the radial direction shall be time-averaged. The conditions under which this approximation is valid will be given in Section VI.

We proceed to show how the system of equations breaks up into manageable pieces. The continuity equations are already satisfied. From Eq. (7) one finds, according to Eq. (5), the only component of B:

$$B_\phi = B_0 \sin\omega t = \frac{1}{\omega} E_0'(r) \sin\omega t \tag{10}$$

Using Eq. (4) one obtains the current density after substitution of Eqs. (7) and (10):

$$j_z = \frac{1}{\omega}\left(\omega^2 E_0 + \frac{1}{r}\frac{d}{dr} rE_0\right)\sin\omega t \tag{11}$$

This equation expresses the current as the source of the radiation field.

Now the current shall be calculated as caused by the field. Consider the momentum equations, Eqs. (1A) and (1B). Neither the magnetic force nor the pressure gradient has components in the z-direction. Hence the z-components become:

$$eNE_o \cos \omega t = NM \frac{\partial V}{\partial t}$$

$$-enE_o \cos \omega t = nm \frac{\partial v}{\partial t}$$

The transport terms, $V\text{grad}V$, which often cause difficulties, vanish because of Eq. (8). These equations are easily integrated to give the velocities and the current,

$$V = \frac{eE_o}{M\omega} \sin \omega t, \quad v = \frac{-eE_o}{m\omega} \sin \omega t \tag{12}$$

$$j = \left(\frac{e^2N}{M} + \frac{e^2n}{m} \right) E_o \frac{\sin \omega t}{\omega} \tag{13}$$

Elimination of j from Eqs. (11) and (13) gives an ordinary differential equation for E,

$$\frac{1}{r} \frac{d}{dr} \left(r \frac{dE_o}{dr} \right) + \left(\omega^2 - \frac{e^2N}{M} - \frac{e^2n}{m} \right) E_o = 0 \tag{14}$$

which is nothing but the well-known wave equation in a plasma with variable ion and electron densities, n and N. However, these densities are yet unknown.

Equations for these densities can be found from the radial components of Eq. (1); for the ions one obtains:

$$eN \left[\boldsymbol{E} + \boldsymbol{V} \times \boldsymbol{B} \right]_r - kT \frac{dN}{dr} = 0 \tag{15}$$

The electrical part of the Lorentz force is due to E_r which is related to the densities by Eq. (3)

$$\frac{1}{r} \frac{d}{dr} (rE_r) = e(N - n) \tag{16}$$

The cross product appearing in Eq. (15) can be formed using Eqs. (10) and (12). For ions one obtains

$$eN\left[\boldsymbol{V}\times\boldsymbol{B}\right]_r = -\frac{e^2N}{M\omega^2}E_o\frac{dE_o}{dr}\sin^2\omega t$$

$$= \frac{e^2N}{4M\omega^2}\left(\frac{d}{dr}E_o^2\right)[1-\cos 2\omega t] \qquad (17)$$

and an analogous expression for the electrons. This force is independent of the sign of the charge; it is much larger for the electrons than for the ions. It is expressed as the derivative of the electric field intensity. Together with the minus sign this means that this force always points in the direction of decreasing electric field amplitude, that is, to the electric nodes of the standing electromagnetic wave. This result, although derived for this special geometry, is generally true.

At this point the approximation mentioned earlier is made: only the time average of the force Eq. (17) is retained.* For the ions Eq. (15) now becomes:

$$eNE_r - \frac{e^2N}{4M\omega^2}\frac{d}{dr}E_o^2 - kT\frac{d}{dr}N = 0 \qquad (18)$$

and for the electrons:

$$-enE_r - \frac{e^2n}{4m\omega^2}\frac{d}{dr}E_o^2 - kT\frac{d}{dr}n = 0 \qquad (19)$$

The problem is thus reduced from the original twenty partial differential equations to the solution of four ordinary differential equations, Eqs. (14), (16), (18), and (19). At $r=0$, one may prescribe three boundary values: $N(0)$, $n(0)$, and $E_o(0)$; while the other two are given by symmetry:

$$E_r(0) = 0,\ \frac{dE_o}{dr} = 0$$

III. STATISTICAL APPROACH

In this section we shall use an alternate method, which is perhaps more elegant if less transparent physically. Equations (14), (16), (18), and (19) can be derived by starting from the equations of motion for an individual particle in the average field of all the others. Collisions between ions and electrons will be neglected, which corresponds exactly to the as-

* See Section VI.

sumption made in the previous section that there be no friction between the ion gas and the electron gas. The (infrequent) collisions between like particles are taken into account implicitly later on when use is made of the equilibrium distributions in phase space.

The motion of an electron in the field given by Eqs. (7) and (10) is described by the following Lagrangian,

$$L = \frac{m}{2}\left[r^2 + (r\dot{\phi})^2 + \dot{z}^2 \right] + \frac{e\dot{z}}{\omega} E_o(r) \sin \omega t + eU(r) \quad (20)$$

where the second term represents the interaction with the radiation (vector potential times velocity) and the third term the radial electrostatic field due to charge separation:

$$-\frac{dU}{dr} = E_r \quad (21)$$

Since L does not depend explicitly on ϕ or z one has immediately

$$m\dot{z} + \frac{e}{\omega} E_o \sin \omega t = p_z \quad (22)$$

$$mr^2 \dot{\phi} = p_\phi \quad (23)$$

where the momenta p_z and p_ϕ are constants. Equation (22) is quite remarkable. It asserts that the z-component of velocity, apart from a constant, is given by the electric field at the point at which the particle finds itself. Since the velocity may have any direction, the particle may have come from points of widely differing field amplitude. Nevertheless, its oscillating velocity at the distance r from the axis is simply

$$-m/e \int E_z(r,t)dt$$

In a more general field this is not true. The current density becomes

$$j_z = e\left[N\dot{Z} - n\dot{z} \right]_{av}$$

where N and n are the number of ions and electrons per unit volume; the average is taken over all momenta p_z which are distributed at random. Hence

$$j_z = \frac{1}{\omega}\left(\frac{Ne^2}{M} + \frac{ne^2}{m} \right) E_o \sin \omega t \quad (24)$$

which is the same expression as obtained in the continuous model. This simple relation between current and field does *not* hold in arbitrary fields

when collisions are negligible, that is, when the mean free paths exceed the wave length. The wave equation, Eq. (14), follows immediately as a consequence. Equation (16) is of course equally valid.

To make further progress one has to examine the equation for the radial acceleration

$$\frac{d}{dt}\frac{\partial L}{\partial \dot{r}} = \frac{\partial L}{\partial r}$$

or

$$m\ddot{r} = m\dot{r}\dot{\phi}^2 + \frac{e\dot{z}}{\omega}\frac{dE}{dr}\sin\omega t + e\frac{dU}{dr}$$

After elimination of ϕ and z by means of Eqs. (22) and (23) this becomes

$$m\ddot{r} = \frac{p_\phi^2}{mr^3} - \frac{e^2}{4m\omega^2}\left(\frac{d}{dr}E_o\right)^2 [1 - \cos 2\omega t] + \frac{ep_z}{m\omega}\frac{dE}{dr}\sin\omega t + e\frac{dU}{dr} \tag{25}$$

We shall again time-average the force which appears on the right-hand side:*

$$m\ddot{r} = \frac{p_\phi^2}{mr^3} - \frac{e^2}{4m\omega^2}\frac{d}{dr}(E_o^2) + e\frac{dU}{dr} \tag{26}$$

This approximation is exactly equivalent to the one made in the continuous model. This simplified equation of motion can evidently be derived from a single, time-independent potential

$$\Phi = \frac{e^2 E_o^2(r)}{4m\omega^2} - eU(r)$$

According to statistical mechanics the equilibrium density distribution of electrons in this potential field at the temperature T is given by

$$n(r) = n_o \exp\left(+\frac{eU}{kT} - \frac{e^2E_o^2}{4m\omega^2kT}\right) \tag{27}$$

and analogously for ions,

$$N(r) = N_o \exp\left(-\frac{eU}{kT} - \frac{e^2E_o^2}{4m\omega^2kT}\right) \tag{28}$$

These two equations are exactly equivalent to Eqs. (19) and (18), as may

* In Section VI, the conditions are given under which this is valid.

be seen by taking the logarithmic derivative of Eqs. (28) and (27) and making use of Eq. (21). It is satisfying to see that the continuous model and the statistical treatment lead to exactly the same system of equations.

IV. APPROXIMATE SOLUTION NEGLECTING CHARGE SEPARATION

In this section the radiation field and the plasma density shall be obtained for the limit of infinite Coulomb interaction ($e \to \infty$; e^2/m, e^2/M fixed). In this case no charge separation can occur and the problem is greatly simplified. The results thus obtained represent fairly well the main features of the radiation confinement as long as $h/\lambda << 1$ where $h = \sqrt{kT/e^2n}$ is the Debye shielding distance and $\lambda = 2\pi/\omega$ is the wave length of the applied field.

From Eqs. (27) and (28) one obtains the product Nn of the densities which does not contain the (infinite) Coulomb interaction. The requirement, that there be no charge separation

$$N = n$$

immediately yields:

$$n = n_o \exp\left[-\frac{e^2E_o^2}{8\omega^2kT}\left(\frac{1}{m}+\frac{1}{M}\right)\right] \tag{29}$$

This expression is substituted into Eq. (14) which becomes an ordinary, non-linear, second-order differential equation for $E_o(r)$:

$$\frac{1}{r}\frac{d}{dr}\left(r\frac{dE_o}{dr}\right) + \left\{\omega^2 - e^2n_o\left(\frac{1}{m}+\frac{1}{M}\right)\exp\left[-\frac{e^2E_o^2}{8\omega^2kT}\left(\frac{1}{m}+\frac{1}{M}\right)\right]\right\}E_o = 0 \tag{30}$$

Equation (30) can be brought into a more convenient dimensionless form. Using the following transformations:

$$x = \omega r \tag{31}$$

$$u^2(x) = \frac{e^2E_o^2(r)}{8\omega^2kT}\left(\frac{1}{m}+\frac{1}{M}\right) \tag{32}$$

$$\alpha = \frac{n_oe^2}{\omega^2}\left(\frac{1}{M}+\frac{1}{m}\right) \tag{33}$$

one obtains

$$u'' + \frac{1}{x}u' + (1 - \alpha e^{-u^2})\,u = 0 \tag{34}$$

with the boundary conditions: $u(0) = u_o$; $u'(0) = 0$; $u(b\omega) = 0$.

The first two conditions determine $u(x)$, while the last determines b, the cavity radius. The fields and densities in terms of the function $u(x)$ are:

$$E_o(r) = \frac{u(x)}{\sqrt{\alpha}} \sqrt{8n_o kT} \tag{35}$$

$$B_o(r) = \frac{u'(x)}{\sqrt{\alpha}} \sqrt{8n_o kT} \tag{36}$$

$$n = N = n_o e^{-u^2} \tag{37}$$

The solution $u(x)$ depends on two parameters α and u_o. The parameter α is a measure of the transparency of the plasma to the radiation, since the depth of penetration of an electromagnetic field is

$$d = \frac{1}{\omega \sqrt{\alpha - 1}}$$

The cases of interest are obtained by choosing $\alpha > 1$ and $u_o < 1$. The first inequality requires the plasma to be dense enough to be a good reflector; the second assures that only a small amount of the radiation penetrates to the core of the plasma.

With these parameter values it is not difficult to perceive the general shape of the solution $u(x)$ (Fig. 2): For small values of x, u itself is small and e^{-u^2} about unity, so that the differential equation has the solution

$$u = u_o J_o (i \sqrt{\alpha - 1}\, x)$$

This is a rapidly growing function, which therefore soon leaves the domain of its validity. As u becomes larger than $\sqrt{ln\, \alpha}$ the differential equation simplifies to the ordinary Bessel equation with the solution

$$u = AJ_o(x) + BN_o(x)$$

The actual solution smoothly bridges these two approximating ones (Fig. 2).

The plasma density, being proportional to e^{-u^2} remains fairly constant near $x = 0$ and then drops off very rapidly. The slope of $u(x)$ has a maximum at x_1 which defines a radius $a = x_1/\omega$. It will be called the plasma radius, because most of the plasma lies inside a cylinder with radius a. Thus the plasma is really confined. As α is increased, the density curve, e^{-u^2}, becomes more rectangular. For smaller values of α it falls off more gradually, as seen in Fig. 3, which shows a case in which α is 14.6.

If the solution $u(x)$ is continued beyond x_2 where its first maximum occurs, the plasma density e^{-u^2} increases again. In a practical arrange-

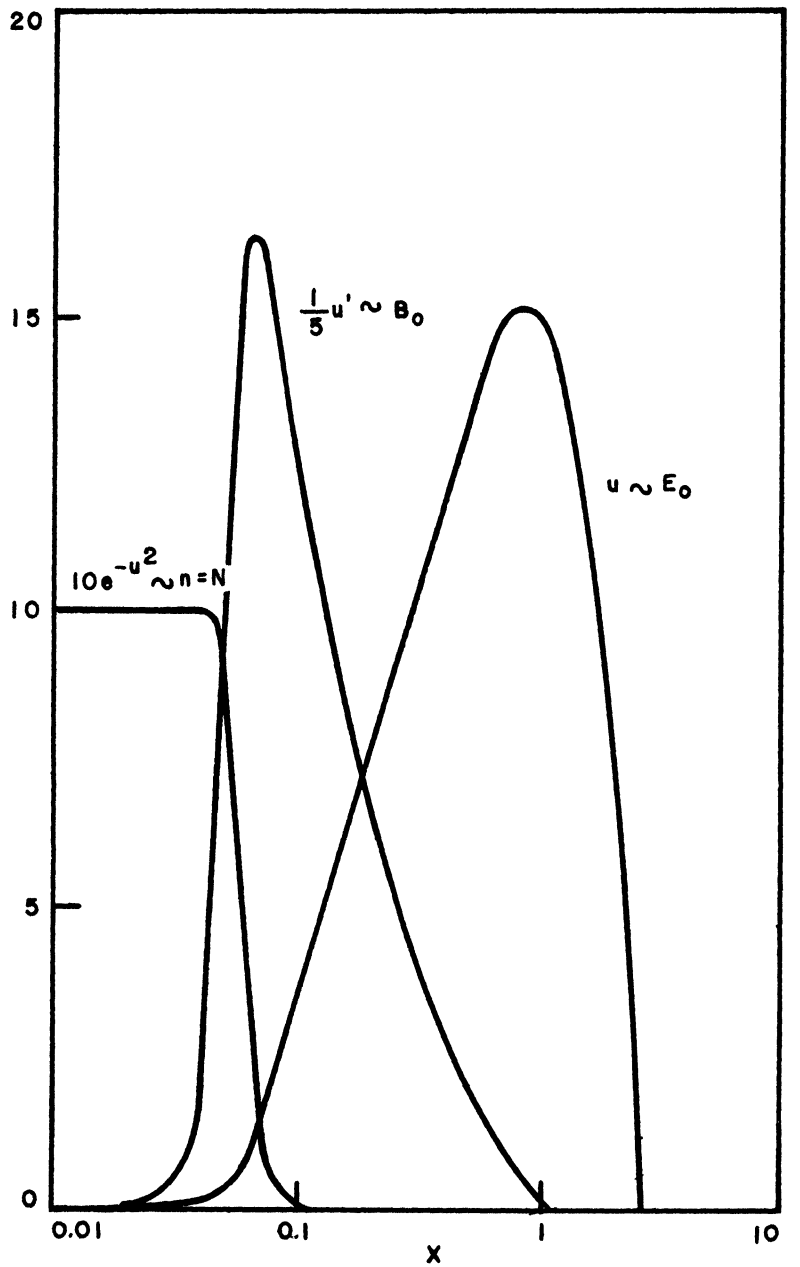

FIG. 2. Fields and plasma density vs. radius: results of integration carried out for $u_0 = 10^{-2}$, $\alpha = 10^4$. Scales are given by Eqs. (31), (35), (36), and (37).

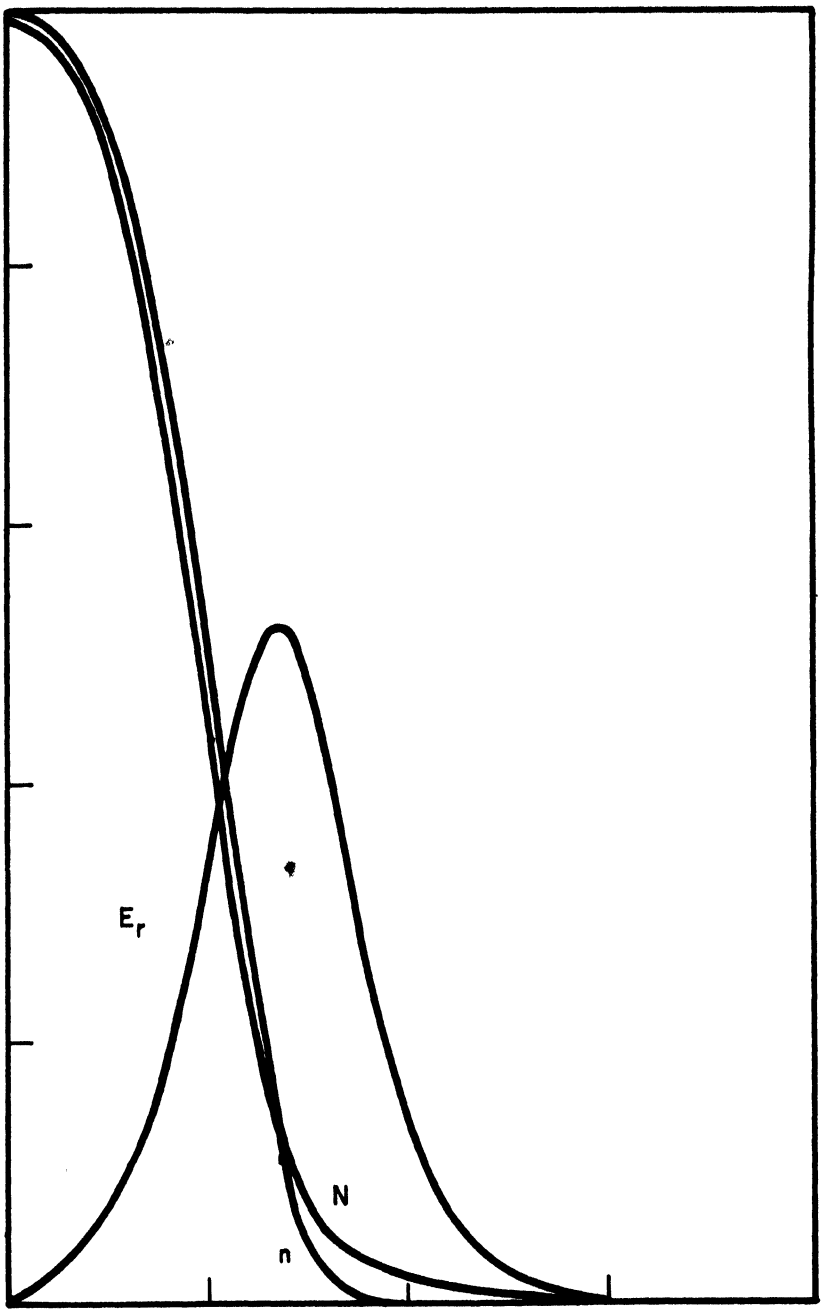

FIG. 3. Radial electric field and charge separation. Scale not given.

ment, however, one wants the density to be large only at the center $x = 0$. Beyond x_2 the particle density should stay small.

To achieve this, assume that the plasma has been removed at points $x > x_2$. Mathematically this means setting $\alpha = 0$ in Eq. (34) for $x > x_2$. The discontinuity thus introduced in the higher derivatives of u is extremely small, since at x_2 the term αe^{-u^2} equals $\alpha e^{-u_{max}^2}$ which is practically zero. Thus the solution u continues after x_2 as an ordinary cylinder function according to Eq. (9). The first zero of u, namely $x_3 = \omega b$, marks the radius of the cavity wall.

Physically this removal of plasma upsets the equilibrium at x_2 where the particle density drops from e^{-u^2} to zero. Consequently particles will escape at a rate given by the product of their density at $x_2 = \omega r_2$ and their thermal velocity

$$2\pi r_2 n(r_2) \sqrt{\frac{kT}{m}}$$

The total number of particles confined is approximately

$$\pi a^2 n_o$$

Thus the half life of the confinement is about

$$t = \sqrt{\frac{m}{kT}} \frac{a^2}{2r_2} e^{u^2(x_2)}$$

which is an exceedingly long time. Hence practically no leakage of plasma occurs.

Finally let us examine $u'(x)$ which represents the magnetic field B according to Eq. (36). At x_1, u' has a sharp maximum. Outside this point it behaves nearly like the magnetic field in a coaxial line, while inside it drops rapidly to zero in a manner familiar from the skin effect in wires. The B field and hence the magnetic pressure may be much larger at the plasma ($r = a$) than at the cavity wall ($r = b$), particularly if a/b is small. This effect is due to the cylindrical geometry and occurs only for the TM mode with no ϕ variation.

V. CHARGE SEPARATION

The exact solution of Eqs. (14), (16), (18), and (19) takes account of the charge separation. As Fig. 3 shows, this is a small effect in the regions in which the plasma density is high. As the density decreases for larger distances from the axis, the Debye shielding distance increases and therefore large differences in ion and electron densities will occur. The electron density is larger than the ion density at the center of the

plasma column and smaller in the surface layer, consistent with the notion that the radiation pressure is exerted primarily on the electrons while the ions are held by the charge separation field E_r which is also plotted in Fig. 3.

It may be worth while to make a few remarks about a peculiar mathematical difficulty that arises in the solution of the system of Eqs. (14), (16), (18), and (19). Unlike linear equations, this system does not permit one to determine the singularities of the solutions independently of the initial conditions. It can be shown that the system possesses solutions which are singular in one or the other of the densities, N or n. More precisely, the singularity which may occur at *any* point is a second-order pole in one density, the other density having a second-order zero at that point. This can be seen easily by substituting

$$\left.\begin{aligned} N &= \frac{2kT}{e^2 (r - r_0)^2}\ ; n = \text{const}\ (r - r_0)^2\ ; \\ E_r &= \frac{2kT}{e\ (r - r_0)}\ ; E_0 = (r - r_0)^s, s = \tfrac{1}{2}\left(1 + \sqrt{1 + 8\,\frac{kT}{M}}\right) \end{aligned}\right\} \quad (38)$$

into Eqs. (14), (16), (18), and (19) and observing that they are satisfied by the leading terms in the neighborhood of r_0. The possibility of these singularities is very surprising since in the physical reality an accumulation of charges such as given by the first of Eq. (32) is clearly impossible.

Suppose now that a solution of the system of equations is attempted by step-wise integration. As soon as an error is made, the integration will follow one of the singular solutions. From the coefficient of the second-order pole of N it is apparent that the singularity develops in a distance $h = \sqrt{kT/e^2 N_r}$ (Debye length) where N_r is the value of the correct solution at the point where the error is made. Since h is much smaller than the interval of interest it is obvious that a solution cannot be found by step-wise integration.

The curves of Fig. 3 have been obtained by a relaxation method. One starts out with a guess of N and n (obtained for instance from the approximate solution neglecting charge separation), calculates E_r and E_0 from Eqs. (14) and (16). With the quantities so found the left sides of Eqs. (18) and (19) are evaluated, which will not vanish; they represent the forces tending to push the plasma into equilibrium. From these forces one obtains more accurate distributions N and n, whereupon the cycle is repeated. A provision is made whereby the total number of charges in the interval is held fixed so as to avoid singular solutions. This method

was adapted for machine computation by A. B. Troesch,* the result of which is plotted in Fig. 3.

VI. PLASMA OSCILLATIONS

So far the oscillating part of the containing force, Eq. (17), has been neglected. It may be taken into account as a perturbation if the scalar potential is allowed to be time-dependent. Thus, in the Lagrangian Eq. (20) $U(r)$ is replaced by

$$\tilde{U}(r, t) = U(r) + \delta U(r\, t)$$

whence

$$\tilde{E}_r(r, t) = E_r(r) + \delta E_r(r\, t), \quad \delta E_r = -\frac{\partial}{\partial r}\delta U$$

The equation for the radial acceleration of an electron now becomes, instead of Eq. (26):

$$m\ddot{r} = \frac{p_\phi^2}{mr^3} - \frac{d}{dr}\left(\frac{e^2E_o^2}{4m\omega^2} - eU\right) + \frac{\partial}{\partial r}\left[\frac{ep_z}{m\omega}E_o \sin \omega t + \frac{e^2E_o^2}{4m\omega^2}\cos 2\omega t + e\delta U\right] \tag{39}$$

The solution is assumed to be

$$\tilde{r}(t) = r(t) + \delta r(t)$$

where $r(t)$ satisfies Eq. (26), that is, Eq. (39) without the last term, and δr is expected to turn out small. Hence to first order

$$m\frac{d^2}{dt^2}(\delta r) = \frac{\partial}{\partial r}\left[\frac{ep_z}{m\omega}E_o(r) \sin \omega t + \frac{e^2E_o^2(r)}{4m\omega^2}\cos 2\omega t + e\delta U(r, t)\right]\Bigg|_{r=r(t)} \tag{40}$$

From this equation it is easy to see that the perturbation of the potential must be of the form

$$\delta U(r, t) = U_1(r) \cos 2\omega t$$

Because of the occurrence of $r(t)$ Eq. (39) cannot be integrated exactly. However, if the frequencies contained in $r(t)$ are much smaller than the

* Ramo-Wooldridge Corporation, Computer System Division.

frequency of the applied force, ω/π, one obtains a good approximation for δr by simply integrating the trigonometric functions of Eq. (40) twice:

$$m\delta r = -\frac{\partial}{\partial r}\left[\frac{ep_z}{m\omega^2}E_0 \sin \omega t + \frac{e^2E_0^2}{16m\omega^2}\cos 2\omega t + \frac{eU_1}{4\omega^2}\cos 2\omega t\right]$$

For the purpose of an estimate of the condition in which this is valid one may define the highest frequency contained in $r(t)$ by

$$\ddot{r} = -\Omega^2(r)\cdot r$$

Using for the acceleration only the part due to the confining force, one obtains

$$\Omega^2 = \frac{1}{r}\frac{d}{dr}\frac{e^2E_0^2}{4m^2\omega^2}$$

and

$$\left(\frac{\Omega}{\omega}\right)^2 = \frac{2}{x}\frac{d}{dx}(u^2)\frac{kT}{m}$$

where x and u have the meaning of Eqs. (31) and (32). Thus the condition in question is

$$\frac{m}{kT} >> \left[\frac{2}{x}\frac{d(u^2)}{dx}\right]_{\max}$$

The value of the right side of this inequality depends on the sharpness of the boundary between field and plasma (see Section IV). It is large for a very sharp boundary and becomes small if the density of the plasma falls off more gradually. Thus, for a given temperature the distribution cannot be made arbitrarily sharp.

The average displacement, ξ, of electrons at a given point is obtained by averaging δr over the randomly distributed momenta p, hence

$$\xi = -\frac{d}{dr}\left[\frac{e^2E_0^2}{16m^2\omega^4} + \frac{eU_1}{4m\omega^2}\right]\cos 2\omega t \tag{41}$$

For ions one obtains similarly

$$\Xi = -\frac{d}{dr}\left[\frac{e^2E_0^2}{16M^2\omega^4} - \frac{eU_1}{4M\omega^2}\right]\cos 2\omega t \tag{42}$$

If the perturbations of the densities are denoted by δN and δn the continuity equations yield

$$\delta n + \frac{1}{r}\frac{\partial}{\partial r}(r\xi n) = 0$$

$$\delta N + \frac{1}{r}\frac{\partial}{\partial r}(r\Xi N) = 0 \tag{43}$$

From Eq. (3) one has

$$\operatorname{div} \delta \boldsymbol{E} = e\,(\delta N - \delta n) \tag{44}$$

Elimination of δN, δn between Eqs. (43) and (44) leads, after integration, to

$$\delta E_r = -\frac{dU_1}{dr}\cos^2 \omega t = e\,[\xi n - \Xi N] \tag{45}$$

The three Eqs. (42), (41), and (45) can now be solved for dU_1/dr, ξ, and Ξ.

$$\frac{dU_1}{dr} = \frac{\dfrac{e^3}{16\,\omega^4}\left[\dfrac{n}{m^2} - \dfrac{N}{M^2}\right]\dfrac{d}{dr}E_0^2}{1 - \dfrac{e^2 n}{4\,m\omega^2} - \dfrac{e^2 N}{4\,M\omega^2}}$$

$$\xi = \frac{1 + \dfrac{e^2 n}{4\,m\omega^2}}{1 - \dfrac{e^2 n}{4\,m\omega^2}} \frac{e^2}{16\,m^2\omega^4}\frac{d}{dr}E_0^2 \cos 2\omega t$$

$$\Xi = \frac{1 + \dfrac{e^2 n}{4\,m\omega^2}}{1 - \dfrac{e^2 n}{4\,m\omega^2}} \frac{e^2}{16\,M^2\omega^4}\frac{d}{dr}E_0^2 \cos 2\omega t$$

In the last two expressions N/M has been neglected against n/m. The amplitude of the electron oscillations, ξ, is evidently much larger than Ξ. Resonance occurs at a distance r at which

$$\frac{e^2 n}{4\,m\omega^2} = 1$$

that is, where the plasma frequency equals twice the frequency of the applied field.

PLASMA INSTABILITY IN THE INTERPLANETARY MAGNETIC FIELD

E. N. PARKER*

I. INTRODUCTION

Biermann's[1] analysis of the motion of comet tails indicates that gas flows outward continuously in all directions from the sun with velocities of the order of 500 to 1500 km/sec. He suggests that this outward-streaming gas has a density at the orbit of the earth which is normally about 500 hydrogen ions/cm^3, with very much higher densities during occasional violent solar outbursts.

There are arguments that Biermann's outward velocities and densities are too high. We do not wish to become involved in such discussions here, for they are basically concerned with the analysis and interpretation of photographs of comets. We shall, however, point out that during the years of enhanced solar activity (during each peak of the sunspot cycle) there is at all times, apparently, at least some feeble auroral display somewhere in the terrestrial auroral zones. This suggests that there must at all times be hydrogen ions rushing past our planet with velocities of the order of 1000 km/sec.

During the years of solar minimum there is no such evidence. Therefore, we shall discuss both 1000 km/sec and much lower, say 100 km/sec, outward-streaming velocities V_m from the sun.

II. BASIC INTERPLANETARY FIELD

There is, so far as this author is aware, no evidence that the outward gas velocities from the sun reverse themselves; whatever their observed magnitudes may be, the motion is always outward. Since systematic magnetic observations of the sun[2] indicate no field-free regions on the surface

* Enrico Fermi Institute for Nuclear Studies, University of Chicago.

of the sun, and imply no field-free regions in the interior, the gas flowing outward from the sun must be threaded by lines of force of the general solar magnetic field. Continued outward flow will draw out the lines of force into a radial configuration, and this radial field will extend as far into space as the outflowing gas can travel; Davis[3] estimates 200 to 2000 astronomical units (1 a.u. = earth–sun distance of 1.5×10^8 km), which so far as we are concerned is infinitely far. The coronal streamers, which are believed to map the magnetic lines of force, support this theoretical prediction of a radial field.

The coronal streamers suggest that during the years of maximum solar activity, the more complex magnetic fields found in the solar equatorial regions are extended by outward-flowing gas, along with the general solar dipole field. For simplicity we shall consider only the dipole field; our conclusions would not be greatly altered by the more complicated fields near the equator. Thus, if the sun were without rotation, its drawn-out dipole field would be

$$B_r = B_o \left(\frac{R}{r}\right)^2 \cos\theta, \qquad B_\theta = B_\phi = 0 \tag{1}$$

in spherical coordinates. We choose[2] B_o to be of the order of one gauss, in the solar corona where $r = R = 10^6$ km. Hence, at the orbit of the earth, B is only 5×10^{-5} gauss, when one disregards the dependence on θ which does not really apply near the equator.

If we take into account the angular velocity Ω (2.7×10^{-6} radians/sec) of the sun, then we have B_r and B_θ as before, with the azimuthal field

$$B_\phi\,(r,\theta,\phi) = B_o \frac{\Omega R}{V_m} \frac{R}{r} \sin\theta \cos\theta \tag{2}$$

so that the lines of force spiral as shown in Fig. 1. For 1000 km/sec outward velocities, the magnetic lines of force are essentially radial at the orbit of the earth, and do not make an angle of 45° with the radius vector from the sun until 2.5 a.u. For 100 km/sec, 45° is reached at 0.25 a.u., inside the orbit of Mercury; at the earth the lines make an angle of 76° with the radius.

III. THERMAL ANISOTROPY

We have discussed elsewhere[4] the mean free path of a thermal electron or ion, with velocities u_e and u_p, respectively, in a plasma of N electrons and ions per unit volume. The mean free paths of thermal protons and

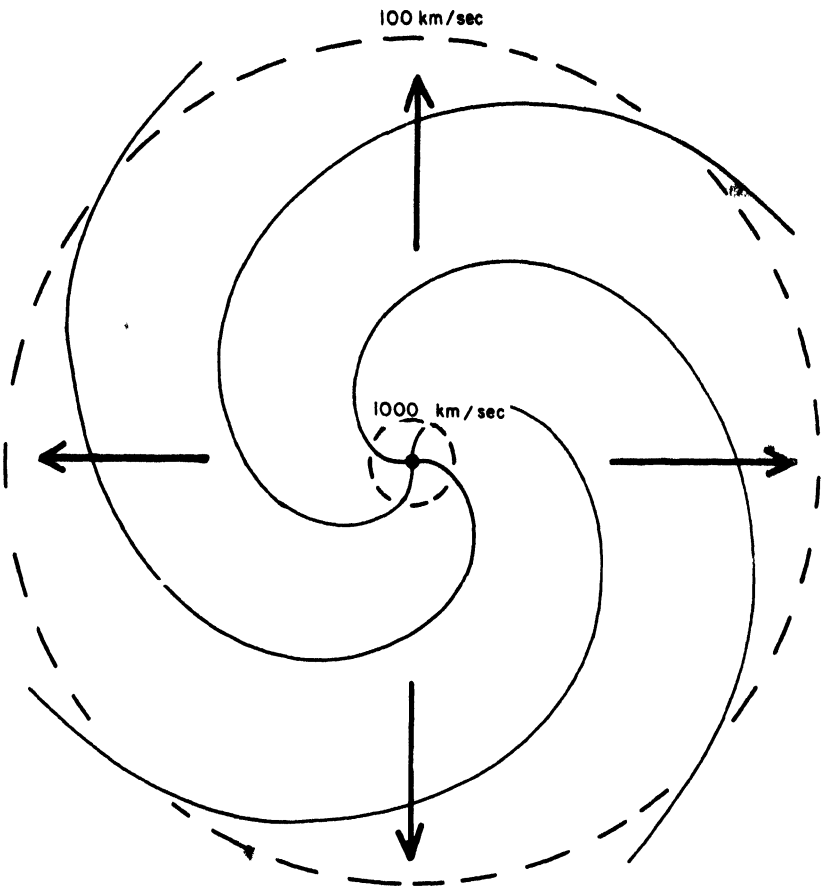

FIG. 1. Lines of force from the rotating sun near the solar equatorial plane, assuming a uniform outward radial gas flow: broken circles represent the scale of the orbit of the earth relative to the spiraling lines of force for the indicated gas velocities.

electrons in a hydrogen plasma are of the same order of magnitude, and depend essentially upon the temperature squared, divided by N. In spite of the great amount of expansion which has taken place since the gas left the sun, one expects* the outward-streaming gas to have temperatures of the order of magnitude of 10^5 °K at the orbit of the earth[5] (for which $u_p \cong 50$ km/sec). $N = 500/\text{cm}^3$ yields[4] a mean free path of the order

* If it should ultimately prove that T is small compared to 10^5 °K, then the collision time would perhaps be so small as to invalidate our conclusions.

of $\lambda \cong 10^{11}$ cm. The collision time for a hydrogen ion is, accordingly, $\tau = \lambda/\mu_p \cong 2 \times 10^4$ sec at the orbit of the earth; for an electron the collision time is negligibly small, 4×10^2 sec.

Now once the gas is as far as the earth, the solar gravitational field may be neglected; escape-energy from the orbit of the earth is 0.8×10^{13} ergs/gm, whereas even 100 km/sec represents 5×10^{13} ergs/gm. Therefore, the outward velocity is essentially uniform and the gas expands in two directions, perpendicular but not parallel to the radius vector from the sun. The characteristic time of expansion is $r/2v_m$, or 7.5×10^4 sec, at the orbit of the earth ($r = 1.5 \times 10^{13}$ cm) with $v_m = 1000$ km/sec.

We note that the expansion time $r/2v_m$ is of the same order as the collision time τ. During one collision time τ, the gas volume will have increased by a factor of the order of $\tau/(r/2v_m)$, and the pressure perpendicular to the radius will have fallen by the same amount. Thus, assuming that the collision after time τ restores isotropy to the colliding particles, the mean anisotropy is of the order of $v_m\tau/r$, which is 0.13 with the numbers used here. The pressure perpendicular to the radius vector will be of the order of 13 per cent less than the radial pressure.

Now the mean free path varies with temperature T and density N as $\lambda \propto T^2/N$, if we neglect the slower variation of logarithmic quantities in the complete expression.[4] Supposing the orbit of the earth to be beyond the region of coronal heating,[5] we may believe that T and N are related approximately adiabatically. $T \propto N^{\gamma-1}$. Thus, since the thermal velocity u_p is proportional to $T^{1/2}$, the ion collision time τ varies as $N^{(1/2)(3\gamma-5)}$. But for a monatomic gas $\gamma \cong 5/3$, so that the collision time is roughly independent of N, and hence independent of the distance from the sun. Therefore, the degree of anisotropy $v_m\tau/r$ decreases as $1/r$ with increasing distance from the sun.

IV. PLASMA INSTABILITY

The dynamical equations of a tenuous plasma for the velocity component u_n perpendicular to the magnetic field B (supposed to be of large scale) is[6]

$$\rho \frac{du_n}{dt} = -\nabla_n(P_n + B^2/8\pi) + (1/4\pi)\,[(B \cdot \nabla)B]_n\,(1 + \xi) \quad (3)$$

$$\partial B/\partial t = \nabla \times (u_n \times B), \quad (4)$$

where ρ is the density, and the subscript n denotes the component perpen-

dicular to $\boldsymbol{B}$. We see that the form of these equations differs from the usual hydromagnetic equations only in the factor* $1 + \xi$, where

$$\xi = 4\pi (P_n - P_s)/B^2 \tag{5}$$

with P_s representing the pressure parallel to $\boldsymbol{B}$.

Consider the perturbation of a large-scale field $\boldsymbol{B}_0 = \boldsymbol{e}_z B$ (where $\boldsymbol{e}_x$, $\boldsymbol{e}_y$, and $\boldsymbol{e}_z$ represent unit vectors along the coordinate axes) by a plane transverse field $\boldsymbol{b} = \boldsymbol{e}_y \varepsilon(z,t)$. Then the total magnetic pressure $(B^2 + \varepsilon^2)/8\pi$ varies by terms only second order in ε, and consequently so do P_n, P_s, and ξ. Neglecting all second-order terms in ε, Eqs. (3) and (4) reduce to

$$\rho \partial u_n/\partial t = (B/4\pi)\ (1 + \xi)\ (\partial \varepsilon/\partial z),$$
$$\partial \varepsilon/\partial t = B \partial u_n/\partial z.$$

Eliminating u_n we have the hydromagnetic wave equation,

$$\partial^2 \varepsilon/\partial t^2 - (1 + \xi)\ (B^2/4\pi\rho)\partial^2 \varepsilon/\partial z^2 = 0. \tag{6}$$

Now suppose that P_s is sufficiently greater than P_n that $1 + \xi$ is a negative quantity. Then it is readily shown[8] that a perturbation ε of wave length Λ will grow exponentially with a characteristic time

$$\frac{1}{\omega} = \frac{\Lambda}{2\pi}\left[\frac{\rho}{(P_s - P_n) - B^2/4\pi}\right]^{1/2}. \tag{7}$$

If B is of the order of $\frac{5}{4} \times 10^{-5}$ gauss (at the earth's orbit), then the magnetic pressure is only 10^{-10} dynes/cm^2, whereas 500 hydrogen atoms/cm^3 at 10^5 °K yields 70 times this amount. Thus, if the anisotropy $(P_s - P_n)/P_s$ is as large as 0.13, estimated in Section III, we may neglect the term $B^2/4\pi$ in Eq. (7), rewriting $1/\omega$ as

$$\frac{1}{\omega} \cong \frac{\Lambda}{2\pi}\frac{\sqrt{3}}{u_p}\left(\frac{P}{P_s - P_n}\right)^{1/2} \tag{8}$$

* The reader is to be warned that similarity in form, while meaningful in the special case we are considering, can be very deceptive in general. Neither the pressures P_n and P_s, nor the motion u_s parallel to $\boldsymbol{B}$, are as easily computed as in the classical hydromagnetic case. The reader is referred to the general treatment by Watson, Kaufman, and Chandrasekhar,[7] of the stability of the pinch effect, which, as it turns out, contains as a special case the instability discussed here. Their general discussion will illustrate how narrowly the present development has sailed between the mountainous rocks of complexity.

where P is the mean pressure, to be computed from the root-mean-square thermal velocity u_p by the relation $P = pu_p^2/3$. The characteristic time of growth is 1.5×10^4 sec, or 4 hr, for a wave length of 10^6 km at 10^5 °K with $(P_s - P_n)/P = 0.13$; shorter wave lengths grow in amplitude at correspondingly greater rates.

Remembering that the pressure anisotropy is inversely proportional to the radius, we see that far beyond the orbit of the earth, $1/\omega$ will approach infinity and we may have stability at great distances.

V. DISORGANIZED INTERPLANETARY FIELD

In Section II we suggested that Biermann's comet analysis, with a 1000 km/sec gas motion outward from the sun, yields an essentially radial solar magnetic field throughout interplanetary space within 2.5 a.u. of the sun. In Section III we suggested that the anisotropic expansion of the outward-flowing gas would yield an anisotropy of the order of 0.1 in the thermal motions, with the pressure greatest, parallel to the radius vector from the sun. Hence, if the magnetic field is essentially radial, we conclude that the pressure P_s parallel to $\boldsymbol{B}$ is greater than P_n perpendicular. It follows that the radial field is unstable to transverse perturbations and will become waved or kinked, and we predict that the inner solar system is surrounded by a thick shell of a disordered magnetic field, shown in Fig. 2, as a consequence of the instability of the basically radial field.

We cannot, of course, fix the boundaries of this disorganized shell with any degree of accuracy on the basis of the above calculations. Beyond 2.5 a.u. the magnetic field is primarily azimuthal, thus it is P_s which will become small as a result of the expansion. Other kinds of instabilities can then occur.[8] Inside the earth's orbit, where the field is radial, B^2 increases with decreasing r as $1/r$.[4] Thus $1 + \xi$ may soon become positive as we move inward from the earth's orbit, and no instability will be possible.

We must turn, then, to inferences concerning the interplanetary field structure obtained from the onset and decay of the anomalous cosmic ray intensity produced by solar flares. The observed sharp onset implies[9] that between the earth and the sun the magnetic field is radial (or otherwise $< 10^{-6}$ gauss). The fact that the subsequent decay of the cosmic-ray intensity is not exponential, but more nearly $t^{-3/2}$ until the intensity has fallen very low, requires[10] that in some way the inner solar system be surrounded by a thick disorganized field of the order of 10^{-5} gauss extending from 1 or 2 a.u. out to about 5 a.u. We suggest that this thick shell,

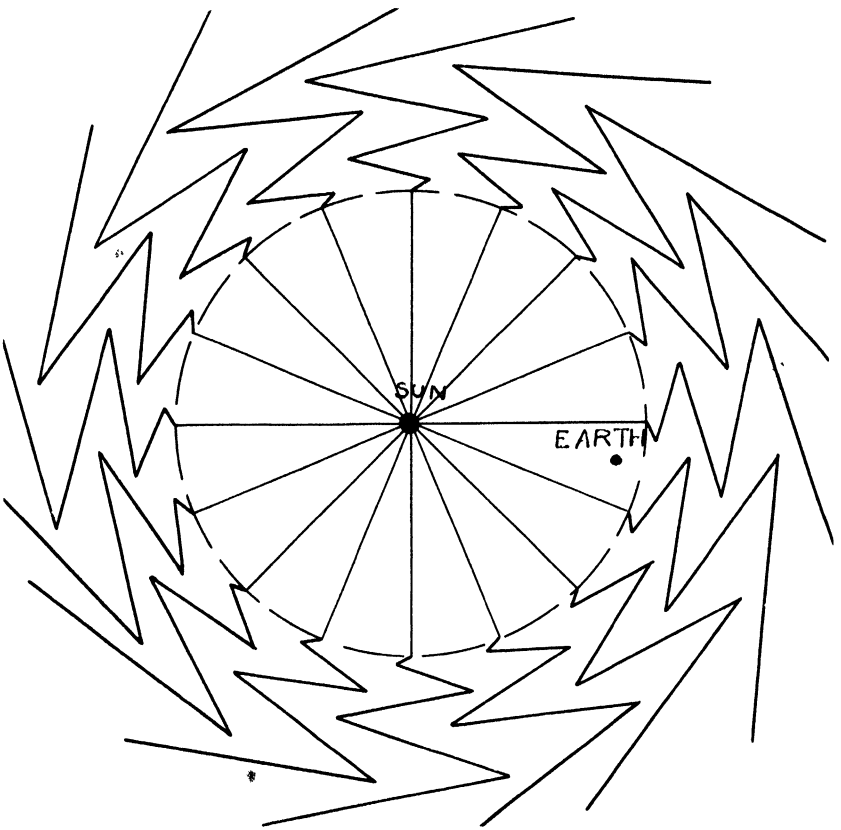

FIG. 2. Schematic diagram of the shell of disordered field enclosing the smooth radial field of the inner solar system. Solar rotation has been neglected.

required by the cosmic-ray observations, is just the region of instability in the radial solar field.

Obviously there are many possible variations on the simple spherical model which we imply here. For instance, if we have a smooth radial field inside the disorganized shell, then cosmic-ray particles cannot get across the radial field easily from their origin in flares near the solar equatorial plane, and it is not necessary, so far as the cosmic-ray observations are concerned, that the shell extend over the poles of the sun.

Such a model is not unreasonable when we remember that the radial

field, consisting of the extended solar dipole field, vanishes on the equatorial plane of the sun. And in the limit as $B \to 0$ we have instability no matter how small the anisotropy may be. Thus instability, and disordering, would be most likely in the vicinity of the equatorial plane, particularly if our rough numerical guesses have greatly overestimated the degree of anisotropy.

We should note, while we are mentioning the radial field vanishing on the equatorial plane, that once the onset of instability occurs, there will of course no longer be a field-free plane through which cosmic-ray particles might easily escape from the inner solar system.

Finally, in closing, we shall consider the possibility that the outward-streaming gas has radial velocities of only 100, rather than 1000 km/sec, as has sometimes been argued. If the density is as low as 5 ions/cm^3, then the degree of anisotropy, $(P_s - P_n)/P = v_m\tau/r$, is essentially unaltered. But we find from Eq. (2) that the magnetic field is now tightly coiled, and 1 gauss at $r = R$ yields 20×10^{-5} gauss at the orbit of the earth. $B^2/4\pi$ is now large compared to $P_s - P_n$, and no instability and no disordered shell are to be expected. Thus neither can we account for the prompt arrival of cosmic-ray particles from solar flares because the field is not radial, nor can we account for their subsequent slow decay. We suggest, therefore, that at least during years of solar activity, the high velocities suggested by Biermann are present in the inner regions of interplanetary space together with the radial field and the disordered shell.

REFERENCES

1. L. Biermann, Z. Astrophys. **29**, 274 (1951); Z. Naturforsch. **7a**, 127 (1952); Observatory **107**, 109 (1957).
2. H. W. Babcock and H. D. Babcock, Astrophys. J. **121**, 349 (1955).
3. L. Davis, Phys. Rev. **100**, 1440 (1955).
4. E. N. Parker, Phys. Rev. **107**, 830 (1957).
5. E. N. Parker, Astrophys. J. (submitted).
6. E. N. Parker, Phys. Rev. **107**, 924 (1957).
7. S. Chandrasekhar, A. N. Kaufman, and K. M. Watson, Ann. Phys. (in publication).
8. E. N. Parker, Phys. Rev. (in publication).
9. J. A. Simpson, Suppl. Nuovo Cim. (in publication).
10. P. Meyer, E. N. Parker, and J. A. Simpson, Phys. Rev. **104**, 768 (1956).

SECTION 3

HIGH-SPEED FLUID DYNAMICS

EXPERIMENTS USING A HYDROMAGNETIC SHOCK TUBE*

VERNON H. BLACKMAN† AND BRYAN NIBLETT‡

Two methods for producing high-velocity plasmas in a low-density gas have received considerable attention recently. Kolb[1] at NRL, as well as the group at Lockheed,[2] has carried out studies with a T-type discharge tube similar to that originally used by Fowler. In this geometry, the current discharge in the tube is drawn between metal electrodes, and the return current is directed so as to produce a Lorentz force on the spark plasma.

Another method of producing currents which can then lead to an interaction with an external magnetic field and resultant forces on the gas is to induce an electrodeless discharge in the gas.[3] An attractive advantage of this technique is the possibility of obtaining plasmas without electrode contamination. In order for this approach to work, the electric field induced by a rapidly varying magnetic field must be strong enough to cause a breakdown in the gas, and the induced current loops must be closed in the gas, thus eliminating the need for electrodes. To produce such a field, the geometry indicated in Fig. 1 was used at Princeton University. A low-inductance condenser is discharged through a single-turn copper coil wrapped about a glass tube. The induced E field is in the tangential (θ) direction and, as shown by Fig. 2, has its maximum value at the surface of the glass tube. The electric field (about 900 volts/cm maximum for most of the work reported here) was sufficient to cause an electrodeless breakdown in argon for pressures from the micron region up to 50 mm while in air the upper limit for breakdown was about 10 mm.

The gas breaks down initially at the walls of the tube and implodes inward; then high-velocity plasma is observed to propagate outward in

* This work was supported by ONR and performed at Princeton University.

† Now at Giannini Research Laboratory.

‡ Now at United Kingdom Atomic Energy Authority.

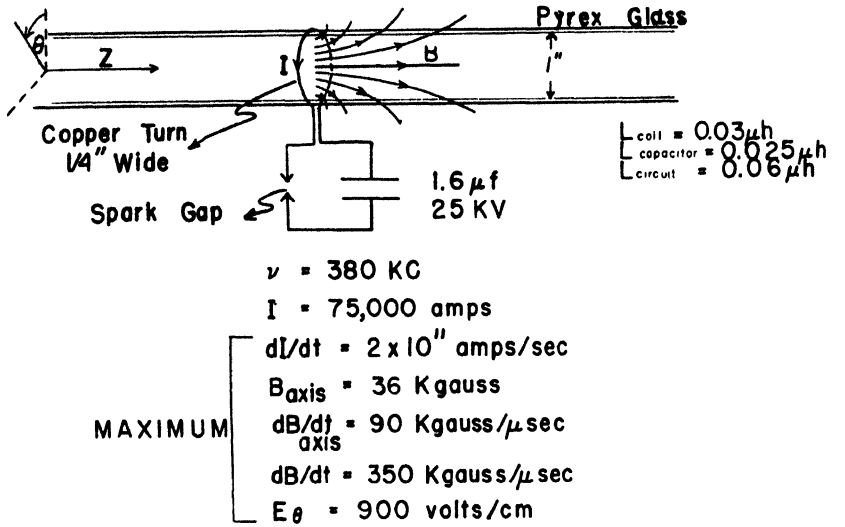

FIG. 1. Schematic diagram of apparatus for producing high-velocity plasmas

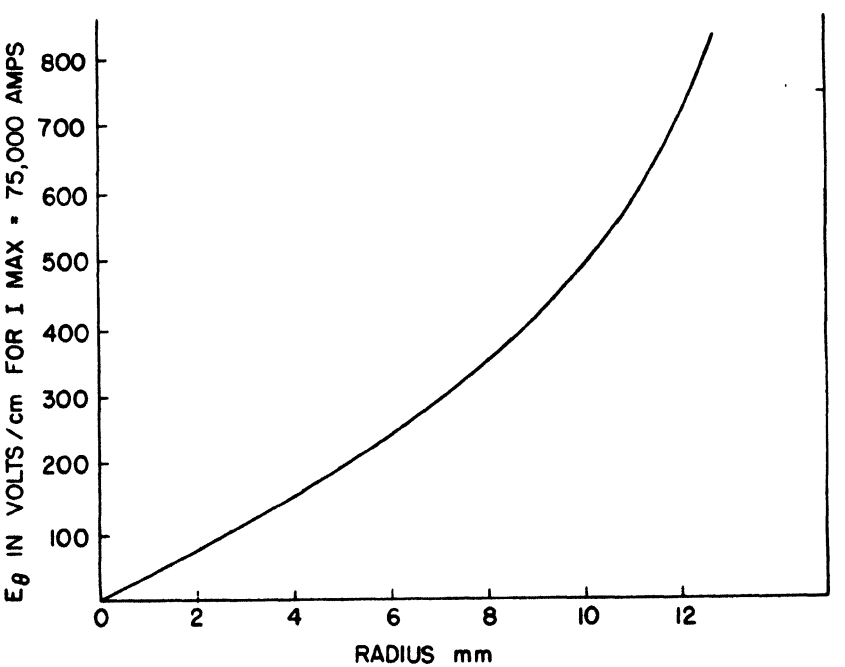

FIG. 2. Dependence of induced electric field on radial position in the plane of a circular loop of 1.5 cm radius at a ringing frequency of 380 kc/sec.

both directions from the plane of the coil. Rotating drum photographs have been used to measure the velocity and attenuation of the plasma as a function of distance from the coil. Photographs taken with a slit perpendicular to the direction of the shock propagation show that the shock becomes plane within about three tube diameters. Typical streak photographs are shown in Fig. 3.

A series of measurements were carried out to study the breakdown process and the relation between electric field strength and gas pressure at the onset of breakdown.* The electric field induced in the gas was varied by changing the charging voltage on the condenser while the inductance remained constant. A number of tests were conducted for each pressure and the reproducibility of breakdown was reasonably good. The results for air are shown in Fig. 4. It can be seen that the minimum breakdown field for a frequency of 380 kc/sec occurs at a pressure of about 0.3 mm Hg pressure and at a field strength of about 380 volts/cm. The experimental error in both field and pressure readings was about 12 percent for each point. For comparison, the results for breakdown in air for DC fields between metal electrodes as given in Meek and Craggs have also been included. It is only possible to make an order of magnitude comparison between these graphs because the Townsend theory, rather than the diffusion criterion, determines the breakdown pressure limit of a gas between metal electrodes. Some points were also taken in argon and helium at higher pressures and these measurements agreed fairly well with the curves of Meek and Craggs and also Schumann.

The delay between the initiation of the external current and the gas breakdown in the tube was also determined. The light from the spark gap was viewed with a photocell which triggered an oscilloscope and the light from the tube discharge was picked up with another photocell and viewed on the trace. The time lag for light to appear in the tube after the condenser discharge started was 1.3 μsec, just half of the 2.6 μsec period of a full oscillation. Thus, most evidence showed that in this setup for the given discharge conditions, the gas breaks down on the second half of the first cycle. When the same experiments were repeated at near-critical pressure the tube took a full cycle to break down.

Since this method can produce relatively plane shock waves of moderate strength ($M = 10$–30) at a distance of 10 to 20 cm from the coil, studies were undertaken to determine the ionization times of various gases. Photographs taken with the streak camera record the motion of

* The authors are grateful to Mr. John Wells for assistance with these measurements.

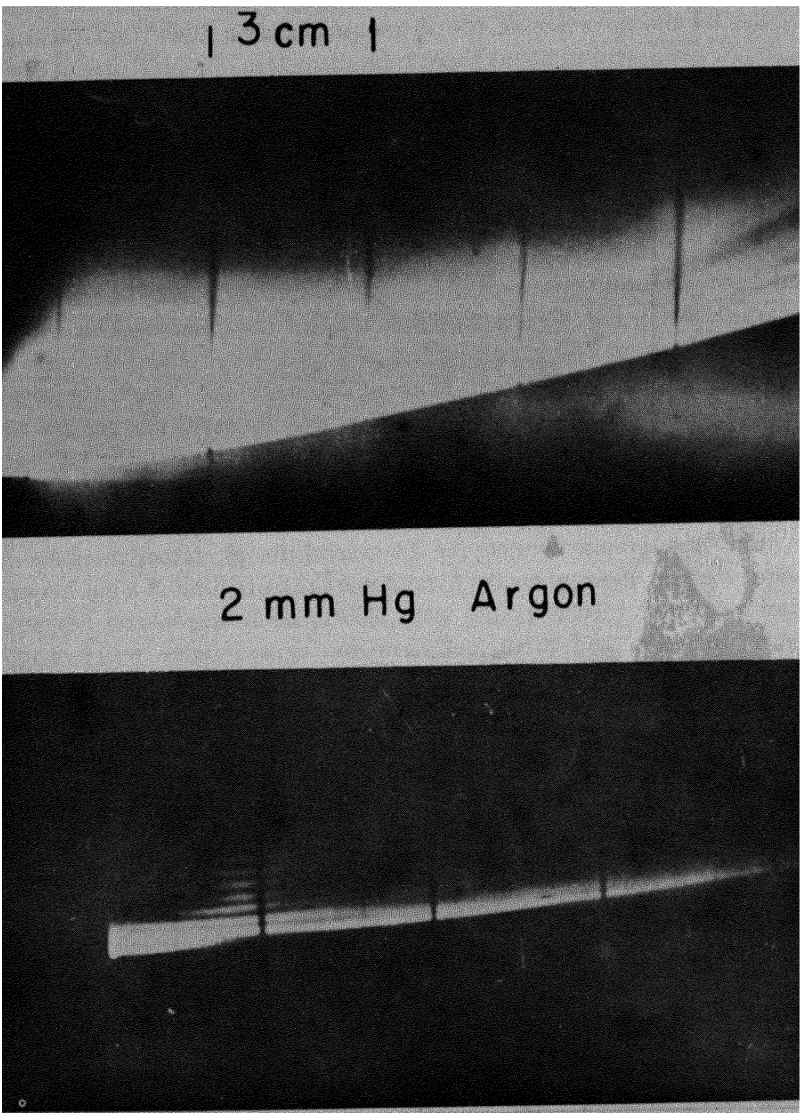

FIG. 3. Typical streak camera photographs; time is vertical and distance horizontal

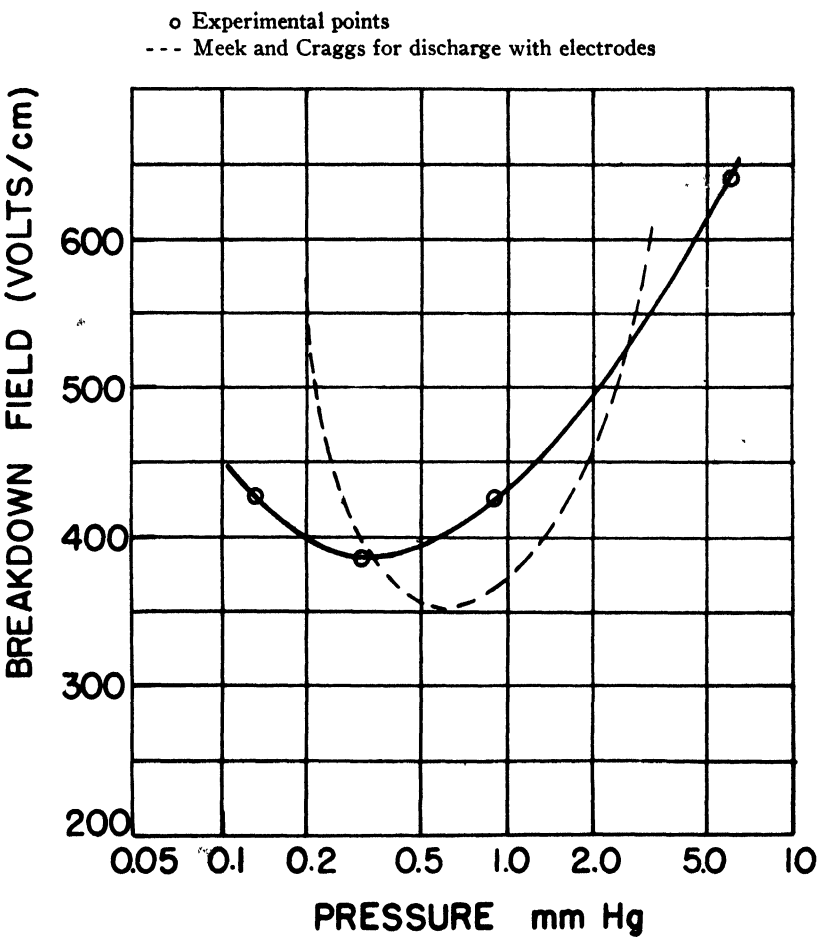

FIG. 4. Dependence of breakdown field strength on gas pressure at a frequency of 380 kc/sec.

the luminosity behind the shock wave since the shock front itself is not visible on the photographs, and this luminosity is observed experimentally to have a sharp front. For the noble gases the luminous front is taken as coincident with the point at which ionization equilibrium is attained.[4] The ionization time is very short for strong shocks and the luminous front and the shock front are coincident, but as the wave decays the shock front draws progressively further ahead of the luminosity; the intermediate dark space is the region in which the gas "relaxes" to its equilibrium condition.

The essential problem, therefore, is to determine on each film the locus of the shock front. The position of the shock front was determined by reflecting the wave from the plane face of a one-inch-diameter metal slug placed in the tube at appropriate distances from the coil. When the shock wave is reflected from the face of the slug the enthalpy of the gas is approximately doubled and the ionization time is decreased by a factor of five or more. Thus an error of 20 percent or less is incurred by assuming the reflected shock and luminous front to be coincident.

A series of shocks were fired into argon at forepressures between one and two millimeters of mercury and the reflecting slug was placed at varying distances from the coil in order to vary the Mach number of the incident shock at reflection. Typical reflection photographs are shown in Fig. 5; the reflected shock, appearing earlier in time than the incident luminous front, can be seen clearly for the shocks in argon and air but not

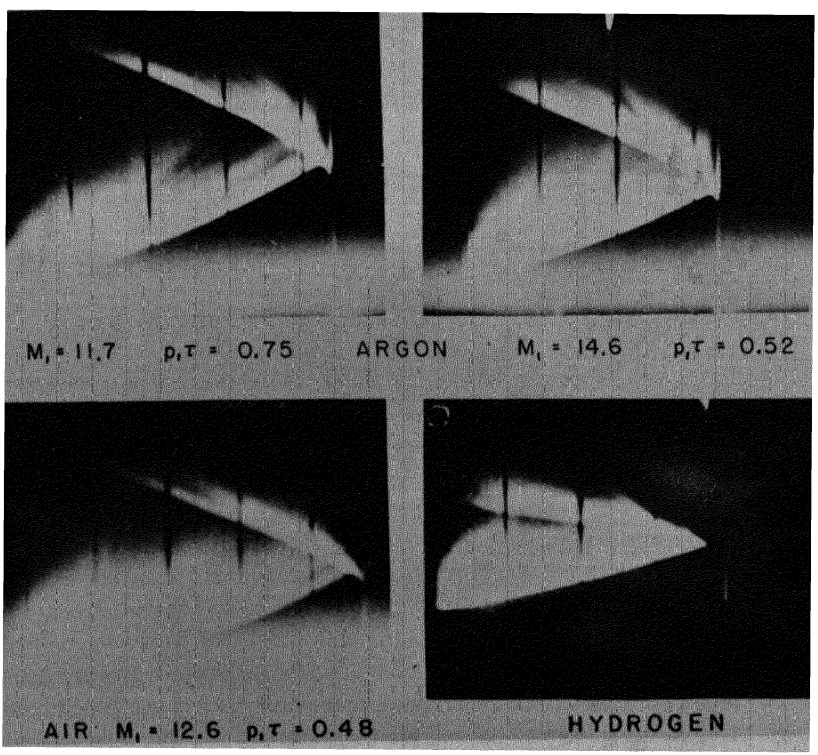

FIG. 5. Reflection photographs showing the reflected shock appearing as a spike for argon and air. Values of $p_1\tau$ are in cm Hg-usec.

in hydrogen. If a series of pictures are taken with the same gas pressure and the same capacitor voltage the streak records can be accurately superimposed and a "master" diagram constructed showing the locus of the luminous front and the shock front. Such a master diagram is shown as Fig. 6. The Mach number of the shock can be obtained from the angle α

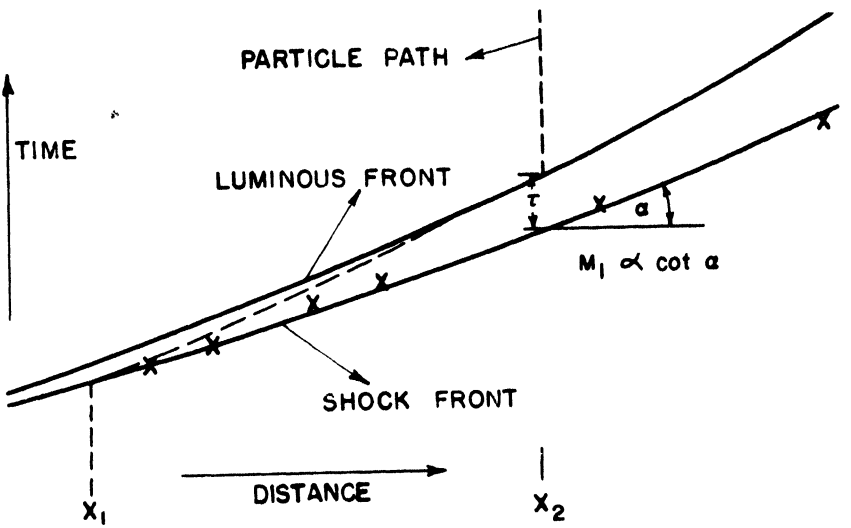

FIG. 6. Diagram indicating the method of evaluating ionization times from streak photographs.

and the film speed, and the distance τ along the time axis is a measure of the ionization time. This measured time τ must be multiplied by the mean density ratio across the shock to give the true ionization time.

The results for argon are plotted in Fig. 7 in terms of $\log p_1\tau$ versus $1/T_{A0}$, where p_1 is in centimeters of mercury and τ is in microseconds. The temperature immediately behind the shock front is T_{A0}. These argon measurements are compared with the more extensive and accurate results by Petschek and Byron.[4] Agreement is reasonably good for short ionization times, but increasingly poorer for longer times.

The most serious source of error is the attenuation of the incident shock. The gas sample which reaches equilibrium ionization at a distance x_2 from the coil (see Fig. 6) passed through the shock further upstream at a distance x_1 where the Mach number was greater. The Mach numbers quoted in this work are thus too low and represent minimum values.

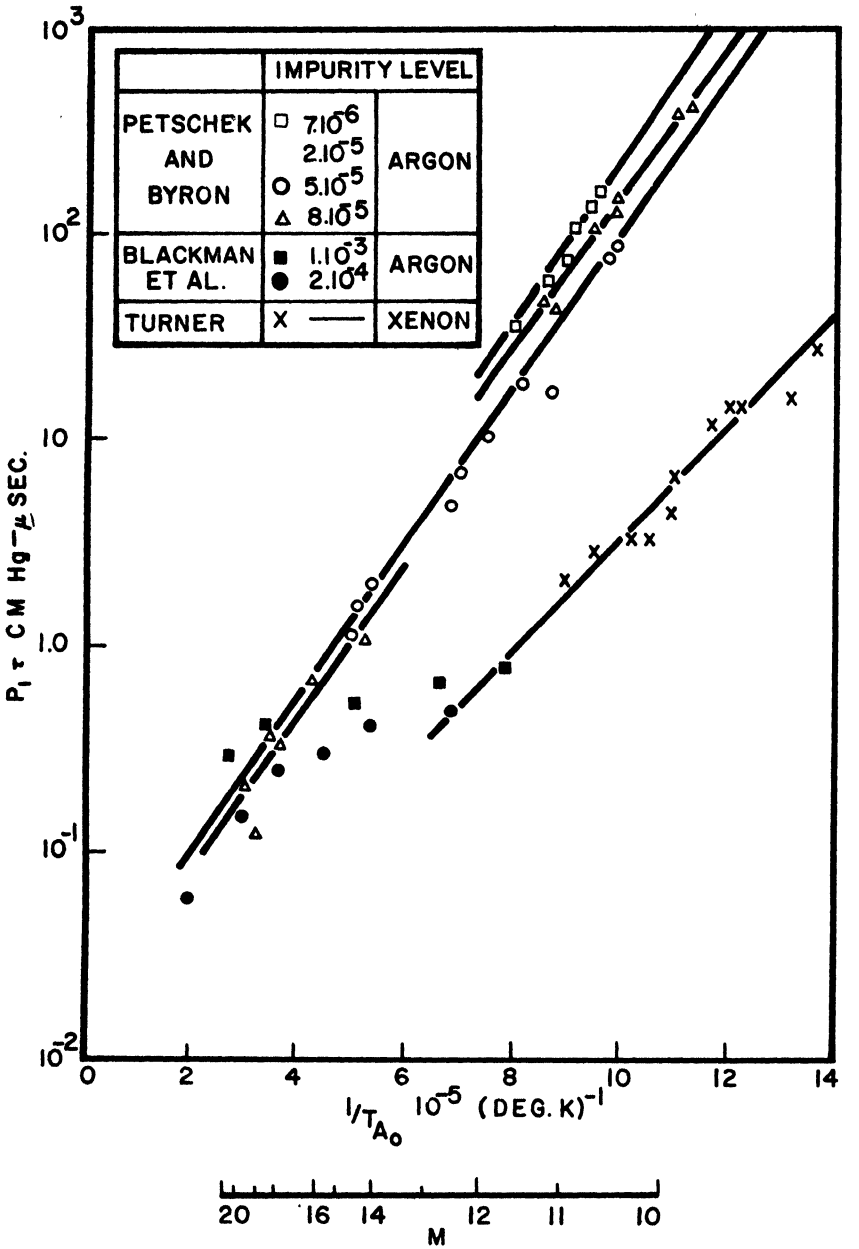

FIG. 7. Results of ionization time measurements for argon

For the range of ionization times over which there is reasonably good agreement between the measurements for argon reported here and the previous results of Petschek and Byron, the time lag of the luminous front in air has also been measured. A typical streak photograph of a shock reflection in air is also included in Fig. 5. The results are plotted in Fig. 8 as log $p_1\tau$ versus Mach number, where once again the Mach number given represents a minimum value. The experimental points fall roughly on a straight line when plotted in this manner.

It is believed that the radiation is produced mainly by processes which involve free electrons. This assumption seems reasonable since in the range of photographic sensitivity the radiation is produced principally by oxygen free-free and oxygen free-bound transitions together with nitrogen

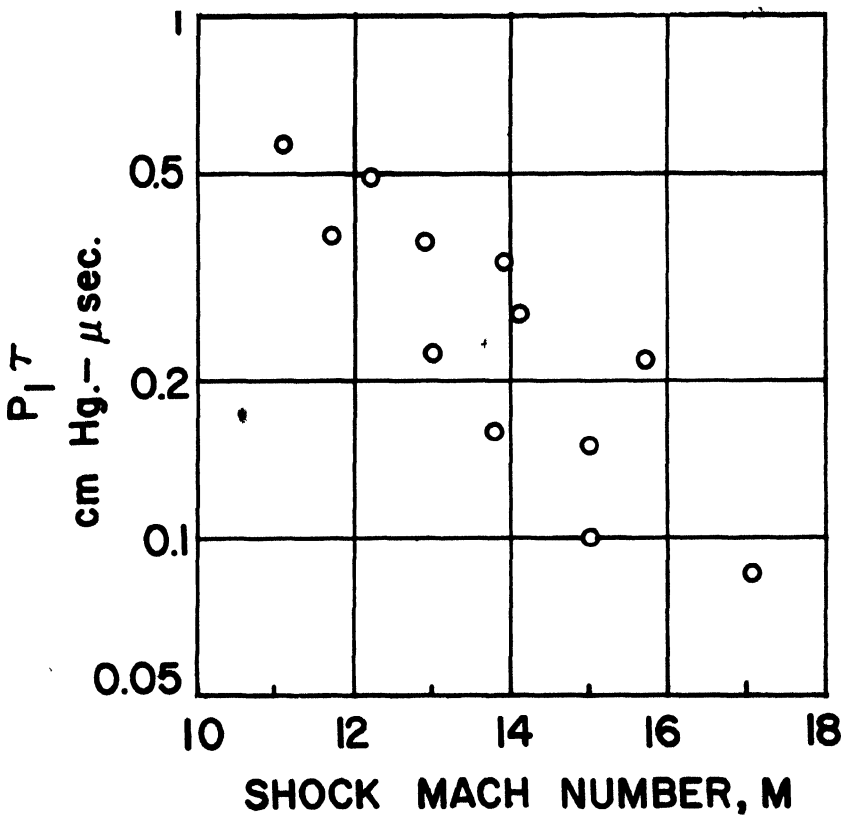

FIG. 8. Results of ionization time measurements for air

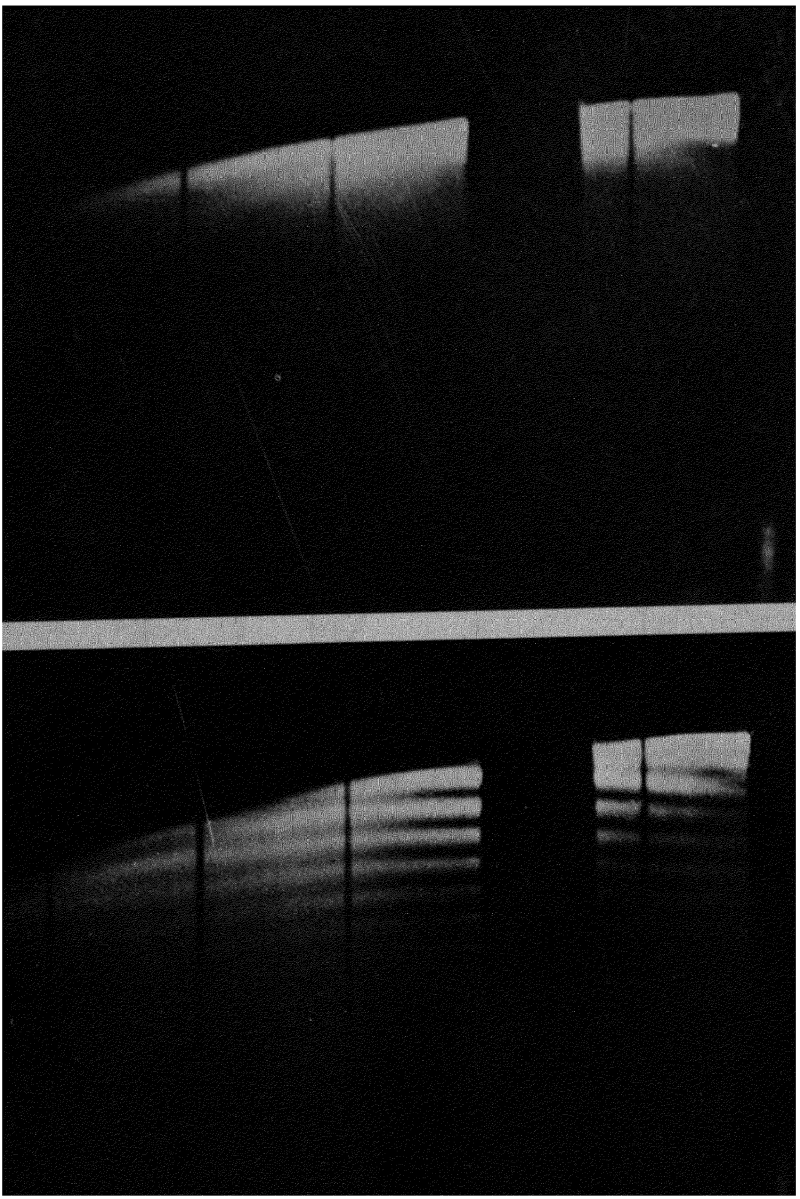

FIG. 9. Shock wave moving into a "magnetic funnel": field is zero in the upper picture.

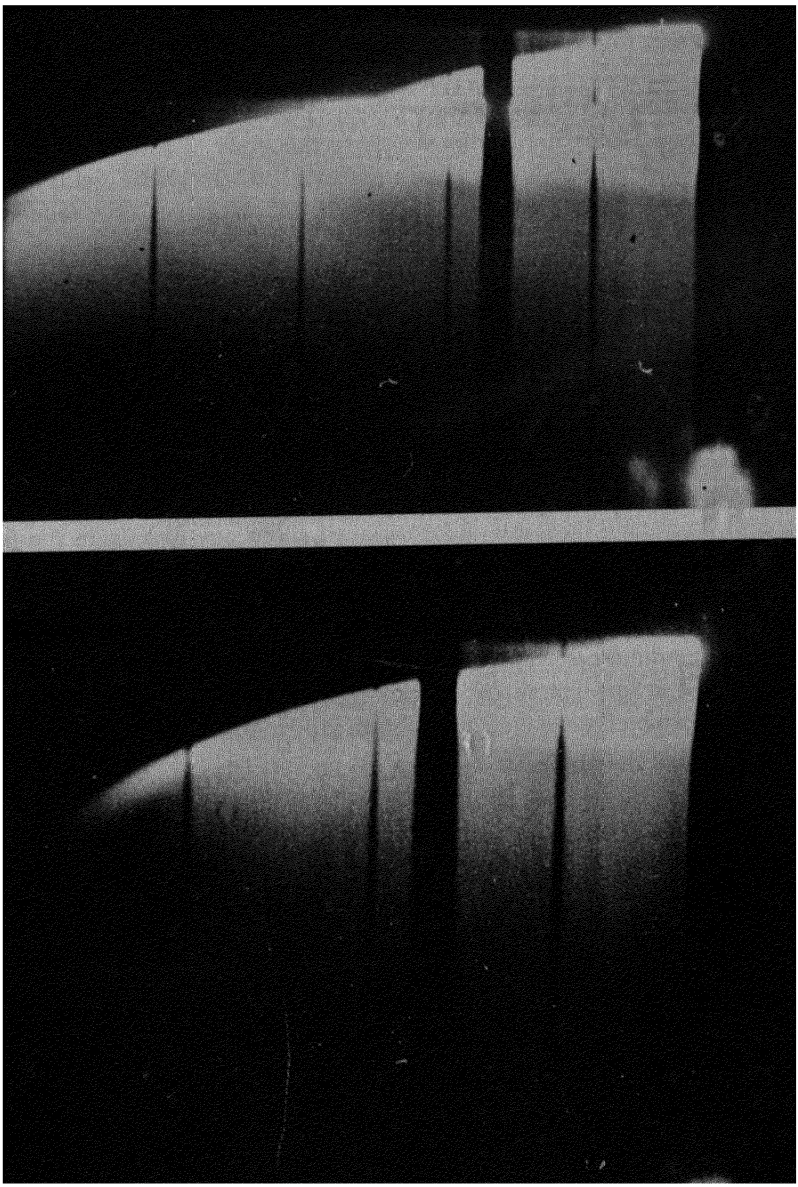

FIG. 10. Two identical coils; the left one to produce a shock and the right one to attempt accelerating it: in the upper picture,only the left-hand coil is fired; in the lower, the right-hand coil is fired an instant later.

band spectra which are likely to be excited by free electrons.[5] Thus the luminous front is taken to be coincident with the ionization front and the times given in Fig. 8 represent approximate values for the ionization time in air.

This method of producing high-velocity plasmas, utilizing an electrodeless discharge, lends itself immediately to the study of shock interactions and the interaction of high-velocity plasmas with magnetic fields; additional coils can be put about the tube and fired in various time sequences to study such effects.

In one experiment a shock from a single turn coil was allowed to pass through the magnetic field of an adjoining twenty-turn axially symmetric coil. Streak photographs, taken through a slit on the axis of the tube, indicate that there was no noticeable change in the shock speed as it moved through the field region. Figure 9 shows such a streak photograph. The slowly varying magnetic field due to the twenty-turn coil puts energy into the ionized gas behind the incident shock at each half cycle.

Attempts were made to push the plasma behind the incident shock by means of a second one-turn coil positioned about one inch from the first coil. Figure 10 shows a photograph of an attempt to accelerate the shock by means of magnetic forces exerted by the buildup of current in the second coil. In this case the incident shock wave was allowed to progress about two centimeters beyond the second coil before this coil was triggered. No increase in incident shock velocity could be noted until the secondary shock, formed by the second coil in the already ionized gas, caught up with the incident shock.

REFERENCES

1. A. C. Kolb, Phys. Rev. 107, 345–50 (1957).
2. S. W. Kash, "Experiments at Lockheed Missile Systems Division," Magnetohydrodynamics. Stanford Univ. Press (1957).
3. H. E. Petschek, "Experiments at AVCO," Magnetohydrodynamics. Stanford Univ. Press (1957).
4. H. E. Petschek and S. Byron, Annals of Phys. 1, 270–315 (1957).
5. J. C. Keck, E. Kivel, and T. Wentink, Jr., "Emissivity of High Temperature Air," AVCO Research Report No. 8 (1957).

VELOCITY MEASUREMENTS IN MAGNETICALLY DRIVEN SHOCK TUBES

S. W. KASH, J. GAUGER, W. STARR, AND V. VALI*

In magnetically driven shock tube systems, the discharge is arranged in such a manner that the strong magnetic fields induced by the discharge current are used to impart energy or motion to the gas in the discharge region. Such systems provide a means of producing relatively high-temperature ionized gases, and should be useful for the studies of the properties of these gases. To determine the temperatures obtainable with air, a series of shock pulse velocity measurements were made over a range of densities.

Two somewhat different shock tube systems employing internal electrodes were used. One system was similar to the T-type employed by Fowler[1] and Kolb,[2] in which the electrodes are mounted perpendicular to the axis of the shock tube section. In the second system the electrodes were mounted concentric with the axis of the shock tube to form a conical or funnel discharge volume. In both systems the electrodes were mounted at one end of the shock tube section and the firing of the discharge initiated shock pulses which traveled down this section. Neither system was electrically damped. The discharge in the T-tube initiated a series of pulses which interacted as they advanced down the shock tube section. The funnel discharge apparently initiated a single shock pulse.

MEASUREMENTS WITH THE T-TUBE SYSTEM

The T-tube system consisted of a pyrex tube with nickel electrodes in short side arms perpendicular to the axis of the main tube (see Fig. 1). The electrodes were attached to a low-inductance capacitor through an air spark gap. To minimize the inductive leads the electrodes were mounted vertically over the center of the condenser. A backstrap (the lead connected to the upper electrode) was passed directly behind the discharge tube. The spark gap was triggered by an induction coil. The electrical

* Lockheed Missile Systems Division.

quantities of the system were as follows: condenser capacitance 1.1 μf, condenser inductance 0.04 μh, circuit inductance 0.26 μh, applied voltage 28 kv, discharge ringing frequency 300 kc.

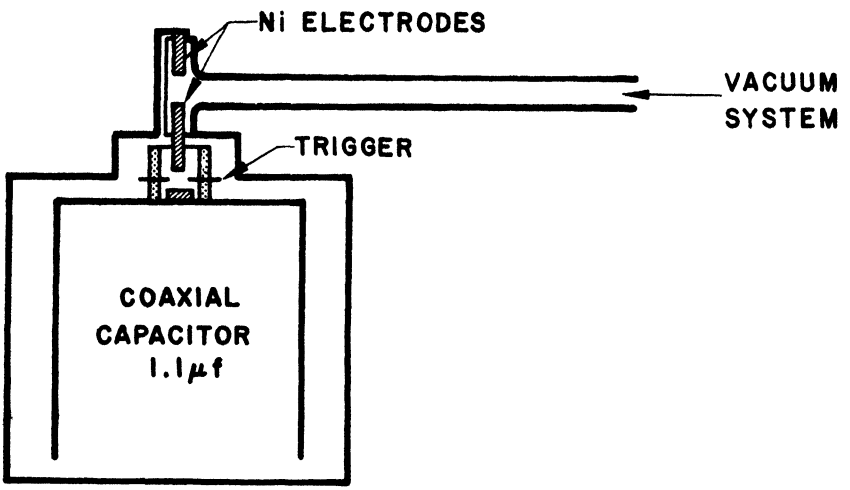

FIG. 1. Schematic diagram of T-tube system

Most of the T-tube data were taken with photocells, which were mounted at different positions along the shock tube. Figure 2 shows a typical oscillogram obtained from one of the photocells. In addition to the first shock pulse a series of secondary pulses can be clearly seen. The gas for the secondary pulses is very likely obtained from gas left over in the neighborhood of the discharge plus additional material volatilized off the electrodes and nearby walls during the discharge.

Two different tube diameters were used for the shock tube section, one $1\frac{1}{16}$ in. i.d., the other $\frac{5}{16}$ in. i.d. Data obtained with the first of these two shock tubes are presented in Fig. 3. Here the time for the first luminous pulse to reach a given photocell station is plotted as a function of pressure. The pressure was varied from 0.1 to 100 mm Hg and photocells were stationed at 10, 20, and 30 cm from the discharge. The curves show the effects of energy attenuation and interaction of the first pulse with the secondary pulses. Note in the $1\frac{1}{16}$-in. i.d. curves the absence of a datum

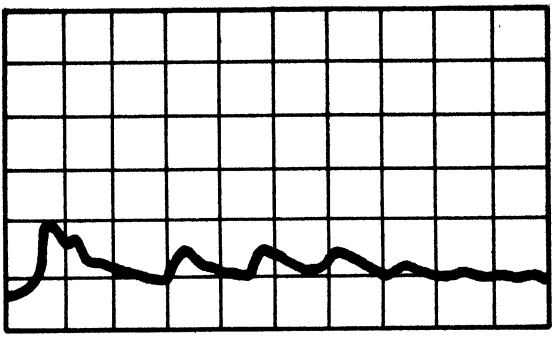

FIG. 2. Photomultiplier oscillogram: pressure, 0.1 mm Hg; sweep speed, 5 μsec per division. (Retouched.)

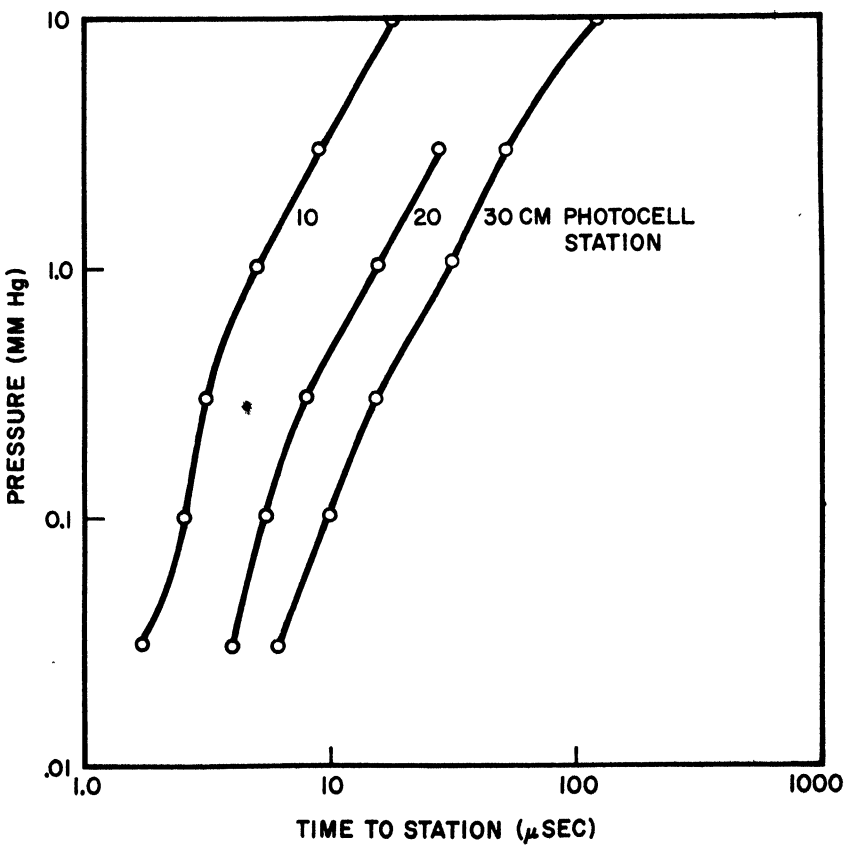

FIG. 3. Position-time data for the 11/16-in. T-tube

point at the 20 cm station. Apparently by the time the first pulse reached the 20 cm station, attenuation had reduced its luminosity below detection. However, somewhere between the 20- and 30-cm station the second shock pulse overtook the first pulse augmenting its energy and making it luminous again. Above 10-mm pressure for the $^{11}/_{16}$-in. tube no luminosity was detected at the photocell stations; luminous pulses were detected, however, up to 100-mm pressure in the $^{5}/_{16}$-in. tube. Although the attenuation of the first shock pulse is greater in the smaller diameter tube, its decrease in energy is offset by the secondary pulses catching up with it, increasing its energy and thereby providing luminous pulses at the higher pressures.

At the relatively low pressures employed in these measurements only a small amount of electrical energy is delivered to the gas by resistive heating. Previous measurements[3] have shown the importance of magnetic fields produced by the discharge for imparting energy and motion to a gas. Since the gas remains in the neighborhood of the electrodes for only a short time, large discharge currents are needed to obtain the strong magnetic fields to accelerate the gas. It is therefore important to minimize the inductance of the discharge circuit. The velocities obtained in the present series of measurements are essentially equal to those obtained with the earlier system using higher inductance condensers. This was achieved with only 430 joules stored in the condenser instead of 1600 joules required previously. In both cases the magnitude of the discharge current was about 2×10^4 amp, the higher capacitance and voltage of the first condensers being offset by their considerably larger inductance.

An estimate of the energy in the first shock pulse can be obtained from one-dimensional strong blast theory. Assuming no energy losses by radiation or conduction to the walls, one has the following relation:

$$x^{3/2} = \frac{3}{2}\int_0^t \left(\frac{\gamma' + 1}{2}\right)\left(\frac{W}{\rho_0}\right)^{1/2} dt, \tag{1}$$

where x is the position of the shock pulse at time t, W is the energy per unit area in the shock pulse (i.e., the total energy imparted to the gas by the discharge), ρ_0 the density in the gas ahead of the shock pulse, and γ' the effective ratio of specific heats.

For a partially dissociated gas γ' varies but only mildly. If it is assumed to be constant, integration of Eq. (1) leads to the relation

$$W = \frac{4}{9}\left(\frac{2}{\gamma' + 1}\right)^2 \frac{\rho_0 x^3}{t^2}. \tag{2}$$

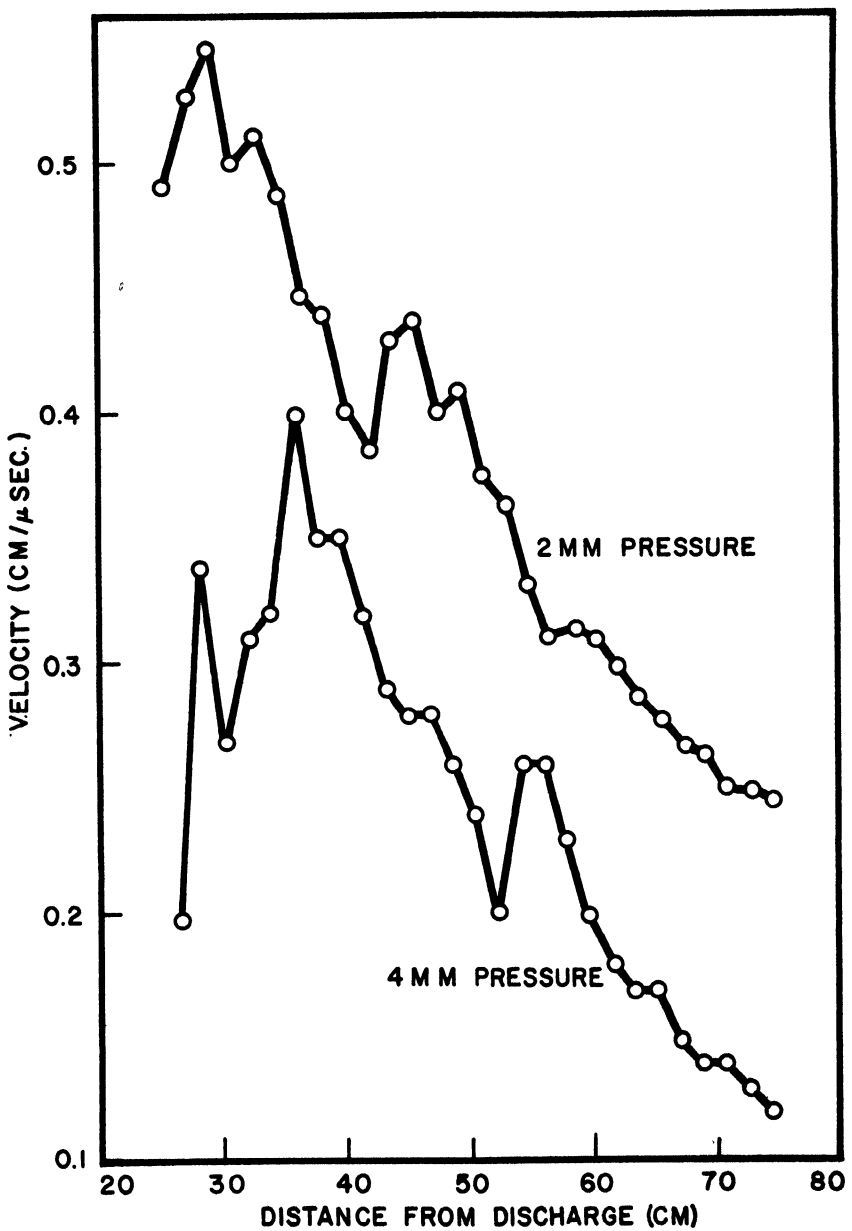

FIG. 4. Velocity in T-tube obtained by microwave reflection.

Figure 4 shows the velocity vs. position as obtained by microwave reflection. The fluctuations in the curves result from a combination of energy attenuation as the first pulse proceeds down the shock tube and energy augmentation as the subsequent pulses catch up with the first one. On the average the velocity decreases more rapidly than the $x^{1/2}$ law which follows from Eq. (2), indicating considerable energy loss as the shock pulse advances down the tube.

MEASUREMENTS WITH THE CONICAL ELECTRODE SYSTEM

The second magnetically driven shock tube system employed axially symmetrical electrodes at one end of the shock tube section. The central electrode and outer electrode were separated by a Teflon insulator and were shaped and spaced to form a funnel discharge region. The details of these electrodes are shown in Fig. 5. The outer electrode was folded back over

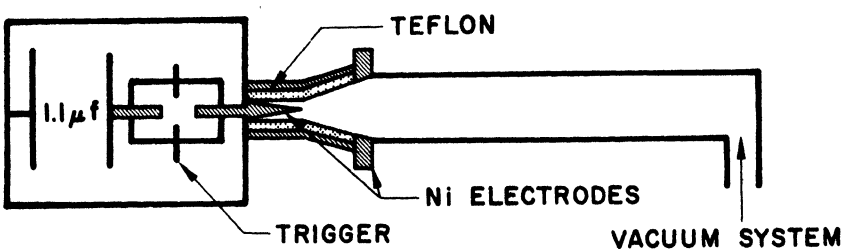

FIG. 5. Schematic diagram of conical electrode system

the conical section so as to confine the magnetic field to the region of the discharge and reduce the inductance of the system. With this arrangement the entire system, from the electrodes through the spark gap to the condenser, was coaxial. The total inductance of the system was 0.085 μh, of which about half was in the condenser. The capacity of the condenser was 1.1 μf and it was charged to 30 kv. The ringing frequency of the system was 520 kc. The inside diameter of the shock tube section was 2 in.

Most of the velocity measurements for the funnel electrode system were made with an electronic camera (image converter), with which a set of five distinct pictures of the gas luminosity could be obtained. The

exposure time per frame could be varied from 0.02 to 0.5 μsec; the time between frames could be varied from 0.5 to 25 μsec. The image converter was triggered by a photocell looking along the axis of the shock tube.

The position-time data obtained on the funnel system could be represented by the simple relation $t = ax^n$.

In Fig. 6 it can be seen that n decreases with decreasing pressure, ap-

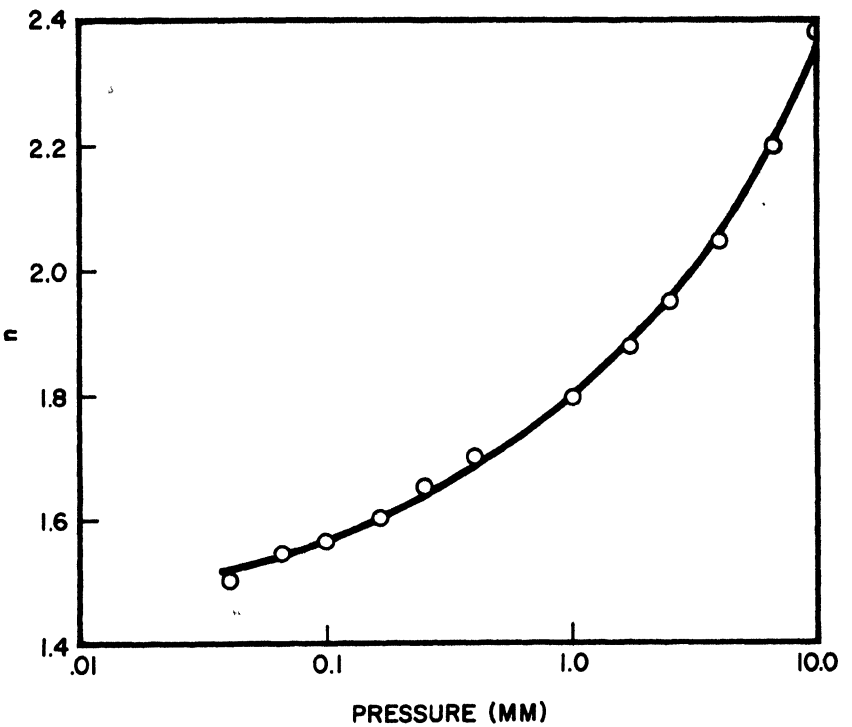

FIG. 6. Exponent of the power law relation used for fitting position-time data

proaching the value 1.5 at the lower pressures, showing that the energy attenuation per unit length of shock pulse travel decreases as the pressure is lowered. Figure 7 presents a plot of the quantity $\rho_0 x \dot{x}^2$, which is very nearly equal to the energy in the shock pulse, as a function of position at each pressure. The values for x and $\dot{x}$ were obtained from the relation $t = ax^n$. This figure again illustrates that the energy attenuation per unit distance traveled increases with pressure.

In order to give some idea of the temperature range obtained in these measurements, the temperature in the shocked gas has been plotted in

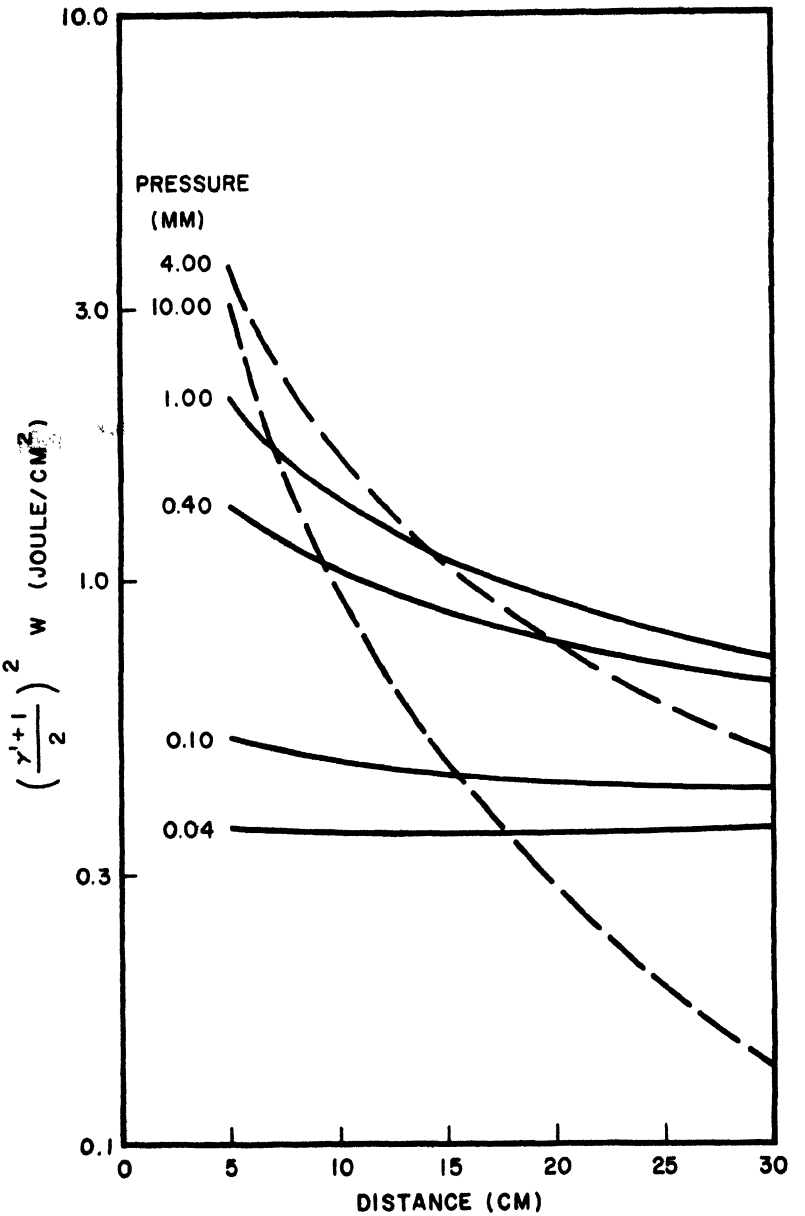

FIG. 7. Energy in the shock pulse

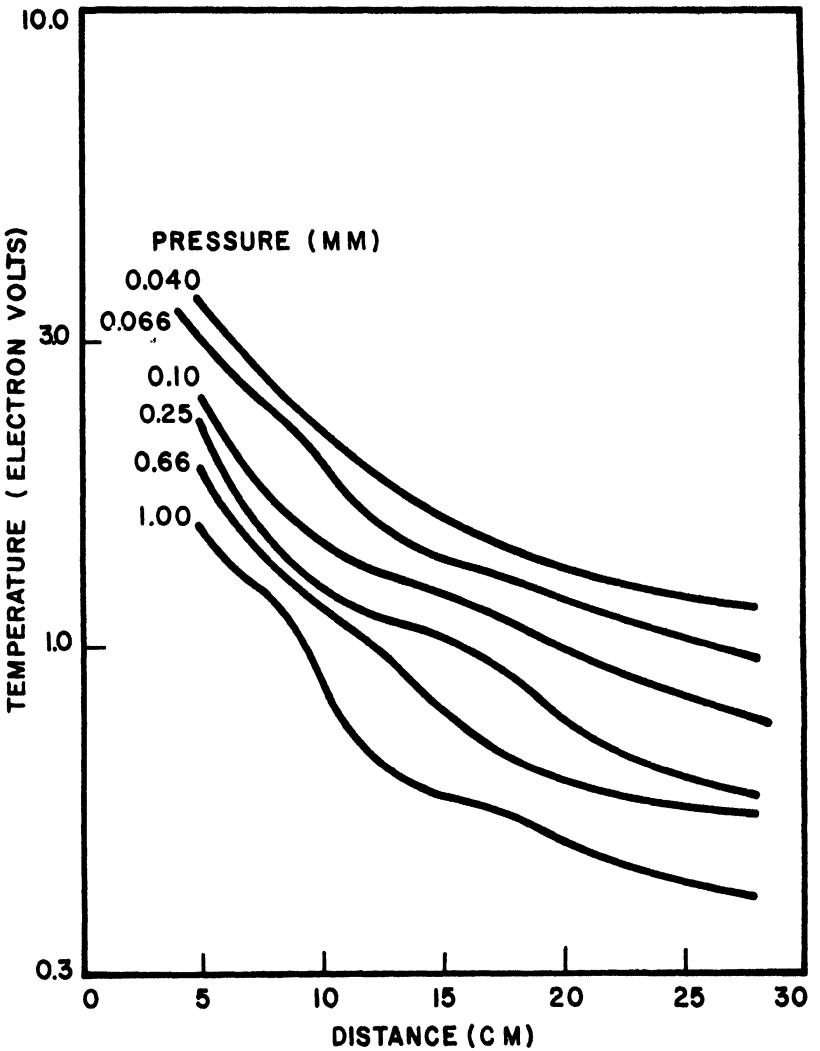

FIG. 8. Temperature in the shock pulse

Fig. 8 as a function of position and pressure. For these curves the temperature was obtained from the strong shock relations, using the data presented by Gilmore[4] and velocity values obtained from the relation $t = ax^n$. The effective ratio of specific heats γ' was also obtained from the strong shock relations, and was found to vary between 1.10 and 1.15. Accordingly, 75 to 90 percent of the non-flow energy in the gas was in dissocia-

tion and ionization. The wiggles shown in the curves of Fig. 8 reflect variations of γ' in this temperature range.

The measurements with the funnel system gave no evidence of any secondary pulses. The first surge of discharge current apparently drives out most of the gas in the funnel. Observation on the erosion of the central electrode supports the hypothesis that the funnel discharge is cylindrically symmetric. After a series of discharges the conically tapered electrode took on a symmetrical hollow-ground appearance. Other discharge firings with a smooth spherical electrode produced a symmetrical dimple at the center of the electrode.

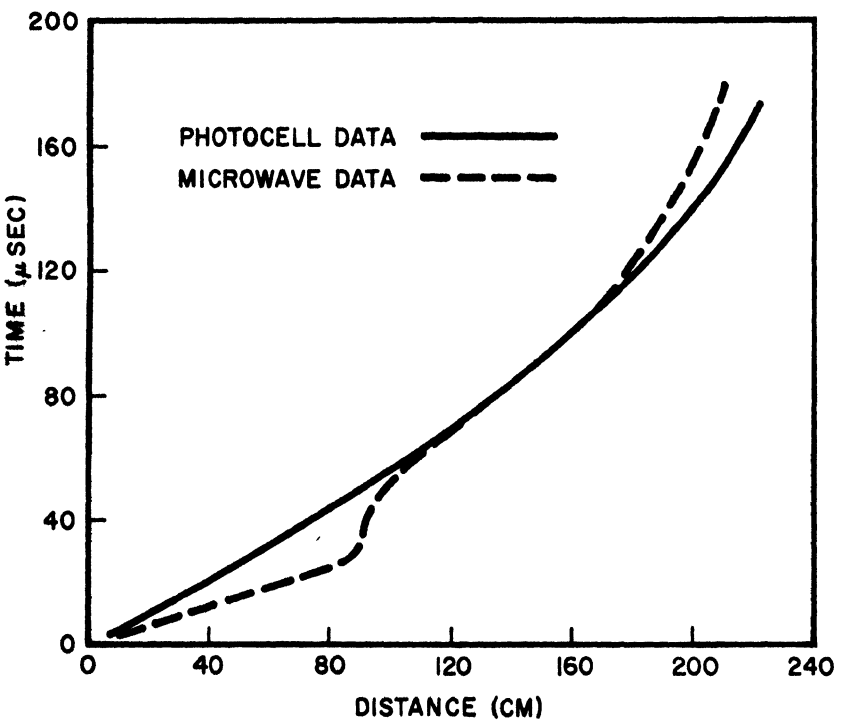

FIG. 9. Comparison of photocell and microwave position-time data

In another set of velocity measurements the funnel system was modified to provide a considerably longer shock tube section. For this purpose the coaxial section leading from the condenser was bent 90° so that the axis of the shock tube was now horizontal and a shock tube section of about three meters was attached to the system. The spark gap was eliminated,

thereby compensating for the inductance added by the longer coaxial section between the condenser and the electrodes. To produce a discharge, the full condenser voltage (for these measurements 30 kv) was applied directly to the electrodes and the discharge was initiated by slowly leading air into the system. With this arrangement the pressure at which the discharge fired could not be controlled very well; the firings usually occurred between 20 and 100 microns. The displacement-time measurements were made with microwave reflections and with photomultipliers. A comparison of the two sets of measurements for a pressure of 20 microns is shown in Fig. 9. At first the microwave positions lead those of the photocell, then the two sets of measurements agree, and finally the microwave positions lag behind the photocell positions. If the shock velocity obtained from the microwave measurements is plotted against position or time, it would appear that the shock pulse undergoes a rapid deceleration followed by a rapid acceleration. Since it is difficult to explain such behavior, one is strongly inclined to accept the photocell position-time data as a reference and seek other explanations for the microwave data. The region where the microwave measurements lead the photocell measurements might be explained by assuming pre-ionization in the gas ahead of the shock by either ultraviolet radiation or electrons emanating from the discharge itself. In this region the velocity is approximately constant, whereas beyond it follows the relations $t = ax^{3/2}$ reasonably well. The region where the microwave measurements lag behind the photocell measurements might be explained by assuming that the ionization had dropped sufficiently so that the microwave signals were beginning to penetrate the gas.

REFERENCES

1. R. G. Fowler, W. R. Atkinson, W. D. Compton, and R. J. Lee, Phys. Rev. **88**, 137 (1952).
2. A. C. Kolb, Phys. Rev. **107**, 345 (1957).
3. R. K. M. Landshoff, in Magnetohydrodynamics. Stanford University Press, 1957.
4. F. R. Gilmore, Equilibrium Composition and Thermodynamic Properties of Air to 24,000° K, RAND Report 1543, August 1955.

MAGNETIC CHANNELING OF A STRONG SHOCK*

F. R. SCOTT, W. P. BASMAN, E. M. LITTLE, AND D. B. THOMSON†

INTRODUCTION

In the study of plane high-velocity shocks, one serious deterrent to a quantitative understanding of the conditions behind the propagating disturbance has been the strong interaction with the containing walls. The following experiment was initiated to minimize this effect and also to examine a specific interaction of a shock-produced plasma and a magnetic field. Although this is by no means a complete study, it does include interesting macroscopic measurements. Also, it shows that a strongly ionizing shock produced outside an axial magnetic field will channel along the axis using the magnetic field as a "wall." In the configuration used, measurements indicate that the magnetic interaction does not contribute any noticeable heating of the shock-produced plasma as it channels.

APPARATUS

For these experiments the shock was produced by a low-inductance linear discharge tube with a hollow electrode.[1] Figure 1 is a schematic diagram of the system. The shock propagates along the axis into the cylinder attached to the hollow electrode. Because this hollow electrode is a solid ring conductor, there is good isolation between any alternating magnetic field in the tapered shock tube and any alternating field in the cylinder. Any mixing will decrease the strength of the plane shock by allowing axial flow along lines of force between the two fields. Also, mixing makes any measurements of the interaction of hydrodynamic shock with a magnetic field ambiguous.

* The symposium report was presented by F. R. Scott who is now with General Atomic Division of General Dynamics Corp.

† Los Alamos Scientific Laboratory.

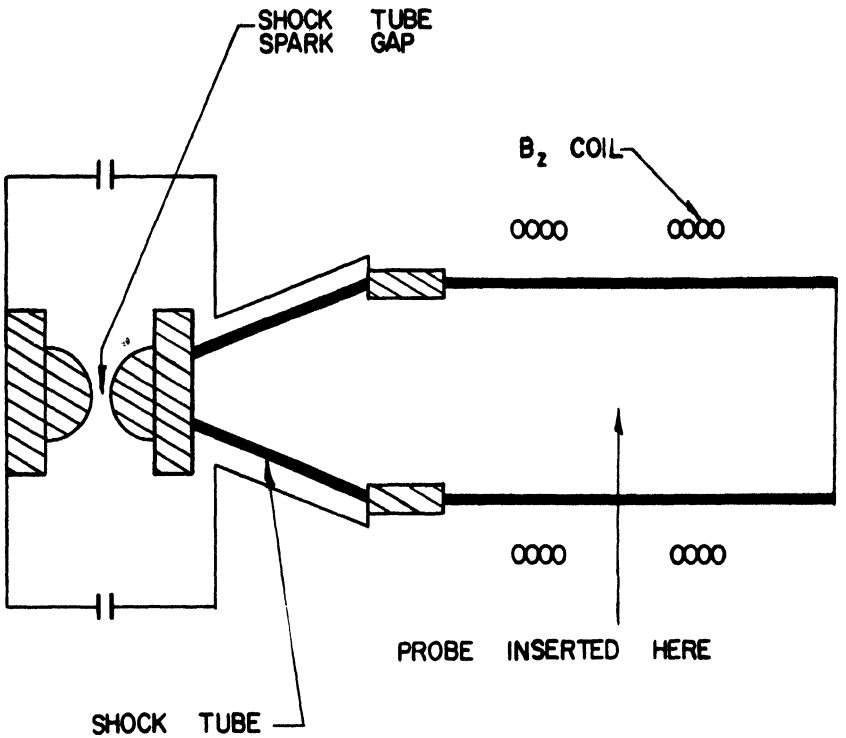

FIG. 1. Schematic diagram of the system producing the shock

The electrical system for the production of the shock consisted of twelve 1-μfd condensers, rated at 25 kv. Each condenser was connected in parallel to a coaxial spark gap through a separate length of RG 8/U cable. The spark gap was coaxially connected to the tube. This system had a ringing frequency of 160 kc and a peak current of 200,000 amp at 20 kv. To study the effects of the resulting shock on a magnetic field, a separate low-frequency, low-voltage bank of eleven 100-μfd condensers supplied current to a solenoid wound around the cylinder. The half cycle period of this system was 6000 μsec, and axial fields up to 6000 gauss were produced in the cylinder.

For these experiments, the slow axial field was triggered first. Then when the field had reached a maximum B_{z0}, the shock tube was discharged. For a typical shock velocity of 8 cm/μsec, the time for the shock to transverse the length of the axial coil was less than 3 μsec, a time small compared to the period of the field. During the time of interest the magnetic field was essentially constant.

MEASUREMENTS

The shock produced by the tapered tube was studied with a Los Alamos rotating mirror "smear" camera. Figure 2 is a typical shock velocity

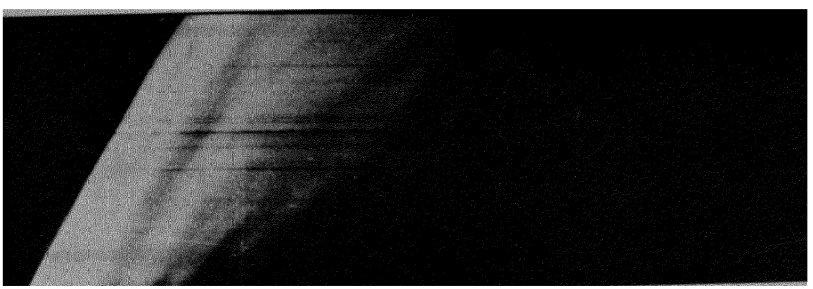

FIG. 2. Smear photograph of the shock; velocity picture

"smear" picture. The slit of the camera was aligned along the center axis of the cylindrical tube, so that the resulting picture gave a plot of light intensity distribution along the axis versus time. The luminous shock velocity is observed on this picture.

These observations resulted in a value of 8 cm/μsec for the velocity of shocks going into deuterium initially at 50-micron pressure. This velocity remained unchanged to within the experimental error of about 0.5 cm/μsec by application of axial fields B_{z0} up to 6000 gauss.

Figure 3 shows a typical shock profile picture. The slit of the smear camera was aligned perpendicular to the tube axis so that the resulting picture gave a plot of the diameter distribution of the light emitted by the hot gas as a function of time. Figure 3 was taken for the case of no axial magnetic field and indicates that the shock front is essentially plane, but does interact strongly with the walls. The intense light and the curvature of the edges of the shock front indicate a strong interaction. Mono-

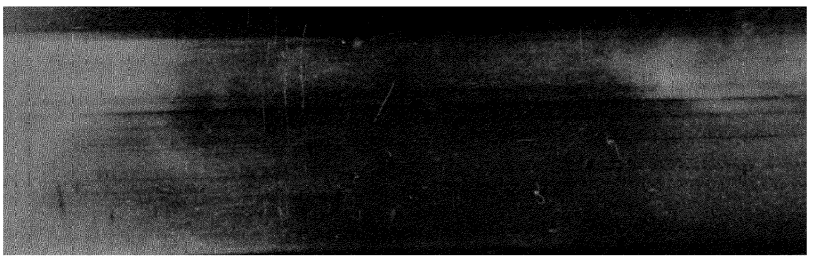

FIG. 3. Smear photograph of the shock; profile picture

chromator observations of silicon emission lines at this time also show that the inside surface of the tube pyrex wall has been evaporated.

Figure 4 shows a typical luminous shock profile "smear" picture for the case of a 3400-gauss axial field. It can be seen that the luminous front was confined to a radius considerably less than the wall radius. After the

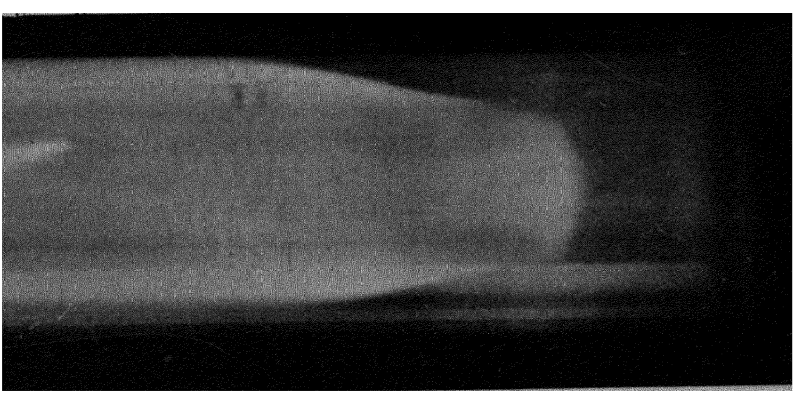

FIG. 4. Profile smear photograph showing the channel effect

shock front has passed, the resulting hot plasma diffuses radially outward through the magnetic field. The diffusion time is about 4 μsec for this picture. It has also been observed with magnetic probes that the axial field diffuses back through the hot gas to near the center of the tube in this time. Since the shock travels the length of the axial field coil in about one-half the time it takes the gas to diffuse to the wall, there is a time in which the plasma is contained by the axial field all along the length of the tube. Observation of the current in the axial field coil also supports this contention.

This channeling of a strong shock by an axial magnetic field was studied in more detail with magnetic probes. The small probes used were first developed in this country by Louis Burkhardt and Ralph Lovberg[2] to measure current distributions in conventional pinch tubes. A typical probe consisted of 30 turns of No. 44 wire wound on a lucite form of area 0.03 cm². The probe coil was inserted in a ⅛-in.-diameter hollow quartz tube. The leads from the coil were brought out from the probe tube through an Armstrong cement seal. The other end of the probe tube was sealed off from the vacuum. A typical probe and its envelope is shown in Fig. 12 of Hugh Karr's article. The probe was inserted in the linear glass tube through a small hole in the cylinder wall. A neoprene disk covered with vacuum grease was used to seal the vacuum between the probe tube and the hole. Crude lucite forms held the probe assembly in place. The distance from the axis of the discharge tube to the probe coil could be varied without breaking the vacuum.

The probe signal was integrated and displayed on a Tektronix 541 oscilloscope. Since the plane of the probe coil was perpendicular to the axial field, the voltage pulse across the probe was proportional to the time rate of the change of this field, and hence the integrated signal was proportional to the field. This integrated signal was observed on a 20-μsec oscilloscope trace. The trace was started when the axial magnetic field had reached the maximum, so that the unperturbed signal appeared as a straight horizontal line displaced from zero by an amount proportional to the strength of the axial field. The shock tube was triggered just after the oscilloscope trace was initiated, so that the perturbation due to the shock appears at the middle of the scope trace.

As mentioned before, the outward motion of the magnetic field lines is opposed by a diffusion-like slipping back toward the center. The probe signals were analyzed at the time for which the displacement of field lines from the center of the cylinder had reached a maximum, which occurred 0.5 μsec after the initial field disturbance.

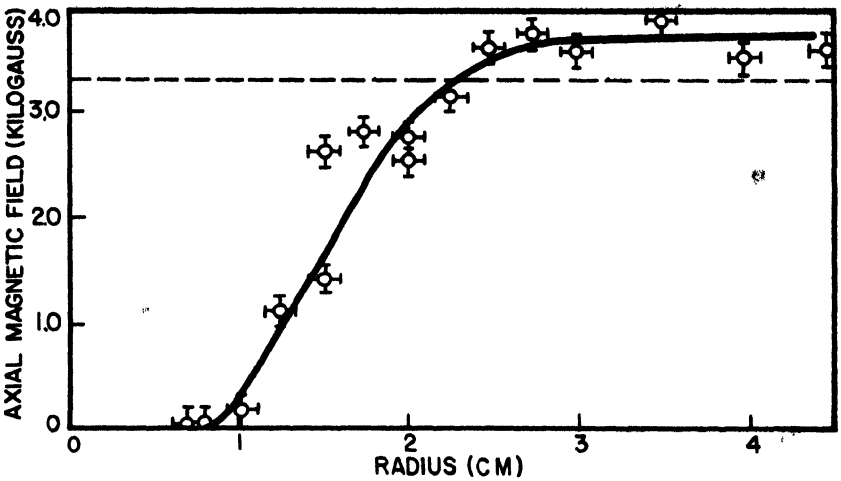

FIG. 5. Radial dependence of the axial field 1/2 μsec after the initial disturbance for an initial field of 3400 gauss.

Figure 5 is a typical plot of the radial dependence of the axial magnetic field 0.5 μsec after the initial field disturbance. This curve shows that there is a region along the axis where the axial field has been removed by the plasma. There is also a region of mixed plasma and field called the sheath, and finally near the tube wall there is a region of increased axial magnetic field with no plasma (as indicated also by the smear camera). Two pertinent radii are evident from Fig. 5, the outer radius where the axial field becomes uniform, and the inner radius where the magnetic field goes to zero. These two radii are plotted in Fig. 6 as functions of the initial axial field strength. Both radii are decreasing functions of the field strength as might be expected. The distance between them, called the sheath region, is relatively constant.

In the absence of an axial magnetic field, an equilibrium shock moving at 8 cm/μsec into deuterium initially at 300° K and 50 microns raises the temperature to 10^5 °K and the pressure to 5.3×10^5 dynes/cm^2 with a density increase by a factor 5.9. The magnetic field producing an equivalent pressure is 3.65 kg which lies within the range of B_{z0} used in these experiments.

An independent value of the equilibrium temperature can be obtained from the radial diffusion time of the magnetic field through the plasma. If one assumes a constant final temperature for 4 μsec after passage of the front and accepts Spitzer's[8] formula for the conductivity of a fully ionized

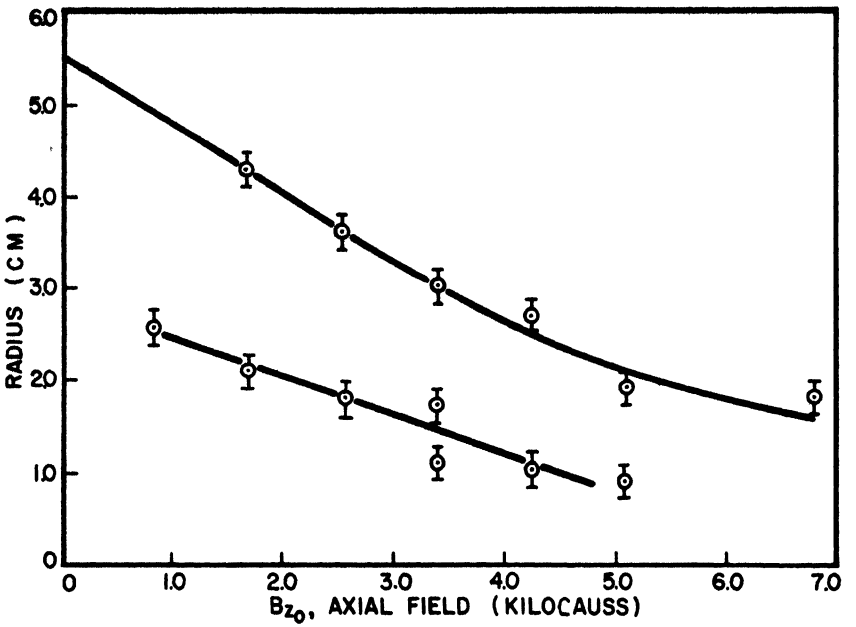

FIG. 6. Inner and outer radii of the channel as a function of initial axial field strength

deuterium gas, an electron temperature of 8×10^4 °K is obtained for a radial and folding diffusion time of 3.5 μsec. This is a gross measurement which certainly needs more data but does indicate a relatively hot plasma 20 cm behind the shock. This result says nothing about the density distribution. Observation of an increase of current in the axial field coil during the time of the shock passage through the coil also indicates that a good conductor occupies a portion of the volume of this coil for at least 4 μsec.

CONCLUSIONS

Although this study was by no means complete, some conclusions can be drawn from the results. First, the shock disturbance does channel along the axis with a radius dependent on the axial magnetic field. Second, the sheath thickness does not vary noticeably with the magnetic field. Third, the observed axial velocity does not vary with the axial magnetic field.

REFERENCES

1. Vernal Josephson, J. Appl. Phys. **29**, 30 (1958).
2. Louis Burkhardt and Ralph Lovberg, Los Alamos Report LA-2131.
3. Lyman Spitzer, Physics of Ionized Gases. Interscience Publishers (1956).

HYDROMAGNETIC EFFECTS IN COUETTE AND STOKES FLOW

H. W. LIEPMANN*

INTRODUCTION

There exist only a few problems for which the equations of motion of a viscous fluid can be integrated. One of these is Couette flow, i.e., the shear flow of a fluid contained between two infinite plates moving relative to each other in their own plane. For incompressible fluids, Couette flow is trivial and is used as the typical example which can be found in almost any elementary physics text; the extension to magneto-hydrodynamics is also well known. Couette flow of a compressible fluid is much more interesting since the interplay between viscous dissipation and heat transfer is involved. The solution for compressible fluids was given by Illingworth[1] some years ago, and the extension to a dissociating or ionizing gas has been recently given.[2,3] In fact Couette flow represents the only case for which a solution, valid for a complete Mach number and Reynolds number range, is known.

It is usually possible to translate the results on Couette flow in such a way that they apply at least qualitatively to flow in a boundary layer where the essential physical phenomena are also due to shear motion. The direct integration of the boundary layer equations is much more involved and cumbersome. Only the case of constant conductivity has so far been carried through.[4]

It is, therefore, instructive to solve the Couette flow problem of a real gas in the presence of a magnetic field. Here the shear motion heats the gas, ionization takes place, and the resulting motion of a conducting gas interacts with the magnetic field. This problem was studied in cooperation with Dr. Z. Bleviss of Douglas Aircraft Co., and some of the main features

* Guggenheim Aeronautical Laboratory, California Institute of Technology.

and results are given in the following; details will be covered in a forthcoming paper by Dr. Bleviss.

A second example of hydromagnetic effects in viscous fluid flow is the classical case of the slow motion of a sphere. The Stokes drag formula for a sphere is very widely known and applied. It is not widely known, however, that there are convergence difficulties in the theory of general Stokes flow and these have only recently been studied systematically.[5] This problem is mathematically much more difficult than Couette flow and hence one has less freedom in choosing the working fluid. Indeed, the solution of the Stokes problem for a compressible fluid is not known! The presence of the magnetic field affects the character of the Stokes solution at large distances, and hence the hydromagnetic effects cannot be obtained by simple perturbation analysis. The solution for the motion of a Stokes sphere in an incompressible fluid with an axial magnetic field was found recently by Dr. W. Chester of Bristol University during his stay at the California Institute of Technology.[6]

EQUATIONS OF MOTION

The equations for steady motion of a viscous, compressible fluid of finite conductivity can be written in the form:

$$\textit{Continuity} \qquad \operatorname{div} \rho \boldsymbol{u} = 0 \tag{1}$$

$$\textit{Momentum} \qquad \operatorname{div} \{\rho \boldsymbol{uu} - \mathbf{P} - \mathbf{T}\} = 0 \tag{2}$$

$$\textit{Energy} \qquad \operatorname{div} \{\rho \boldsymbol{u} h_0 - \mathbf{T} \cdot \boldsymbol{u} + \boldsymbol{q}\} = \boldsymbol{E} \cdot \boldsymbol{j} \tag{3}$$

$$\textit{Maxwell} \qquad \operatorname{curl} \boldsymbol{B} = \mu \boldsymbol{j} = \mu\sigma (\boldsymbol{E} + \boldsymbol{u} \times \boldsymbol{B}) \tag{4}$$

Here $\mathbf{P} = -p\mathbf{I} + \boldsymbol{\tau}$ denotes the viscous stress tensor,

$$\mathbf{T} = -\tfrac{1}{2}\left(\varepsilon E^2 + \frac{B^2}{\mu}\right)\mathbf{I} + \varepsilon \boldsymbol{EE} + \frac{\boldsymbol{BB}}{\mu}$$

the Maxwell stress tensor, $\boldsymbol{q}$ the heat flux vector, and h_0 the so-called total enthalpy, i.e., $h + \tfrac{1}{2}u^2$. The rest of the notation is the usual one: MKS units have been used. The permeability has been assumed constant.

REDUCTION OF THE EQUATIONS FOR COUETTE FLOW

The scheme for Couette flow is shown in Fig. 1. The flow is set up by the axial motion of the outer cylinder past the inner one. This geometry

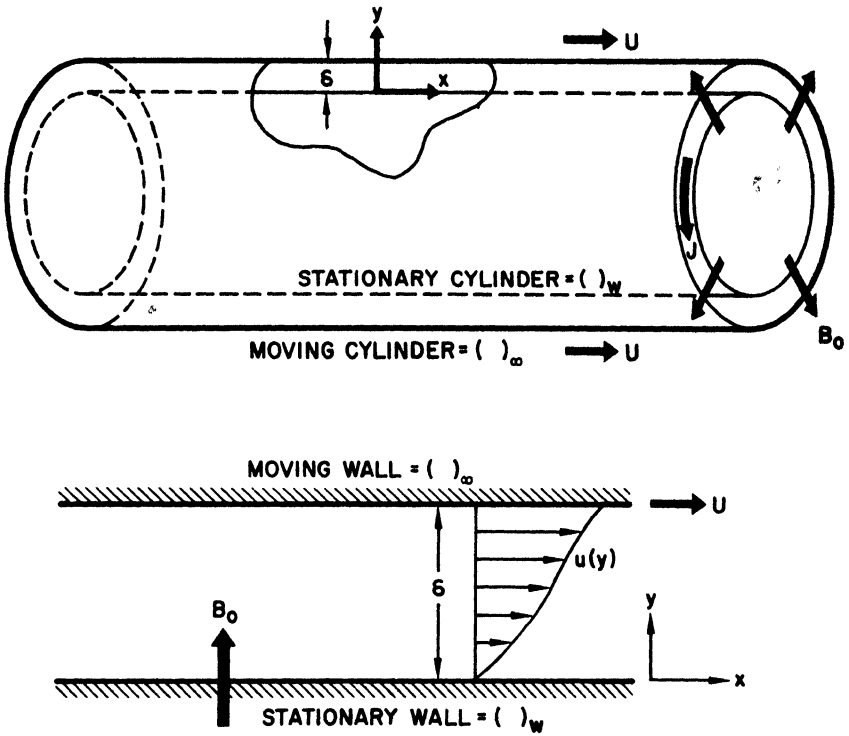

FIG. 1. Scheme for Couette flow

allows closed currents in the gap between the cylinders, and thus leads to simple boundary conditions for the induced magnetic field. Hence the following conditions are impressed by the geometry:

$$\boldsymbol{u} = \{u, 0, 0\}\,; \frac{\partial}{\partial x} = \frac{\partial}{\partial z} = 0\,; \boldsymbol{E} = 0$$

The external magnetic field B is parallel to y. If these conditions are substituted into the equations of motion, Eq. (1) is identically satisfied because one is dealing with pure shear flow. The other three equations reduce to:

$$\frac{d}{dy}\left[\mathbf{P} + \mathbf{T}\right] = 0 \tag{2a}$$

$$\frac{d}{dy}\left[\tau u - q\right] = 0 \tag{3a}$$

with

$$\mathbf{P} = \begin{pmatrix} -p & \tau & 0 \\ \tau & -p & 0 \\ 0 & 0 & -p \end{pmatrix}$$

$$-\frac{dB_x}{dy} = \mu\sigma u B_y = \mu\sigma u B$$

$$B_z = 0 \tag{4a}$$

Hence two components of the Maxwell stresses enter the problem:

$$T_{xy} = \frac{B_x B_y}{\mu}$$

$$T_{yy} = \frac{B_y^2 - B_x^2}{2\mu}$$

BOUNDARY CONDITIONS: APPROXIMATIONS

The moving wall is assumed to be an insulator. Since it is eventually interpreted as an external moving non-conducting fluid this assumption is not restrictive. The induced magnetic field B_x vanishes at infinity and hence at $y = \delta$. Within the inner cylinder $B_x = \text{const}$, since the currents in the annular gap simply constitute a long solenoid.

Shearing stress and heat flux at the boundaries are denoted by τ_w, τ_∞, and q_w, q_∞. Of these q_w or the temperature or the enthalpy is prescribed at the stationary boundary, τ_w, τ_∞ and q_∞ are obtained.

The viscous stress is given by $\tau = \eta(du/dy)$ where η depends on pressure and temperature; the same is true for σ and the thermal conductivity k. The heat flux is written in the form

$$q = -\frac{k}{c_p}\frac{dh}{dy}$$

i.e., in terms of an enthalpy gradient. This is convenient but in the presence of a magnetic field and a real gas not exactly correct. If T denotes the absolute temperature, we can write

$$\frac{dh}{dy} = \frac{\partial h}{\partial T}\frac{dT}{dy} + \frac{\partial h}{\partial p}\frac{dp}{dy}$$

In a magnetic field $dp/dy \neq 0$, and since we have a partially ionized gas $\partial h/\partial p \neq 0$. The product of the two terms is very small in the cases considered here and can be neglected; thus

$$\frac{dh}{dy} \doteq c_p \frac{dT}{dy}$$

Similarly, the effect of the pressure gradient upon η and σ is unimportant for the cases considered here.

Furthermore, the Prandtl number $\mathrm{Pr} = c_p\eta/k$ is assumed constant. This is a convenient but easily removable assumption.

The most stringent assumption concerns the existence of thermal equilibrium: at any point in the channel the ionization and conductivity are assumed to be the ones corresponding to the local conditions of p and T, and to be independent of gradients in pressure and temperature. This is evidently not always correct and the non-equilibrium effects are left for future work. It should be emphasized, however, that heat transfer by diffusion of ionization and dissociation energy is *included*. The coefficient k simply denotes an effective heat conductivity of the mixture; similarly, ε_p denotes the specific heat of the mixture. To work with an "effective" k is always possible in equilibrium and can result at most in a variation of the Prandtl number which is easily taken care of. Indeed, for heat transfer in polyatomic gases this has been the standard procedure. In principle, thermodynamic equilibrium can always be obtained by simply reducing the temperature gradient, i.e., by choosing δ large enough.

The values of pressure and field strength are so restricted that continuum analysis applies. A tensor character of the heat conductivity does not affect the results.

PRINCIPAL RESULTS FOR COUETTE FLOW

The energy equation can be integrated. If q_w, h_w denote the heat flow and enthalpy at the stationary wall respectively, then it follows from Eq.(3a) that

$$\tau u - q = -q_w$$

and thus

$$\frac{1}{2}u^2 + \frac{h - h_w}{\mathrm{Pr}} = -q_w \int_0^y \frac{dy}{\eta} = -q_w \int_0^u \frac{du}{\tau}$$

Consequently the recovery enthalpy, h_r, is given by:

$$h_r = h_\infty + \frac{\mathrm{Pr}}{2} U^2$$

where h_∞ and U are the enthalpy and velocity of the moving wall. *Hence the recovery temperature, i.e., the temperature the wall attains if* $q_w = 0$,

*is not affected by the hydromagnetic effects.** If the temperature or enthalpy at the fixed wall is prescribed, we have for the heat flux

$$q_w = \frac{h_w - h_r}{\Pr} \Big/ \int_0^U \frac{du}{\tau}$$

or in dimensionless form:

$$C_H = \frac{q_w}{(h_w - h_r)\rho_\infty U} = \frac{\tau_\infty}{\rho_\infty U^2} \frac{1}{\Pr \int_0^1 \frac{d(u/U)}{\tau/\tau_\infty}}$$

where τ_∞ denotes the shear stress at the moving wall. But the induced magnetic field B_x vanishes at the moving wall and hence T_{xy} vanishes there. Thus τ_∞ is the total stress on the lower plate as well and consequently a measure for the plate drag. In coefficient form we have,

$$\frac{C_D}{C_H} = 2 \Pr \int_0^1 \frac{d(u/U)}{\tau/\tau_\infty}$$

as a measure of the ratio of drag to heat transfer to the stationary wall. Now if $B = 0$, $T_{xy} = 0$, hence $\tau = \tau_\infty$ and $C_D/C_H = 2 \Pr$, a well-known result. If $B \neq 0$, $\tau + T = \tau_\infty$, hence $\tau \leqq \tau_\infty$ and

$$\int_0^1 \frac{d(u/U)}{\tau/\tau_\infty} > 1$$

Consequently the ratio of drag to heat transfer increases with increasing field. Figures 2 and 3 show some computed values for air for an insulated wall and one at constant temperature. The effect of B is marked.

Shear distributions, velocity distribution, and temperature distribution can be obtained but require an iteration procedure. Figures 4 to 7 show computed results for the temperature and velocity distribution with the product of field strength B and channel height δ as parameter. The values chosen for the velocity, temperature, and pressure correspond roughly to the conditions of a fast missile. Two cases are shown, zero heat transfer

* If the term $\frac{\partial h}{\partial p} \frac{dp}{dy}$ is not neglected, there results a small change in recovery enthalpy.

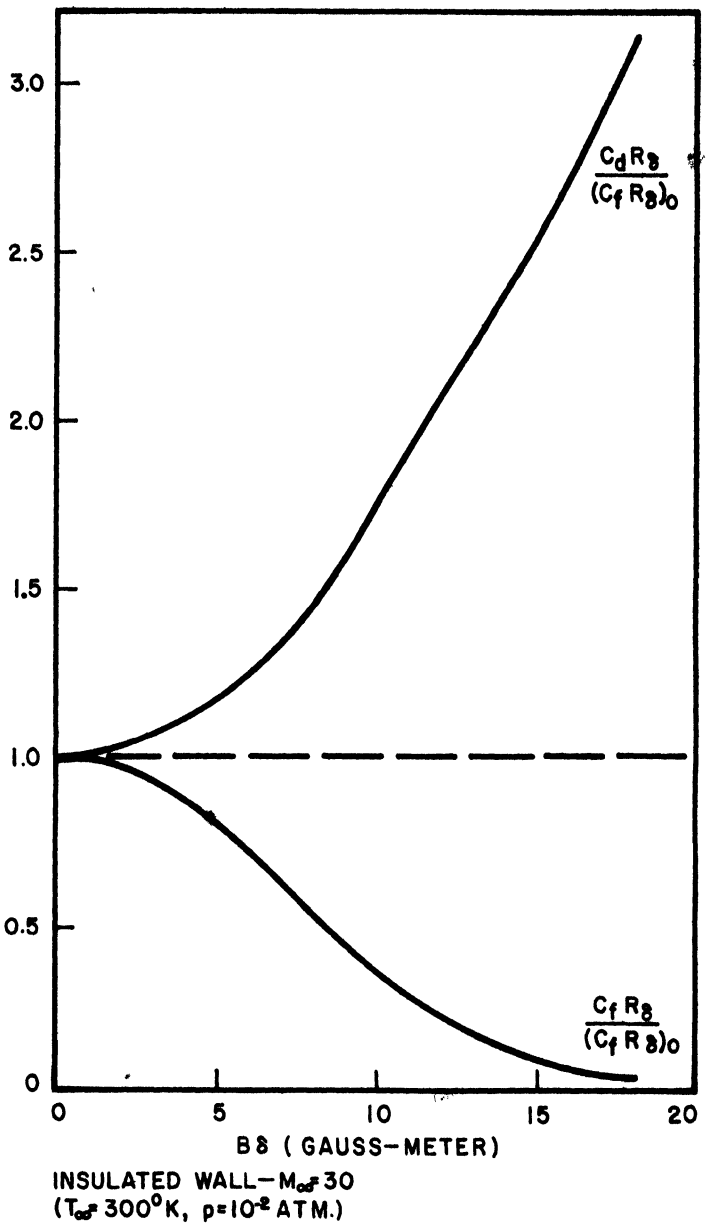

FIG. 2. Ratio of drag to heat transfer for air computed for an insulated wall

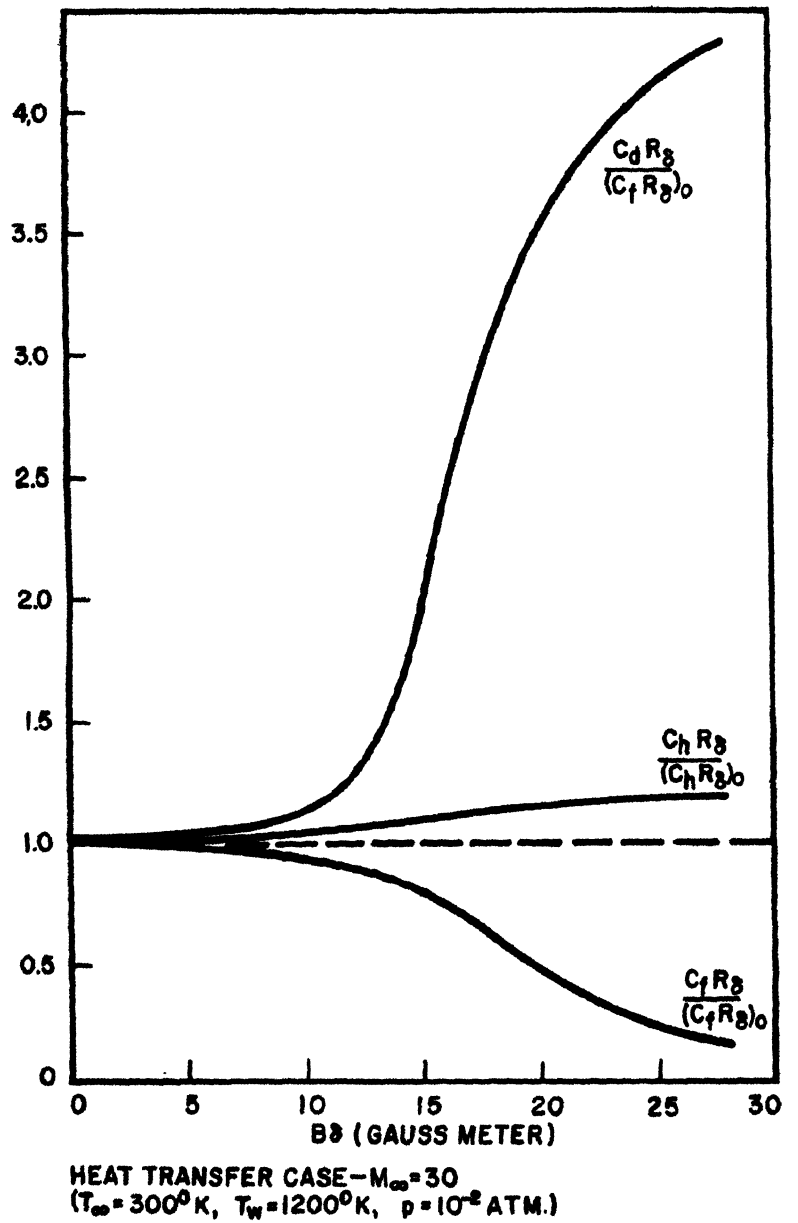

FIG. 3. Ratio of drag to heat transfer for air computed for a wall at a constant temperature.

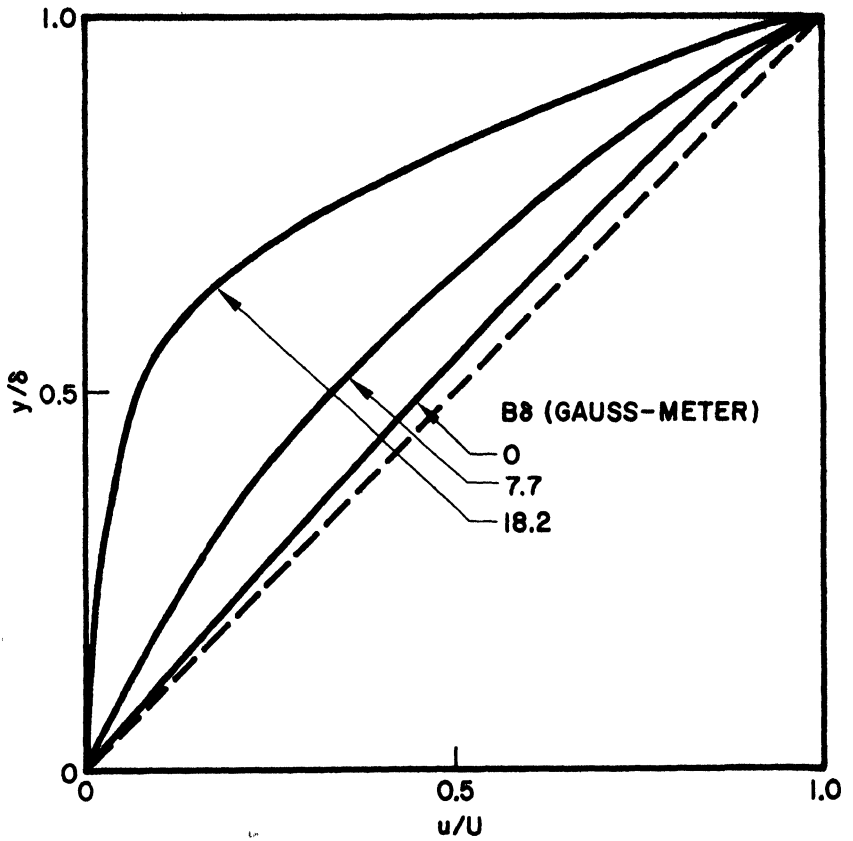

FIG. 4. Velocity distribution for three values of $B\delta$ when there is no heat transfer

and a wall temperature fixed at 1200 °K. Note the shift in the temperature distribution with increasing B. Since the field increases the dissipation and hence raises the temperature, it indirectly also changes the electrical conductivity.

TRANSLATION TO BOUNDARY LAYER FLOW

The transport terms in the equations for a laminar boundary layer with zero axial pressure gradient, as on a long cylindrical body, differ from those for Couette flow; the shearing stress terms are the same. The main

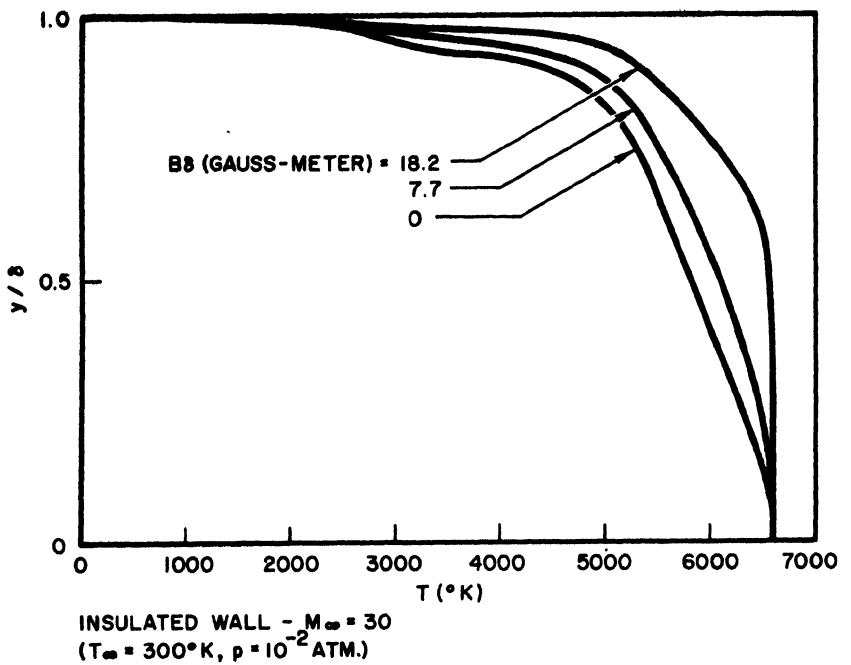

FIG. 5. Temperature distribution for three values of $B\delta$ when there is no heat transfer

effect is the gradual thickening of the laminar layer so that different axial sections of the layer correspond to Couette flow with different δ.

At a given axial station, if one compares boundary layer flow with and without field one concludes that the recovering temperature remains unaffected, and the relative reduction of skin friction and heat transfer is even more pronounced than in Couette flow since the increased dissipation with B makes $\delta_B > \delta_0$. These conclusions agree qualitatively with Rossow's results for a layer with constant conductivity. Also the dissipated energy corresponding to the increased drag with B will appear at the outer edge of the viscous wake of the body.

HYDROMAGNETICS OF STOKES FLOW

Consider the motion of a sphere through a viscous, conducting, incompressible fluid in the presence of a magnetic field parallel to the motion. The flow velocities are assumed so small—i.e., the Reynolds number based on the radius of the sphere less than one—that the transport terms can be neglected. The equations of motion are,

$$\operatorname{div} \boldsymbol{u} = 0$$
$$\operatorname{div} (\mathbf{P} + \mathbf{T}) = 0$$
$$\operatorname{curl} \boldsymbol{B} = \mu\sigma(\boldsymbol{u} \times \boldsymbol{B})$$

The magnetic field opposes the outward motion as the fluid streams around the sphere. The currents flow in circular paths around the axis of motion.

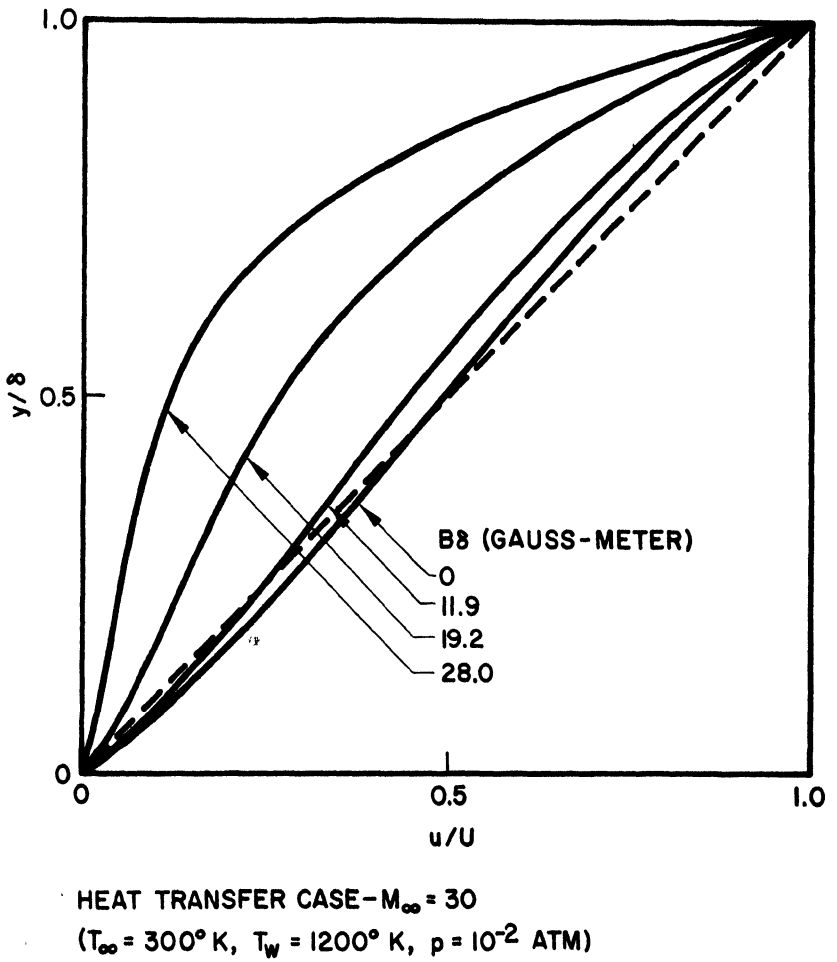

FIG. 6. Velocity distribution for three values of $B\delta$ when there is a heat transfer

Chester[6] has integrated this set of equations and finds that the drag of the sphere for small Hartmann number can be written as:

$$D = 6\pi\eta RU\left\{1 + \frac{3}{8}N_H + \frac{7}{960}N_H^2 + \cdots\right.$$

$$N_H = \sqrt{\frac{\sigma}{\eta}}\,|B|R$$

It is interesting, and at first glance surprising, that the expression for the drag contains a term linear in B. This fact shows that the solution for small B or N_H cannot be obtained by a regular perturbation procedure starting from the known solution for the flow with $B = 0$. That this is true can be seen from two simple arguments.

First, presence of the field adds Joule heating to the dissipation of energy. It is not possible to compute this Joule heat by using the ordinary Stokes solution. If one uses cylindrical coordinates x and r and denotes the velocity components by u and v respectively, one can formally express the Joule heat as

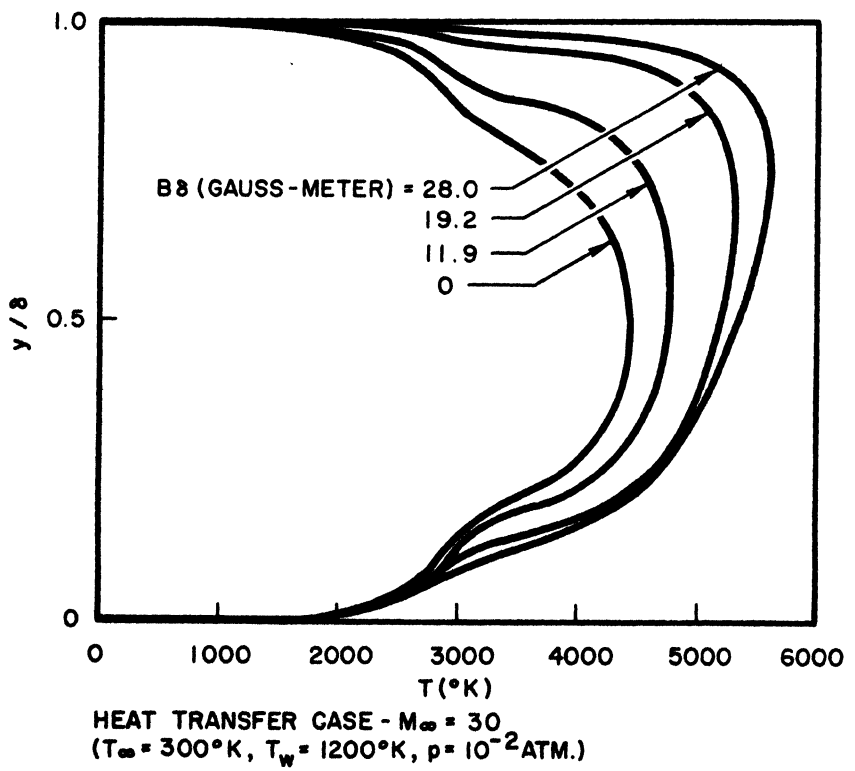

FIG. 7. Temperature distribution for four values of $B\delta$ when there is a heat transfer

$$Q = \sigma B^2 \int_0^\infty \int_0^\infty v^2 \, dx \, r \, dr$$

However, if the v corresponding to the solution for $B = 0$ is inserted the integral diverges at infinity.

Furthermore, the momentum equation can be written in cylindrical coordinates as

$$\eta \nabla^2 u = \frac{\partial p}{\partial x}$$

$$\eta \nabla^2 v = \left(\frac{\eta}{r^2} + \sigma B^2 \right) v + \frac{\partial p}{\partial r}$$

The second equation leads, for $B = 0$, to asymptotic solutions for large r like $v \sim 1/r^2$, $p \sim 1/r^3$. If B is finite, however, no matter how small, there exists a distance r such that $\sigma B^2 >> \eta/r^2$; hence the character of the flow field at infinity is changed and v decreases exponentially.

One may express the same state of affairs by saying there exists a characteristic length

$$L^{-1} \sim \sqrt{\frac{\sigma}{\eta} B^2}$$

and the magnetic field simulates a cylindrical wall of radius L surrounding the fluid flow. It is known that such a wall increases the drag of a Stokes sphere proportional to $1 + \text{const } R/L$; i.e., one can expect here a drag increase of the flow $1 + \text{const } N_H$, in agreement with Chester's solution.

The resulting change in the drag of a small sphere is easily within the range of measurements in mercury, for which the product $|B|R$ in gauss meter is roughly four times N_H. Hence with a few hundred gauss and a sphere of a millimeter diameter, one can expect a change in the drag of more than 10 percent. An experimental investigation of this effect is under way.

REFERENCES

1. C. R. Illingworth, "Some Solutions of the Flow of a Viscous, Compressible Fluid," Cambridge Phil. Soc. Proc. **46**, 469 (1950).
2. H. W. Liepmann and Z. O. Bleviss, "The Effects of Dissociation and Ionization on Compressible Couette Flow," Douglas Aircraft Co. Rept. SM-19831 (1956).

3. J. E. Broadwell, "A Simple Model of the Nonequilibrium Dissociation of a Gas in Couette and Boundary Layer Flow," Douglas Aircraft Co. Rept. SM-22888, August (1957), J. Fluid Mech., in press.
4. Vernon J. Rossow, "On Flow of Electrically Conducting Fluids Over a Flat Plate in the Presence of a Transverse Magnetic Field," NACA TN 3971 (1957).
5. S. Kaplun and P. A. Lagerstrom, "Asymptotic Expansions of Navier-Stokes Solutions for Small Reynolds Numbers"; S. Kaplun, "Low Reynolds Number Flow Past a Circular Cylinder" and "Note on the Preceding Two Papers," Journ. Math. & Mech. **6, 5,** 585–606 (September 1957).
6. W. Chester, "Stokes Flow in a Conducting Fluid," J. Fluid Mech. **3,** part 3, 304–8 (December 1957).